THE EFFECTS OF DIFFERENT CASTING PARAMETERS ON THE MICROSTRUCTURE AND MECHANICAL PROPERTIES OF TITANIUM DENTAL IMPLANT

by

Necati Soydemir

B.S., in M.E., Dokuz Eylül University, 2005

Submitted to the Institute for Graduate Studies in
Science and Engineering in partial fulfillment of
the requirements for the degree of
Master of Science

Graduate Program in Mechanical Engineering

Boğaziçi University

2009

ACKNOWLEDGEMENTS

I am very thankful to many people who have helped me in the preparation of this study. First of all, I would like to thank my advisor Professor Sabri Altıntaş for his guidance and constant support during the preparation of this thesis. I would also like to thank other thesis committee members, Professor Gökhan Baykal and Assistant Professor Nuri Ersoy for their valuable advice and suggestions. I would also like to thank previous thesis committee member Professor Mahmut A. Savaş for his help in this study.

I would like to express my sincere thanks to Mechanical Engineering, Materials Laboratory assistants Önder Albayrak, Nazım Mahmutyazıcıoğlu and Mehmet İpekoğlu for their great help. Also, I am very thankful to Boğaziçi University Mechanical Engineering assistant Kenan Çınar for his great help in metallographic preparation of titanium. I would like to thank Tolga Özdemir and Hüseyin Işıker from AN-KA "Analiz ve Kalite Kontrol Cihazları". I would also like to thank Batu Bütün and Günay Cankurtaran from TÜBİTAK MAM, Materials Institute for their kindly help.

I would like to thank my friend Aziz Önder for his great support about modelling with Solidworks and also for his nice friendship. I am very grateful to my wonderful friends Serhat Terece and Yusuf Tunçay for their unprizable friendship. I am also thankful to my valuable friends Canan Balkan, Orçun Selçuk and Harun Ferit Özbakır for their lovely friendship. I have overcome those hard times with their warm character and nice support.

Finally, I would like to thank my parents Şükrü Ahmet Soydemir and Ayşe Nurhan Soydemir, and my sisters Tuğba Soydemir and Tansu Soydemir. Their love and support made me complete the study and continue this period of graduate degree. My profound prayers go to my dear grandfathers Necati Soydemir and Niyazi Atik, who deceased before the completion of this study. This study is dedicated to them.

This thesis has been supported by Turkish State Planning Agency Project DPT–03K120250 and Tübitak Project 107M556.

ABSTRACT

THE EFFECTS OF DIFFERENT CASTING PARAMETERS ON THE MICROSTRUCTURE AND MECHANICAL PROPERTIES OF TITANIUM DENTAL IMPLANT

Dental implants are used to replace the missing teeth instead of dental bridges. Titanium (Ti) and its alloys are suitable to be the material for dental implants due to their excellent mechanical properties, good corrosion resistance in biological fluids and biocompatibility. But, Ti is a difficult metal to cast because of its high melting point (1670 ± 50 ºC) and great reactivity at high temperatures with elements such as oxygen, hydrogen and nitrogen. By using centrifugal casting, this problem is minimized. Also, in this method, larger force acting on the molten metal is a big advantage to produce sound castings.

The objective of this study is to find the differences between the structures and mechanical properties of dental implants that were produced with different casting parameters (raise time and revolution per minute, rpm). Specimens later are annealed at 700°C to check the microstructure change and Vickers microhardness (HV) values.

Ti Grade 4 (unalloyed pure Ti) was used in this study. ZPrinter 310 equipment (Z Corporation, USA) was used for modelling (rapid prototyping). Wax models were produced by using mould silicone. For casting, a high frequency melting & casting unit (Vacutherm 3.3 Titan, Linn High Therm GmbH, Germany) was used.

It has been found that raising centrifugal speed made a slight decrease in HV. 300/1 Annealed (AN) specimen has the highest HV value. Annealing made a slight increase in HV. After annealing, microstructure is changed and most of the acicular α grains are converted to α grains.

ÖZET

FARKLI DÖKÜM PARAMETRELERİNİN TİTANYUM DİŞ İMPLANTININ MİKROYAPISINA VE MEKANİK ÖZELLİKLERİNE ETKİSİ

Diş implantları, eksik dişlerin yerini doldurmak amacıyla, diş köprüleri yerine kullanılmaktadır. Titanyum (Ti) ve alaşımları, mükemmel mekanik özellikleri, biyolojik sıvılardaki iyi korozyon dayanımları ve biyouyumlulukları nedeniyle, diş implantları için malzeme olmaya uygundurlar. Fakat, titanyum yüksek ergime sıcaklığına sahip (1670 ± 50 ºC) olduğundan ve oksijen, hidrojen ve azot gibi elementlerle yüksek sıcaklıklarda yüksek reaksiyona girme kabiliyetine sahip olduğundan dökümü zor bir metaldir. Santrifüj döküm yönteminde, bu sorun minimize edilir. Aynı zamanda, bu yöntemde, ergimiş metallere etki eden yüksek kuvvet, boşluksuz dökümler üretmek için büyük avantajdır.

Bu çalışmanın amacı, farklı döküm parametreleriyle (yükselme zamanı ve devir) üretilmiş diş implantlarında oluşan yapılar ve mekanik özellikler arasındaki farklılıkları bulmaktır. Numuneler sonra içyapı değişimini ve Vickers mikrosertlik değerlerini kontrol etmek için 700°C'de tavlanmışlardır.

Bu çalışmada Ti Grade 4 (alaşımsız saf Ti) kullanılmıştır. Modelleme (hızlı prototipleme) için ZPrinter 310 cihazı (Z Corporation, ABD) kullanılmıştır. Mum modeller kalıp silikonu kullanılarak üretilmiştir. Döküm için, yüksek frekanslı ergitme ve döküm ünitesi (VACUTHERM 3.3 TITAN, Linn High Therm GmbH, Almanya) kullanılmıştır.

Santrifüj hızı artışının, mikrosertlik değerlerinde kısmi azalmaya yol açtığı görülmüştür. 300/1 numunesi en yüksek mikrosertliğe sahiptir. Tavlama, mikrosertlikte az da olsa bir yükselmeye yol açmıştır. Tavlama sonrası mikroyapı değişmiştir ve iğnemsi α tanecikleri α taneciklerine dönüşmüştür.

TABLE OF CONTENTS

LIST OF FIGURES

LIST OF TABLES

LIST OF SYMBOLS/ABBREVIATIONS

E	Elastic modulus
^{o}C	Celsius
gf	gram force
GPa	Gigapascal
KPa	Kilopascal
mm	Millimeter
MPa	Megapascal
ASTM	American Society for Testing and Materials
BCC	Body centered cubic
BP	Bottom part
CP	Commercially pure
ELI	Extra low interstitial
FCC	Face centered cubic
HEX	Hexagonal close packed
HIP	Hot isostatic pressing
HV	Vickers hardness
ISO	International Organization for Standardization
ITP	International Titanium Powder
LD	Largest diameter
PM	Powder metallurgy
SD	Standard deviation
SEM	Scanning electron microscope
TI	Titanium
UP	Upper part

1. INTRODUCTION

Titanium (Ti) and its alloys have been widely used in medical applications such as dental and orthopedic prostheses. The success of Ti based materials in these applications is due to their excellent mechanical properties, good corrosion resistance in biological fluids and biocompatibility. The high corrosion resistance of Ti in various test solutions is provided by the formation of a very protective oxide layer on its surface. The contact between the metallic implant and the living tissues is made through the oxide layer on the implant surface. This contact allows the osseointegration process [1].

Ti's superior wetting property makes it useable. So, it has been frequently used as a living body material such as dental making–up substance. Ti and its alloys are promising materials in the dental field. Their properties are nearly equal to those of dental gold alloys, and they have low cost [2, 3].

Dental castings are usually made by pressure vacuum casting, centrifugal casting, investment casting and electric discharge machining. In pressure vacuum or centrifugal casting methods, the metal is melted using an electric plasma arc or inductive heating in a melting chamber filled with inert gas or held in a vacuum. The molten metal then is transferred to the refractory mold by centrifugal or pressure vacuum filling [4].

In the area of centrifugal casting, Ti products play an important role. The use of centrifugal casting as a production method is a common technique and it is used for nearly 200 years. The method was used in practice at the beginning of the 19^{th} century and was developed in England by George Enthony in 1809.

The centrifugal casting method is used to make components that are not regular or symmetrical in shape and so cannot be rotated about a central axis. In this method, the centrifugal force generates a high pressure which forces molten metal into the mould cavity. The melt is thrown out by the centrifugal force under sufficient pressure to assure better die filling. Solidification progresses from outer surface to the inside. The axis of rotation may be horizontal or vertical [5, 6].

Producing Ti dental implants with centrifugal casting is very common. Despite its advantages, Ti is an inherently difficult metal to cast. It has a high melting point (1670 ± 50ºC) and great reactivity at high temperatures with elements such as oxygen, hydrogen and nitrogen. Casting Ti with centrifugal casting technique is a good decision, because the centrifugal casting machine can exert approximately 40 – 60 times more force on the metal than the pressure difference casting unit. This force is good enough to produce sound castings [7, 8].

In this thesis, Ti Grade 4 (unalloyed pure Ti) is used in the centrifugal casting process to produce dental implants. For making models, ZPrinter 310 equipment (Z Corporation, USA) is used as a rapid prototyping machine. Wax models are produced by using mould silicone and rapid prototyping model. A high frequency melting & casting unit (Vacutherm 3.3 Titan, Linn High Therm GmbH, Germany) is used as a centrifugal casting device. Two implants are annealed to search microstructure and hardness change.

2. LITERATURE SURVEY

2.1. Titanium

Ti is present in the earth's crust at a level of about 0.6 per cent and is therefore the fourth most abundant structural metal after aluminum, iron, and magnesium. The first suspicion of a new, unknown element present in dark, magnetic iron sand (ilmenite) in Cornwall (United Kingdom) was expressed in 1791 by Gregor, a clergyman and amateur mineralogist. In 1795, Klaproth, a German chemist, analyzed rutile from Hungary and identified an oxide of an unknown element, the same as the one reported by Gregor. Klaproth named the element "Titanium" after the Titans, the powerful sons of the earth in Greek mythology [9].

2.1.1. Properties of Titanium

2.1.1.1. Basic Properties. Some of the basic characteristics of Ti and its alloys are listed in Table 2.1 and compared to those of other structural metallic materials based on Fe, Ni, and Al.

The high reactivity with oxygen leads to the immediate formation of a stable and adherent oxide surface layer when exposed to air, resulting in the superior corrosion resistance of Ti in various kinds of aggressive environments, especially in aqueous acid environments. The much higher melting temperature of Ti as compared to aluminum, the main competitor in light weight structural applications, gives Ti a definite advantage above application temperatures of about 150°C. The high reactivity of Ti with oxygen limits the maximum use temperature of Ti alloys to about 600°C [9].

Table 2.1. Some important characteristics of titanium and titanium based alloys as compared to other structural metallic materials based on Fe, Ni, and Al [9]

	Ti	Fe	Ni	Al
Melting Temperature (°C)	1670	1538	1455	660
Allotropic Transformation (°C)	$\beta \rightarrow \alpha$ (882°C)	$\gamma \rightarrow \alpha$ (912°C)	-	-
Crystal Structure	bcc → hex	fcc → bcc	fcc	fcc
Room Temperature E (GPa)	115	215	200	72
Yield Stress Level (MPa)	1000	1000	1000	500
Density (g/cm^3)	4.5	7.9	8.9	2.7
Comparative Corrosion Resistance	Very High	Low	Medium	High
Comparative Reactivity with Oxygen	Very High	Low	Low	High
Comparative Price of Metal	Very High	Low	High	Medium

2.1.1.2. Physical Properties. The atomic structure of Ti is $1s^2$, $2s^2$, $2p^6$, $3s^2$, $3p^6$, $3d^2$, $4s^2$. The lightly held $3d^2$ and $4s^2$ electrons are highly reactive and rapidly form a tenacious oxide that is responsible for the metal's biocompatibility.

The remaining electrons are relatively stable and tightly bound. At temperatures up to 882°C, pure Ti exists as a hexagonal close packed atomic structure (hex), alpha phase. Above that temperature, the structure is body centered cubic (bcc), beta phase. The metal melts at l665°C.

The elements oxygen, aluminum, carbon and nitrogen stabilize the alpha phase of Ti because of their increased solubility in the hex. Oxygen occupies interstitial sites. Elements that stabilize the beta phase include manganese, chromium, iron and vanadium [10].

ASTM Committee F–4 on Materials for Surgical Implants recognizes four grades of commercially pure (cp) Ti and two Ti alloys. The two alloys are Ti–6Al–4V and Ti–6Al–4V extra low interstitial (ELI). “Extra low interstitial” describes the low levels of oxygen dissolved in interstitial sites in the metal. With lower amounts of oxygen and iron residuals in the ELI alloy, ductility is improved slightly. Cp Ti materials are cp grade I Ti, cp grade II Ti, cp grade III Ti and cp grade IV Ti. Cp Ti is also referred to as unalloyed Ti. All six of these materials are commercially available as dental implants [10].

2.1.1.3. Mechanical Properties. The mechanical properties of Ti, Ti alloys and other natural and implant materials are listed in Table 2.2. It is important to note that while the modulus of elasticity of cp grade I Ti to cp grade IV Ti ranges from 102 to 104 GPa (a change of only 2%), the yield strength increases from 170 to 483 MPa (a gain of 180%) [10].

Table 2.2. The mechanical properties of titanium, titanium alloys and other natural and implant materials [10]

Material	Modulus (GPa)	Ultimate Tensile Strength (MPa)	Yield Strength (MPa)	Elongation (%)	Density (g/cm³)
cp grade I Ti	102	240	170	24	4,5
cp grade II Ti	102	345	275	20	4,5
cp grade III Ti	102	450	380	18	4,5
cp grade IV Ti	104	550	483	15	4,5
Ti–6Al–4V ELI	113	860	795	10	4,4
Ti–6Al–4V	113	930	860	10	4,4
Co–Cr–Mo	240	700	450	8	8,5
316L Steel	200	965	690	20	7,9
Cortical Bone	18	140	-	1	0,7
Dentin	18,3	52	-	0	2,2
Enamel	84	10	-	0	3

Compared with Co–Cr–Mo alloys, Ti alloy is almost twice as strong and has half the elastic modulus. Compared with 316L stainless steel, the Ti–6Al–4V alloy is roughly equal in strength, but again, it has half the modulus. Strength is beneficial because materials

better resist occlusal forces without fracture or failure. Lower modulus is desirable because the implant biomaterial better transmits forces to the bone [10].

At the atomic level, materials differ in yield strength because they differ in resistance to planar slip and dislocation movement. Atoms and localized stresses that prevent dislocation movement raise the yield strength of such materials. In the case of Ti, oxygen dissolves into the crystal lattice as interstitial atoms between Ti ions. The oxygen atoms take up room in the crystal lattice, effectively squeezing the Ti atoms and creating areas of strain within the atomic lattice. Conversely, because the planes of atoms move less as a result of oxygen residuals, ductility is decreased.

The elastic modulus of a material, at the atomic level, measures the attraction of atoms to each other. This attraction depends on the particular atoms involved and to some extent the arrangement of the atoms in the crystal structure. In the case of cp Ti, trace amounts of oxygen do not significantly change the modulus [10].

2.1.1.4. Chemical Properties. Ti's atomic weight is 47.90. Its chemical behavior shows many similarities with silica and zirconium, as an element belonging to the first transition group. Its chemistry in aqueous solution (especially in the lower oxidation states) has some similarities with that of chrome and vanadium. Ti is a transition metal light with a white – silvery – metallic colour. Pure Ti is not soluble in water, but is soluble in concentrated acids. The main oxidation state is 4+, although the states 3+ and 2+ are also known, but are less stable. This element burns in the air when it's heated up to obtain TiO_2 and when it is combined with halogens. It reduces the water vapor to form the dioxide and hydrogen. It reacts in a similar way with hot concentrated acids, although it forms trichloride with chlorhydric acid [11].

2.1.1.5. Crystal Structure. Pure Ti exhibits an allotropic phase transformation at 882°C, changing from a bcc crystal structure (β phase) at higher temperatures to a hex crystal structure (α phase) at lower temperatures. The hexagonal unit cell of the α phase is shown in Figure 2.1a. The lattice parameters are a (0.295 nm) and c (0.468 nm) at room temperature. The resulting c/a ratio for pure α Ti is 1.587, smaller than the ideal ratio of

1.633 for the hex crystal structure. The unit cell of bcc β phase is illustrated in Figure 2.1b. The lattice parameter value of pure β Ti at 900°C (a = 0.332 nm) [9].

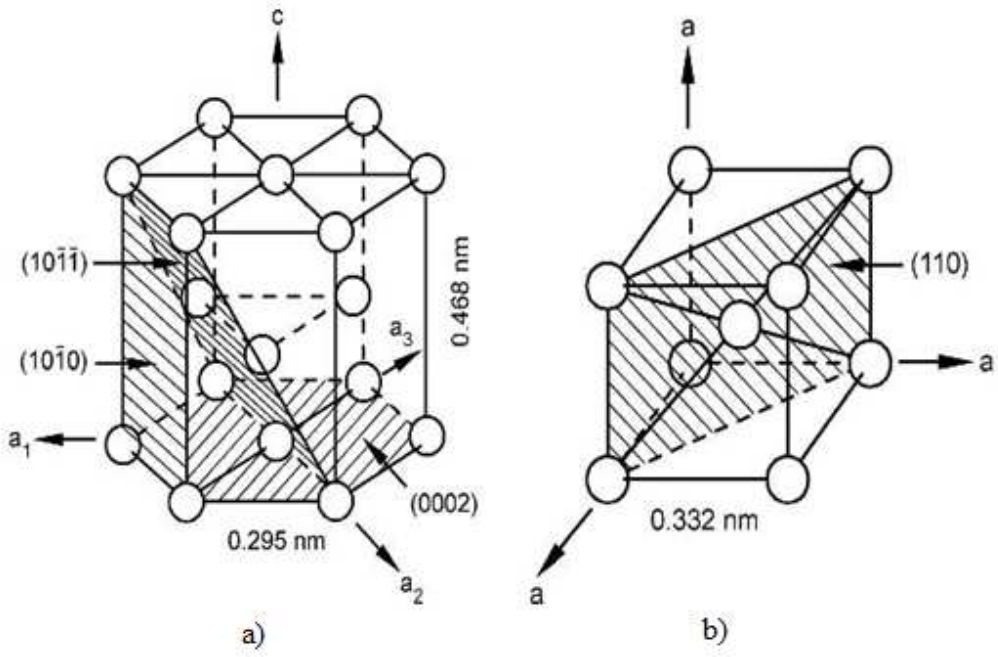

Figure 2.1. Unit cells of titanium a) α phase and b) β phase [9]

2.1.2. Alloy Types of Titanium and Phase Diagrams

Commercial Ti alloys are classified conventionally into three different categories (α, α + β, and β alloys). This classification is illustrated in Figure 2.2 schematically.

The β phase is helpful in controlling the recrystallized α grain size and improves the hydrogen tolerance of these alloys. The four different grades of cp Ti differ with respect to their oxygen content from 0.18 per cent (grade 1) to 0.40 per cent (grade 4) in order to increase the yield stress level. The two alloys Ti–0.2Pd and Ti–0.3Mo–0.8Ni offer better corrosion resistance than cp Ti. Their common names are grade 7 and grade 12 respectively and the iron and oxygen limits are identical to grade 2 of cp Ti. Ti–0.2Pd offers better corrosion resistance, but is more expensive than Ti–0.3Mo–0.8Ni [9].

The α alloy Ti–5Al–2.5Sn (0.20 per cent oxygen) has a much higher yield stress level (780–820 MPa) than the cp Ti grades (grade 4: 480 MPa). It can be used at service temperatures up to 480°C and in its ELI version with 0.12 per cent oxygen also at low

temperatures (–250°C). It is an old alloy, although it is being replaced by Ti–6Al–4V in many applications [9].

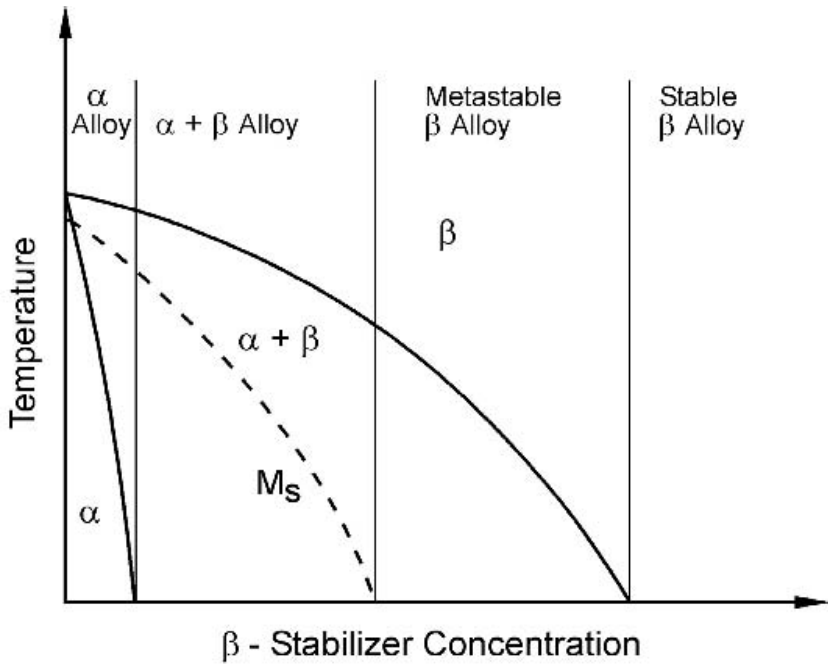

Figure 2.2. Classification of commercial titanium alloys (schematically) [9]

Alloys which contain in equilibrium only a small volume fraction of β phase (less than about 10 volume per cent) are also often called “near α” alloys and their main usage is at high service temperatures. Although they belong per definition to the α + β alloys.

The Ti–6Al–4V alloy contains in equilibrium at 800°C about 15 volume per cent β phase. This alloy has an exceptional good balance of strength, ductility, fatigue, and fracture properties but can be used only up to temperatures of about 300°C. The ELI version of this popular alloy has especially high fracture toughness values and excellent damage tolerance properties. This alloy is the well known, lowest cost and most commercial available Ti alloy. It accounts for 60 per cent of the total Ti production [9, 12].

β alloys like Beta 21S and Beta C are actually metastable β alloys, because they all are located in the equilibrium (α + β) phase region of the phase diagram. Since stable β alloys located in the β single phase field do not exist as commercial materials, the expression β alloys is commonly used and also used for the metastable β alloys [9].

Figure 2.3 illustrates the effect of alloying elements on phase diagrams of titanium alloys (schematically).

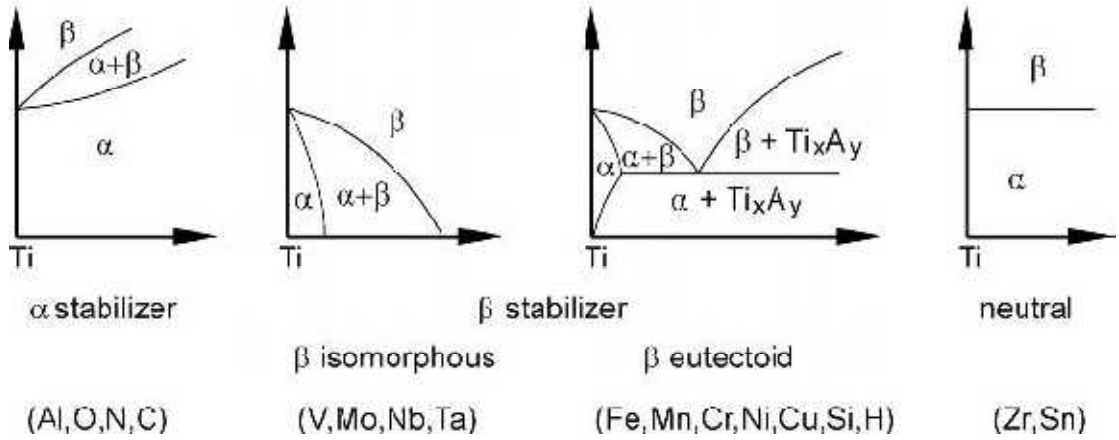

Figure 2.3. Effect of alloying elements on phase diagrams of titanium alloys (schematically) [9]

Aluminum is the most important α stabilizer and is therefore present in many titanium alloys. The binary Ti–Al phase diagram (Figure 2.4) shows that with increasing aluminum content the Ti_3Al (α_2) phase will be formed and that the two phase region (α + Ti_3Al) starts at about 5 per cent Al for a temperature of about 500°C. To avoid any appreciable amount of coherent Ti_3Al precipitates in the α phase, the aluminum content in most titanium alloys is limited to about 6 per cent. From Figure 2.4 it can be seen that for this aluminum level of about 6 per cent the α/β transformation temperature of 882°C for pure titanium is increased to about 1000°C for the two phase region (α + β). In addition to conventional titanium alloys, the Ti–Al phase diagram is also the basis for the titanium aluminides, which are recently developed alloys based on the two intermetallic compounds Ti_3Al (Alpha–2 alloys and the orthorhombic variant, Ti_2AlNb alloys) and TiAl (Gamma alloys) [9].

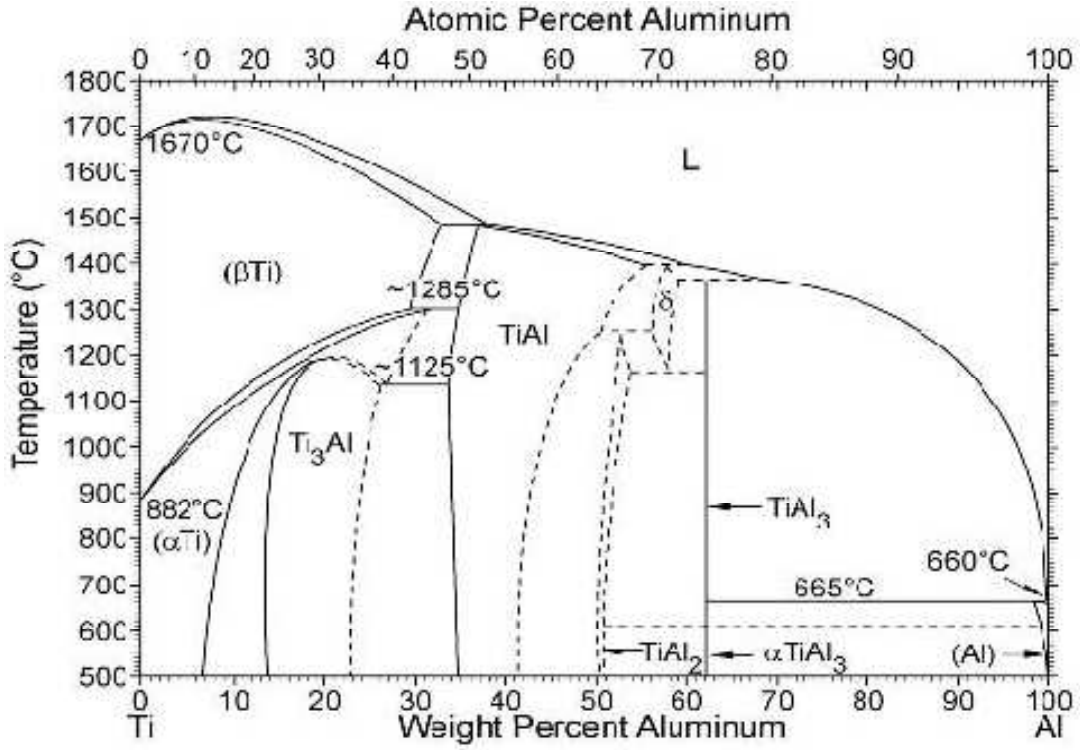

Figure 2.4. Ti – Al phase diagram [9]

From the three most important β isomorphous elements (V, Mo and Nb) the Ti – Mo binary phase diagram is selected (Figure 2.5). This is because it is convenient to calculate equivalent molybdenum content (as in case of an equivalent aluminum content) for all β stabilizers in multi component titanium alloys. The maximum molybdenum content present in conventional titanium alloys is about 15 per cent, so the miscibility gap only adds complexity to the present discussion without helping to understand the effects of alloying additions in the concentration ranges of interest. Indeed, it can be seen from Figure 2.5 that 15 per cent Mo lowers the $\beta \rightarrow \alpha + \beta$ transformation temperature from 882°C for pure titanium to about 750°C. Furthermore, it can be seen from Figure 2.5 that the solid solubility of Mo in the α phase is very low (below 1 per cent). The Ti–V and Ti–Nb phase diagrams are qualitatively similar to Figure 2.5. By adding 15 per cent V, which is also about the maximum vanadium content in conventional titanium alloys, the $\beta \rightarrow \alpha + \beta$ transformation temperature is lowered to about 700°C. The maximum solid solubility of V in the α phase is at 680°C about 3 per cent and therefore much higher as compared to molybdenum. The addition of Nb in conventional titanium alloys is kept within the range of 1–3 per cent, much lower than the maximum amounts of Mo and V. The influence of

Nb on the β → α + β transformation temperature is similar to Mo, the transus is lowered to about 750°C by an addition of 15 per cent Nb [9].

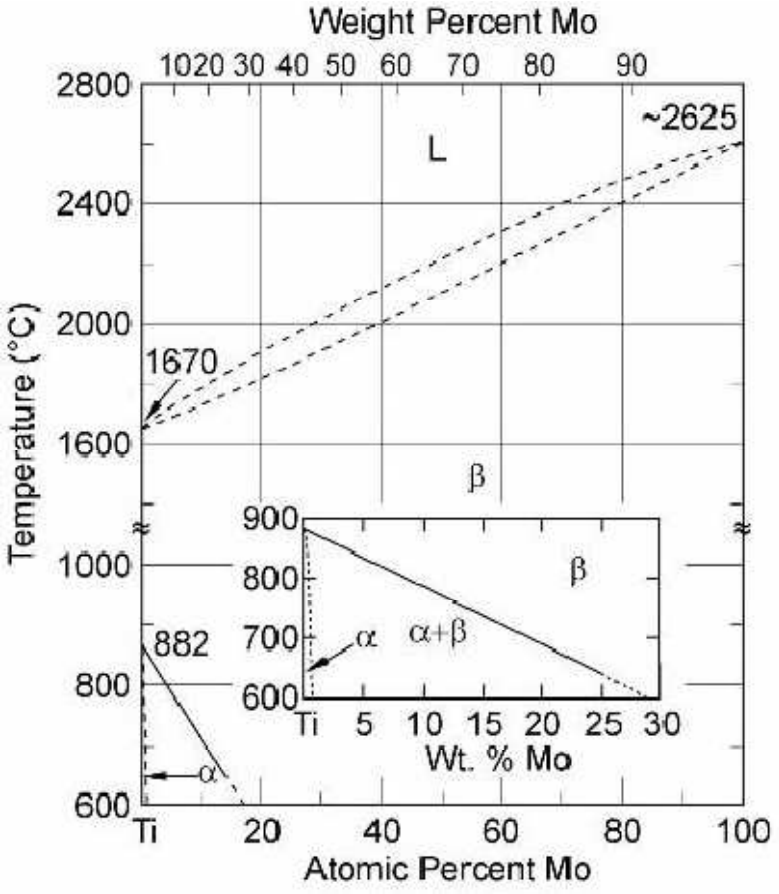

Figure 2.5. Ti – Mo phase diagram [9]

Among the β eutectoid forming elements, the Ti – Cr and Ti – Fe phase diagrams have been chosen and are shown in Figure 2.6 and Figure 2.7 respectively. It can be seen that Cr is an effective β stabilizing element, the eutectoid temperature being 667°C and the eutectoid point lying at about 15 per cent Cr. A characteristic of all β eutectoid forming elements is a low solid solubility in the α phase. For example, in the Ti – Cr system (Figure 2.6) the maximum solubility is only about 0.5 per cent. Consequently, nearly all of the β eutectoid forming element additions partition to the β phase [9].

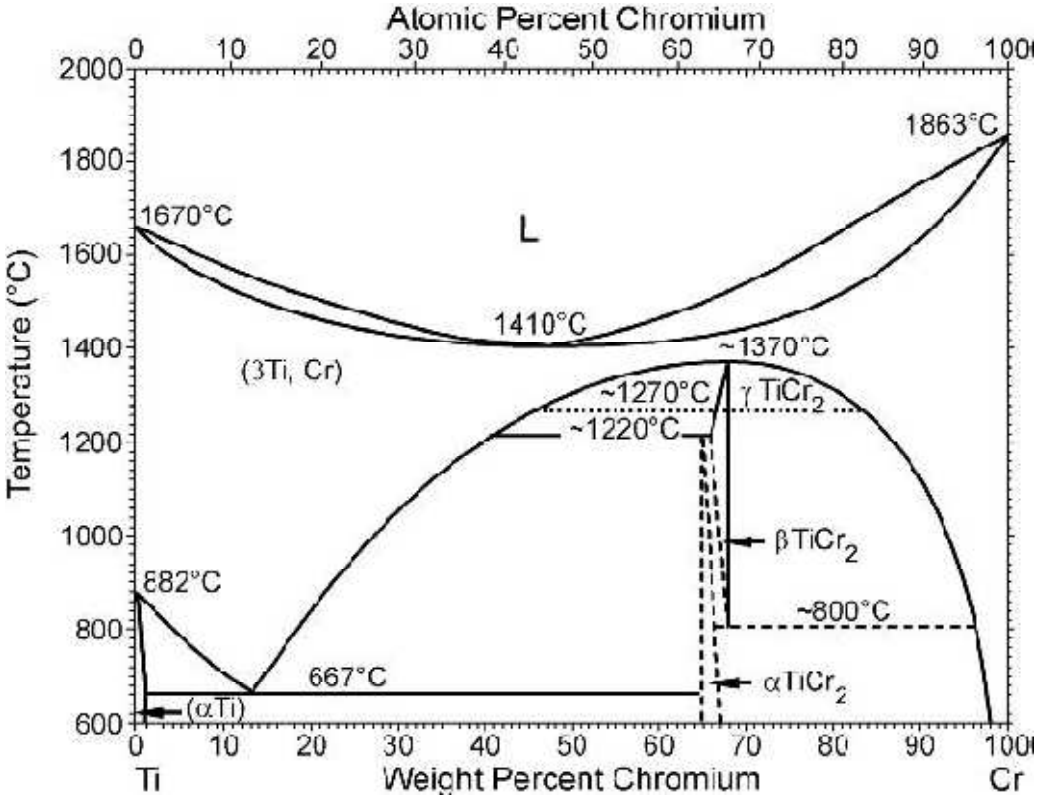

Figure 2.6. Ti – Cr phase diagram [9]

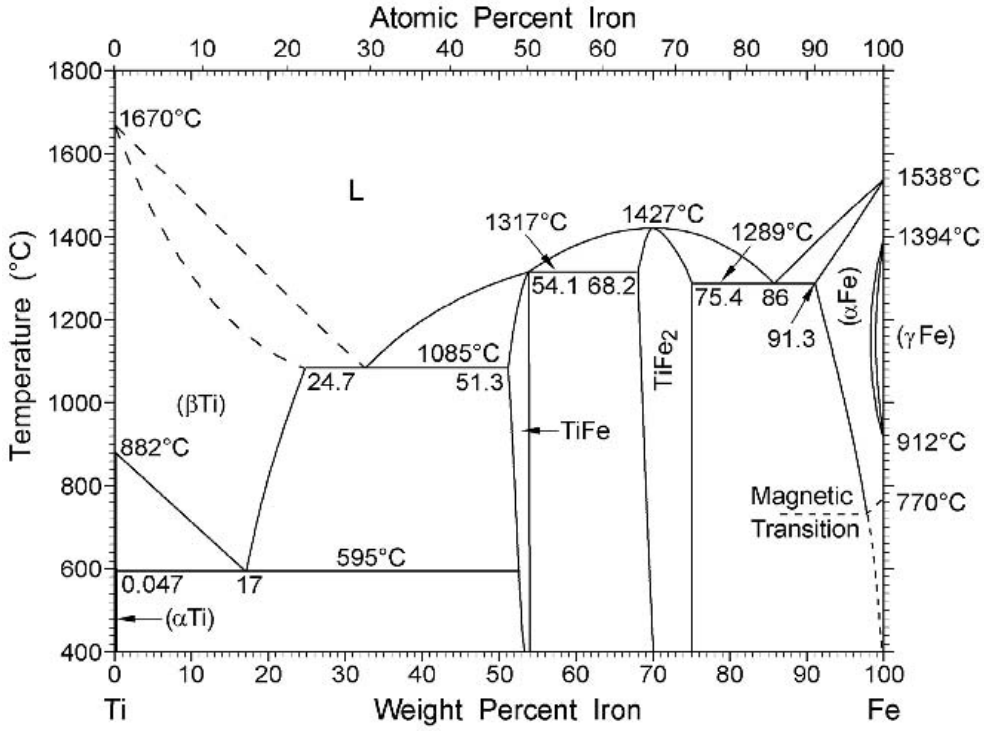

Figure 2.7. Ti – Fe phase diagram [9]

2.1.3. Microstructure of Titanium

The microstructures of Ti can be complex. They are a direct result of composition, processing and post processing heat treatment. The mechanical properties of Ti alloys in a finished shape can be affected by several factors. These factors are:

- Amounts of specific alloying elements and impurities
- Melting process used to make primary ingot
- Number of melting steps
- Method for mechanically working ingots into mill products
- Steps in forging a shape
- Casting process and volume of cast article and use of densification techniques such as hot isostatic pressing (HIP) to reduce casting porosity
- Powder metallurgy (PM) process including method of making powder
- Joining process used to fabricate a structure
- Post processing heat treatment of final step employed in working or fabrication
- Machining process and surface treatment

Transformations on heating and cooling and phase compositions are altered by alloying additions, which are typically classified as alpha or beta stabilizers. Vanadium, iron and hydrogen are beta stabilizers. Oxygen, aluminum and nitrogen are alpha stabilizers.

Pure Ti can be strengthened by alloying, processing and post processing heat treatment. The physical properties of Ti are largely unaffected by processing. However the kinetics of the Ti beta phase transformations that occur during heating, cooling and aging strongly influence microstructure and therefore mechanical properties.

The grain size, grain shape and grain boundary arrangements in Ti have a very significant influence on mechanical properties.

Pure Ti is single phase alpha. The microstructure of cp Ti depends on whether or not it has been cold worked or on the specific type of annealing employed. In a pure Ti, which

contains oxygen and nitrogen, the alpha formed from beta has much more distinctive Widmanstätten structure than does a Ti essentially free of these elements (Figure 2.8) [13].

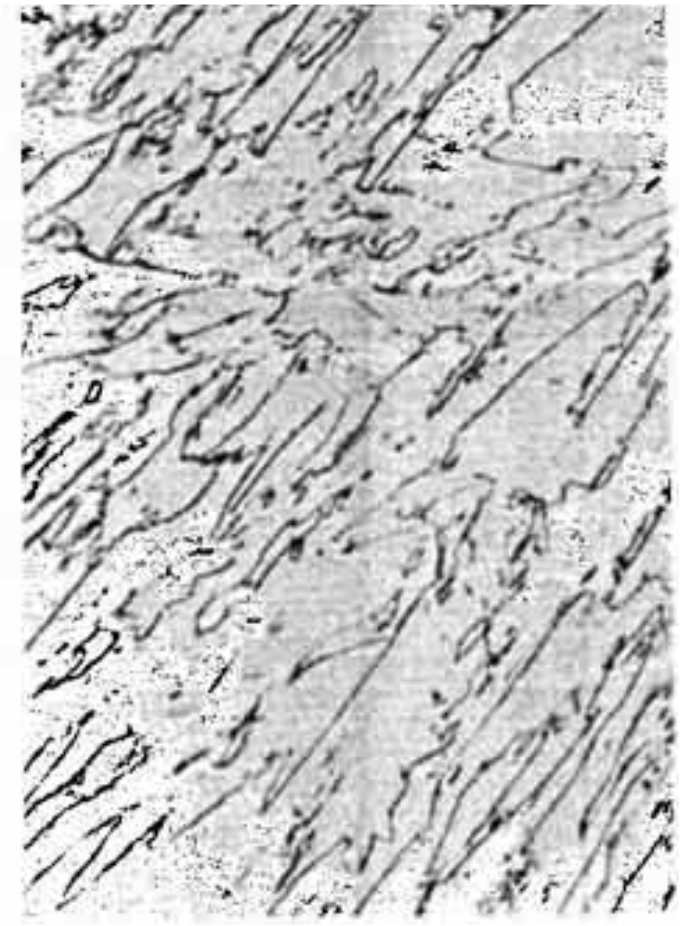

Figure 2.8. Distinctive Widmanstätten structure in pure titanium (150x) [13]

The equiaxed microstructure of Ti after annealing at 800°C (1 hour) in the alpha region is shown in Figure 2.9.

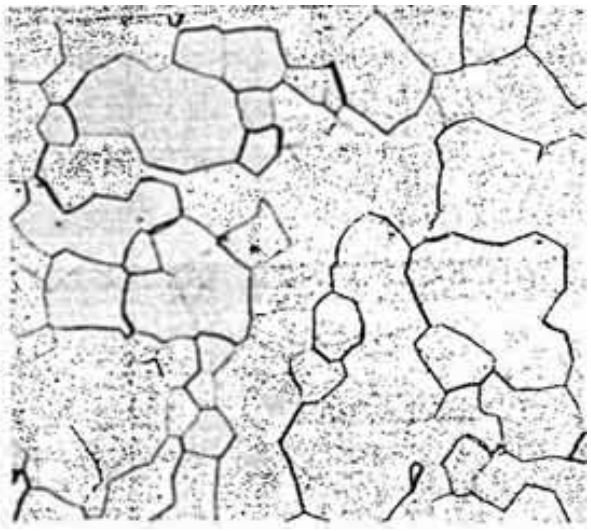

Figure 2.9. Titanium after annealing at 800°C (100x) [13]

The decomposition of beta phase in Ti alloys can take place by martensitic transformations and this frequently happens in the alpha–beta alloys. The beta to martensitic transition is responsible for an acicular (plate like) structure in quenched and/or quenched and aged Ti alloys. In Figure 2.10, the acicular structure of Ti–6Al–4V can be seen (slow cooling). The white plates are alpha and the dark regions between them are beta. This is a typical Widmanstätten structure [13].

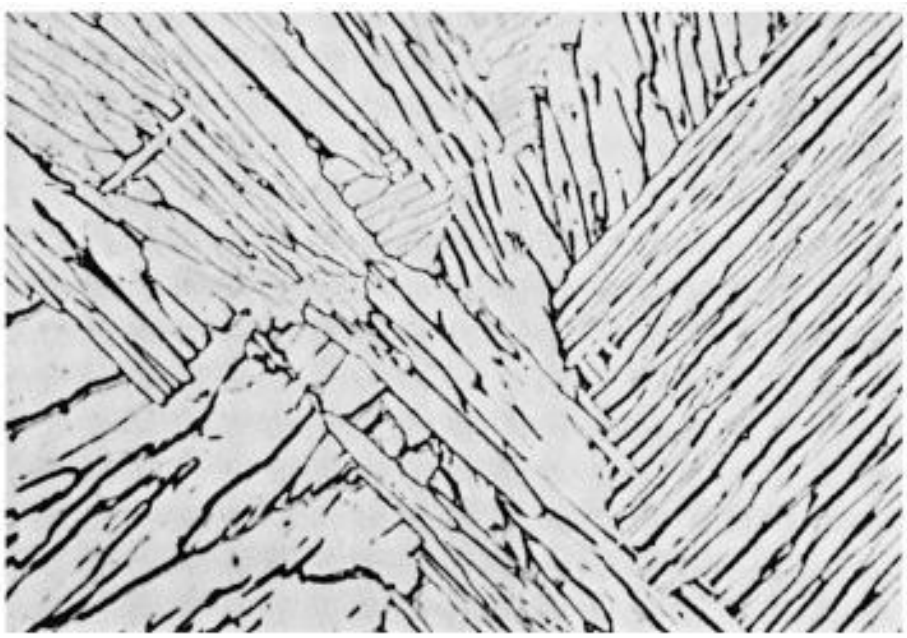

Figure 2.10. Microstructure of Ti–6Al–4V (500x) [13]

Schematic of the development of a Widmanstätten structure in Ti–6Al–4V is illustrated in Figure 2.11.

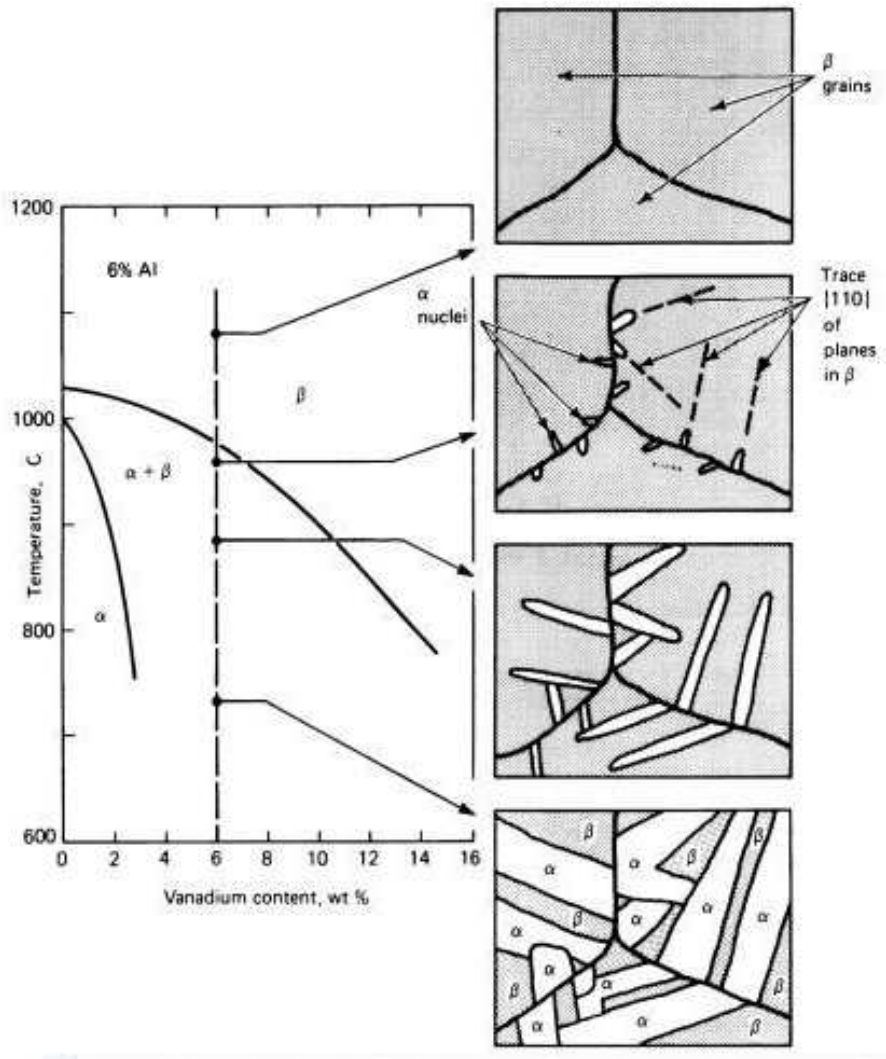

Figure 2.11. Schematic of the development of a Widmanstätten structure in Ti–6Al–4V [13]

There are some studies that involve microstructure of Ti and its alloys. Iijima *et al.* [14] worked about wear properties of Ti and Ti–6Al–7Nb castings for dental prostheses. The purpose of their study is to evaluate the wear resistance of high-strength Ti–6Al–7Nb alloy castings for dental application. Test specimens were cast from commercially pure titanium (cp Ti grades 2 and 3) and Ti–6Al–7Nb alloy ingots, and subjected to a wear test simulating the occlusal loading pattern.

As shown in Figure 2.12, the microstructure of the Ti–6Al–7Nb alloy exhibits a refined two phase structure consisting of an acicular α phase in prior β grains. In the microstructures of cp Ti grades 2 and 3, α grain boundaries were observed [14].

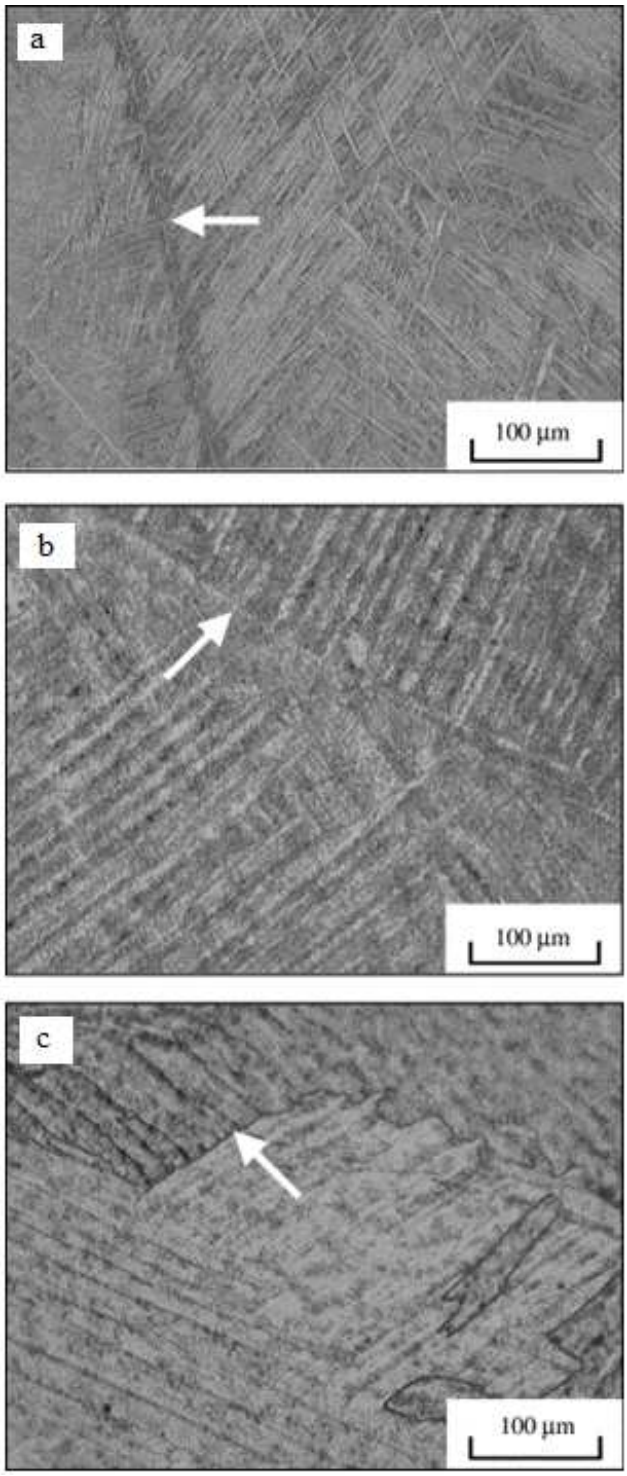

Figure 2.12. Microstructures observed by an optical microscope of castings a) Ti–6Al–7Nb alloy b) CP Ti grade 2 c) CP Ti grade 3 [14]

Ho *et al.* [15] searched about structure and properties of cast binary Ti – Mo alloys. Light micrographs of cp Ti and Ti–Mo alloys are illustrated in Figure 2.13.

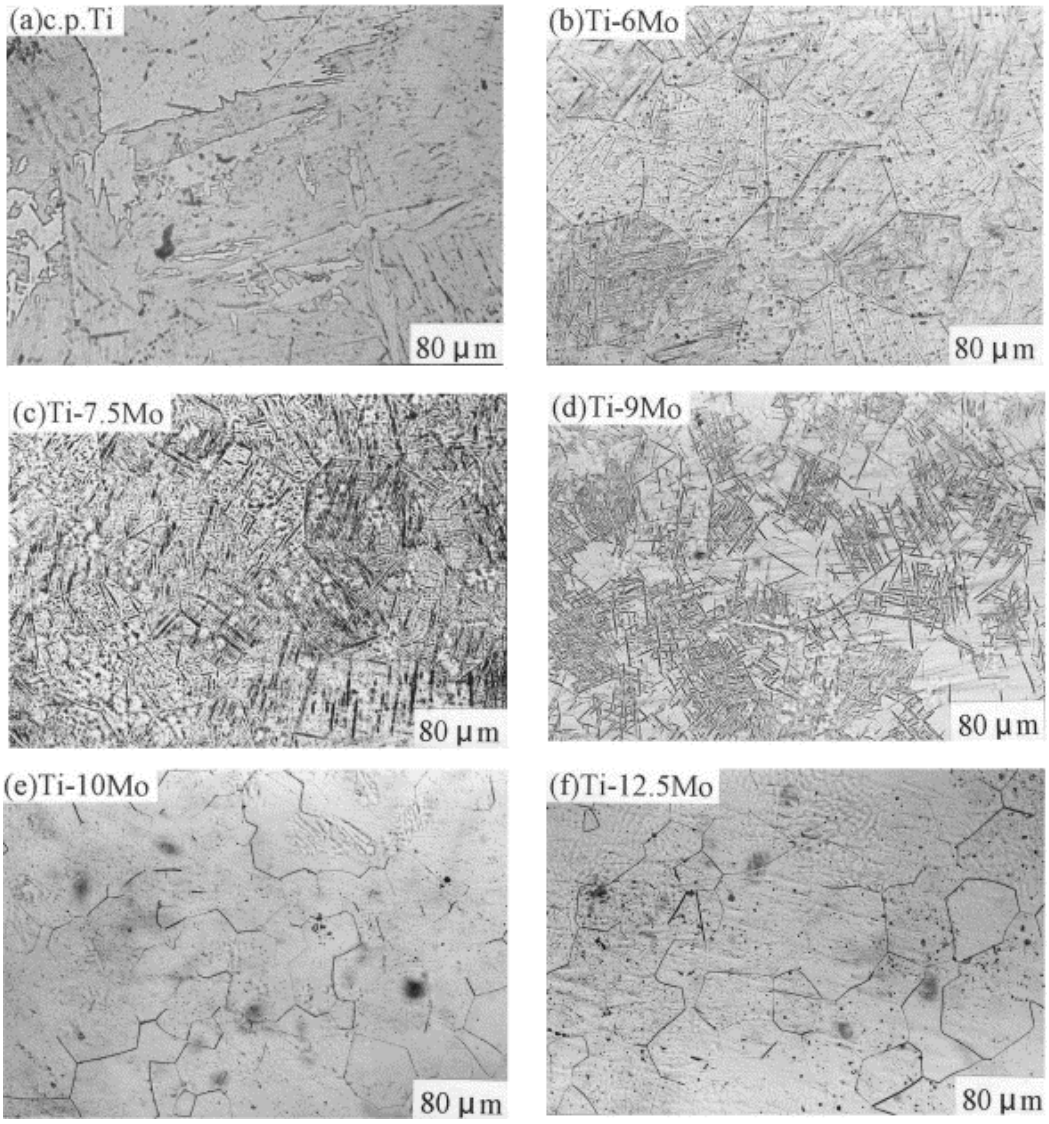

Figure 2.13. Light micrographs of cp Ti and Ti – Mo alloys [15]

The hex cp Ti exhibited a typical rapidly cooled metastable feather like microstructure. When Mo content was 6 weight per cent, the fine, acicular martensitic structure of α″ phase was observed. When Mo content was 7.5 weight per cent, the entire alloy was dominated by the martensitic α″ structure. When the Mo content increased to 9 weight per cent, a significant amount of equiaxed, retained β phase was observed. When the alloy contained 10 weight per cent or more Mo, β phase became the only dominant phase [15].

2.1.4. Processes for Titanium

2.1.4.1. The Hunter Process. The first meaningful extraction of metallic Ti was in 1910 by Hunter who reduced titanium chloride ($TiCl_4$) with sodium at temperatures between 700°C and 800°C. This formed the basis of the Hunter Process. Hunter Process involves the chlorination of rutile (TiO_2) in the presence of coke or other form of carbon. Hunter heated $TiCl_4$ with sodium metal under great pressure in a sealed container called a steel bomb. The result was 99.8 per cent pure Ti. The Hunter Process was successfully used for many years, but the Kroll Process eventually became dominant.

$$TiO_2\,(s) + 2Cl_2\,(g) + C\,(s) \rightarrow TiCl_4\,(l) + CO_2\,(g) \qquad (2.1)$$

$$TiCl_4\,(l) + 4Na\,(l) \rightarrow 4NaCl\,(l) + Ti\,(s)\ [13, 16, 17, 18] \qquad (2.2)$$

2.1.4.2. The Kroll Process. The Kroll process is a pyrometallurgical industrial process used to produce metallic Ti. It was invented in 1940 by William J. Kroll in Luxembourg. After moving to the United States, Kroll further developed the method in 1945 for the extraction of zirconium. The Kroll process replaced the Hunter process for almost all commercial production.

First, titanium dioxide is "carbochlorinated" to produce titanium tetrachloride ($TiCl_4$). The most pure ore of Ti, rutile, is combined with petroleum coke and chlorinated in a fluid bed reactor at 1000°C. Then chlorine gas is passed through the charge making $TiCl_4$, also known as 'tickle'. The resulting condensate liquid of $TiCl_4$ is purified by continuous fractional distillation until it is pure. The recovered chloride is reprocessed and fed back into the system.

Next, $TiCl_4$ is reduced with magnesium and is heated. The reaction is an example of a metal displacement reaction. The reaction is carried out in an argon atmosphere to prevent magnesium or sodium from reacting with oxygen in the air. After several days reaction stops, the pressure rises, and the spongy Ti is crushed and melted into an ingot.

$$2Mg\,(l) + TiCl_4\,(l) \rightarrow 2MgCl_2\,(l) + Ti\,(s) \qquad (2.3)$$

The resulting porous metallic Ti sponge, impurities, and unreacted magnesium are purified by leaching or heated vacuum distillation. The sponge is jackhammered out, crushed and pressed before it is melted in a consumable electrode vacuum arc furnace. It is often remelted to remove inclusions and ensure uniformity [11, 19, 20].

2.1.4.3. The Armstrong (International Titanium Powder) Process. A new method for producing low cost Ti powder is the Armstrong Process. This process produces Ti by the reduction of $TiCl_4$ with sodium, as does the Hunter process. However, International Titanium Powder (ITP) has devised a nearly continuous process in contrast to the batch mode of Hunter. The process, which reduces $TiCl_4$ vapor in a molten stream of sodium to produce pure Ti and NaCl, can also be used to in-situ manufacture Ti–6Al–4V alloy powder. Armstrong Process Ti and Ti–6Al–4V powders were used to produce plate by vacuum hot pressing. Also, thin gage sheet was produced by cold rolling solid-phase sintered Ti and Ti–6Al–4V powder compacts [21, 22]. Figure 2.14 shows the basic Armstrong Process.

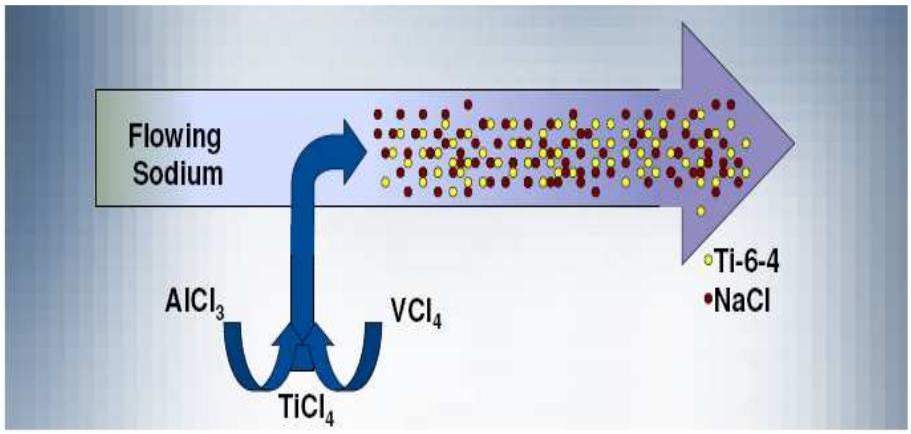

Figure 2.14. The Basic Armstrong Process [23]

2.1.4.4. FFC – Cambridge Process. This process was developed at Cambridge University by D. Fray, G. Z. Chen and T. Farthing and has been licensed to British Titanium. It is illustrated schematically in Figures 2.15. and 2.16 respectively. In this process, solid TiO_2 is immersed in a molten CaCl electrolyte. A TiO_2 powder is formed by conventional ceramic processing into a rectangular sintered cathode incorporating a conducting wire. This cathode is then immersed in the electrolyte with a graphite anode. Continued

electrolysis removes oxygen from the cathode, where it dissolves in the electrolyte and is then removed as O_2, CO or CO_2 at the anode. Simultaneous reduction of several oxides has reportedly allowed production of Ti–6Al–4V alloy [21].

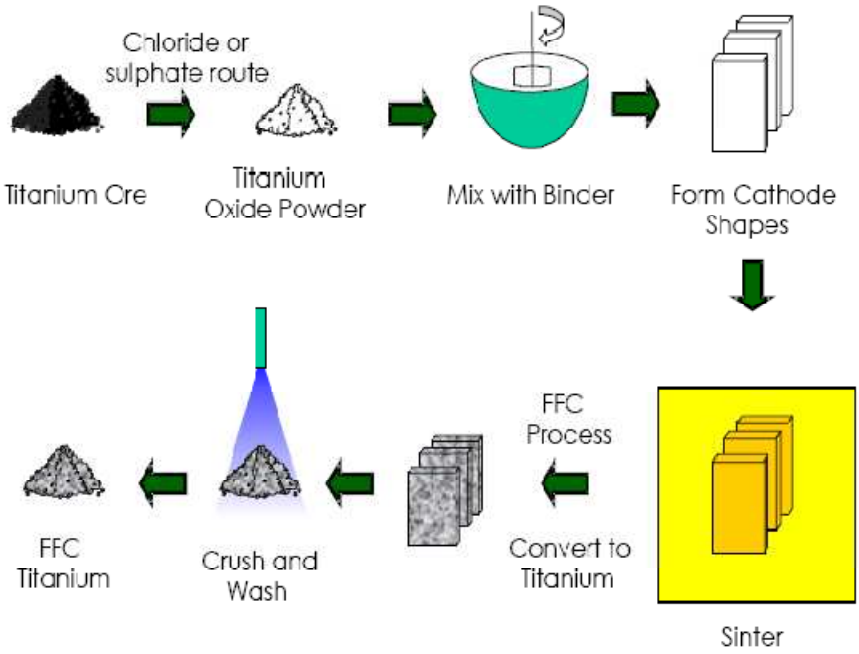

Figure 2.15. Schematic description of the FFC – Cambridge Process [21]

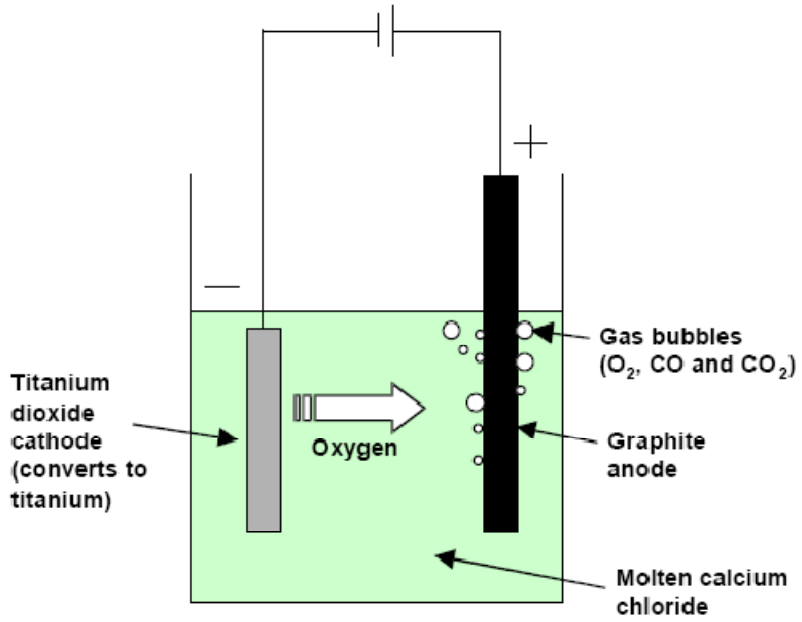

Figure 2.16. Schematic description of the FFC – Cambridge Process Reduction Step [21]

2.1.5. Titanium Manufacturing

The Ti manufacturing consists of five processes:

- Chlorination
- Reduction/vacuum distillation
- Electrolysis
- Crushing, sizing and packing
- Melting

2.1.5.1. Chlorination. First of all, the Ti ore (natural rutile, synthetic rutile, and Ti slag) together with coke as a reducing agent are put in a chlorination reactor. TiO_2 reacts with chlorine gas at high temperatures (1000°C to 1100°C). This reaction separates the oxygen from the Ti, which then bonds with the chlorine, producing dark brown crude titanium tetrachloride. Then, it is purified by continuous distillation to obtain refined titanium tetrachloride with purity of at least 99.9 per cent (colorless and transparent) [24].

$$TiO_2 + C + 2Cl_2 \rightarrow TiCl_4 + CO_2 \quad (2.4)$$

$$(TiO_2 + 2C + 2Cl_2 \rightarrow TiCl_4 + 2CO) \quad (2.5)$$

2.1.5.2. Reduction/Vacuum Distillation. Pure $TiCl_4$ is reacted in a stainless steel reactor with magnesium metal heated to 900°C. $TiCl_4$ is reduced by using magnesium. After the reaction has completed, the magnesium chloride and magnesium included in the lump of Ti are eliminated by high temperature vacuum extraction (vacuum separation process), to leave the Ti. This is mainly the Kroll Process [24].

$$TiCl_4 + 2Mg \rightarrow Ti + 2MgCl_2 \text{ (reduction using magnesium)} \quad (2.6)$$

2.1.5.3. Electrolysis. The magnesium chloride is subjected to electrolysis to decompose it into chlorine and magnesium. The chlorine is returned to the chlorination and purification process. The magnesium is returned to the reduction and vacuum separation process for re-use [24].

$$MgCl_2 \rightarrow Mg + Cl_2 \qquad \text{(electrolysis)} \qquad (2.7)$$

2.1.5.4. Crushing, Sizing and Packing. After reduction and separation, the Ti sponge is crushed by first shearing into large lumps. Then it is divided into smaller pieces using shears and crushers. The pieces are mixed together in a blender to produce a uniform quality. After the Ti sponge has been adjusted into the required particle size and quality, it passes through strict quality control checks before shipment [24].

2.1.5.5. Melting. Pure Ti or Ti alloy ingots are made by melting Ti sponge, with the addition of the alloying elements in the case of Ti alloys. Since Ti reacts readily with oxygen, nitrogen and carbon, the melting process is performed in a vacuum or inert atmosphere. Water cooled copper is used for the crucible. Methods that can be used to melt the Ti are consumable electrode vacuum arc, electron beam and plasma arc. Consumable electrode vacuum arc method is the most widely used method.

The manufacture of Ti ingots starts by forming the Ti sponge and Ti scrap into compacts using a press. These are joined together by plasma arc welding to make the consumable electrode, which goes through an arc melting in a vacuum or inert atmosphere to become the first melt ingot. The melting process starts with an arc forming between the electrode and the crucible. As the electrode melts, the metal runs down and is cooled in the crucible, forming the first melt ingot. The first melt ingots are used as electrodes and melted once more to ensure even quality. After quality control checks, the second melt ingots produced are shipped as a final product [24]. Figure 2.17 shows Ti final product, ingot.

Figure 2.17. Titanium ingot [25]

There is a method of producing a Ti material having enhanced resistance to hydrogen absorption in an aqueous hydrogen sulfide solution, comprising the steps of:

- subjecting a Ti material to cold working with the use of a working oil, with the degree of the cold working being 10 per cent or more of the total cold reduction to produce a cold-worked Ti material
- heat treating the cold worked Ti material at a temperature of from 300°C to 850°C in vacuum or in an inert gas atmosphere to produce a Ti material with a layer of at least one of titanium nitride, titanium carbide and titanium carbonitride formed on the surface
- removing said surface layer to a depth of at least 0.5 µm so that titanium nitride, titanium carbide and titanium carbonitride formed on the Ti material surface is at least partly removed, thereby imparting enhanced resistance to hydrogen absorption in aqueous hydrogen sulfide solutions to said Ti material [26].

2.1.6. Titanium Applications

There are two classical application areas for Ti alloys: airframes and aero engines. In modern aero engines, the weight share of Ti is about 25 per cent being applied mainly in the fan and compressor sections for disks and blades which operate at temperatures up to about 500°C.

In a recent engine, the GE–90 aero engine (Figure 2.18) used for the Boeing 777 aircraft, the large fan blades usually made from Ti–6Al–4V were replaced by polymer composite blades. But, as can be seen from Figure 2.18, still a large number of Ti parts are used in that engine. The most recent advance in the area of blisk (bladed disk) technology has been made by MTU (Daimler Chrysler) by using linear friction welding to attach the blades to the disk. This allows more efficient material utilization making these blisks attractive economically. Linear friction welding also can be used to replace individual airfoils on the blisks as required to repair in–service damage [9].

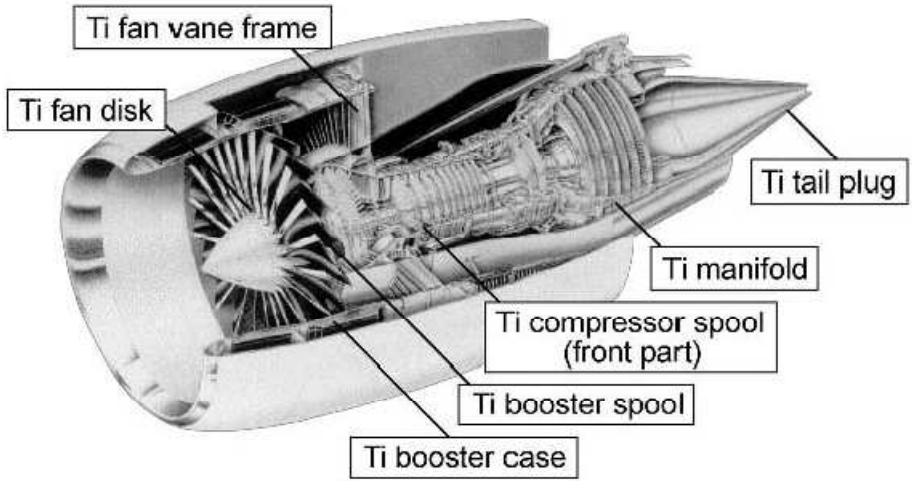

Figure 2.18. Titanium usage in the GE–90 aero engine [9]

In the traditional areas of chemical and power industries using Ti mainly as corrosion resistant material, the usage of Ti in offshore structures has become more common in recent years. One example is shown in Figure 2.19 using Ti as drilling riser string. Because of the requirements for high strength and high fatigue resistance, the Ti–6Al–4V alloy has to be used instead of cp Ti [9].

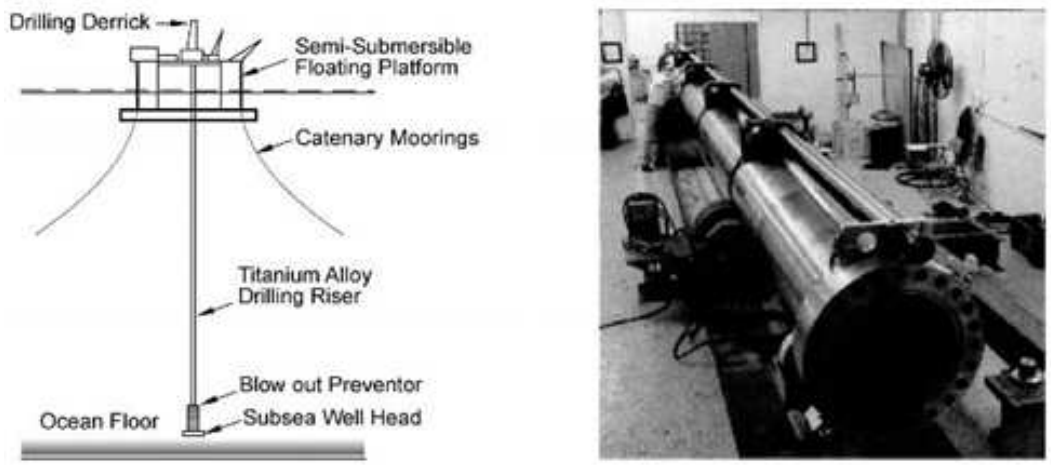

Figure 2.19. Titanium alloy drilling riser a) schematically b) riser string joint [9]

Besides the areas mentioned above, building applications such as exterior walls and roofing material have emerged as a new market for Ti. Using cp Ti as building material has become especially popular in Japan. One example is the Fukuoka Dome (Figure 2.20), built in 1993, which is covered with Ti roofing, retractable for multi-role and all-weather purposes. Each of these building projects uses large quantities of cp Ti leading to the increased usage in the civil engineering area in Japan [9].

Figure 2.20. Fukuoka Dome with retractable titanium roof [9]

Another new area in which Ti use is growing is the area of consumer products, such as spectacle frames, cameras, watches, jewelry and various kinds of sporting goods. The largest application in the area of sporting goods is golf club heads. Other examples are tennis rackets, bicycle frames, etc.

The benefits of Ti golf club heads have been widely publicized and in 1997 about 4500 metric tons of Ti–6Al–4V was used in cast driver heads, such as the ones shown in Figure 2.21. The high strength and the low density of Ti allow a larger club head to be used, which creates a larger area for striking the ball properly while retaining the club head speed [9].

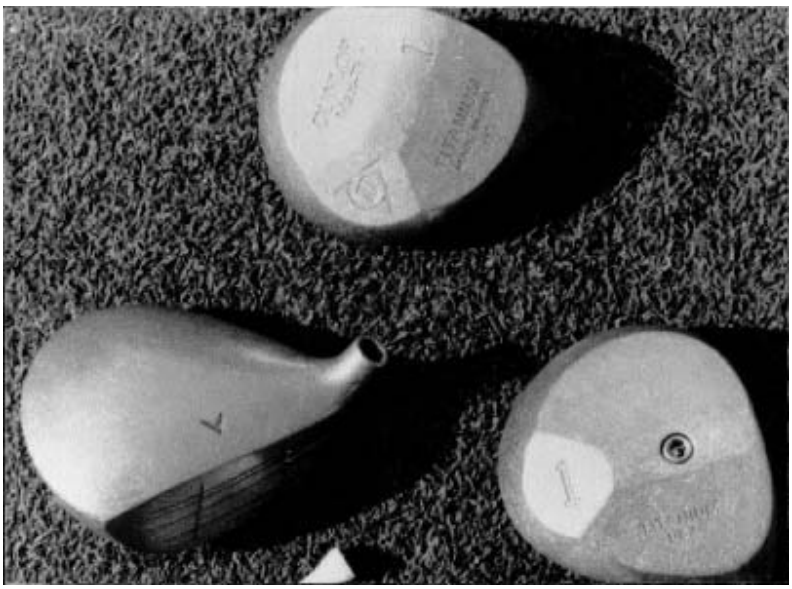

Figure 2.21. Investment cast Ti–6Al–4V golf club heads [9]

Another area to be mentioned in this introduction chapter is the application of Ti in mass produced automobiles. This area also is extremely challenging because of cost sensitivity. Potential parts have been identified, for example valves, valve springs, and connecting rods in the engine area, and suspension springs, bolts, fasteners, and the exhaust system in the car body area. For many years, Ti has been used in high performance vehicles such as Formula One racing cars or off-road racing trucks, but for an application in a family automobile the problem of producing low–cost Ti parts has to be solved. In this context, the cost includes both the raw material and the part fabrication. Successful

introduction of Ti in family automobiles will depend on a significant reduction in one or both of these cost elements [9].

The main usage of Ti is in biomedical field. Commercial pure Ti, Ti–6Al–4V and Ti–6Al–4V ELI are still widely used as representative Ti alloys for implant materials. More recently, V free α + β type alloys such as Ti–6Al–7Nb and Ti–5Al–2.5Fe have appeared as implant materials. In addition, V and Al free α + β type alloys composed of non-toxic elements like Ti–15Sn–4Nb–2Ta–0.2Pd and Ti–15Zr–4Nb–4Ta–0.2Pd have been developed.

Low modulus alloys are nowadays desired because the moduli of alloys are required to be much more similar to that of bone. The β type alloys have been, therefore, developed or are developing. They are composed of nontoxic elements like Nb, Ta, Zr etc. [27].

Table 2.3 shows cp Ti composition according to ISO 5832–2 / ASTM F67 and Ti6Al4V according to ISO 5832–3 and ASTM F136.

Table 2.3. Titanium composition [28]

	Fe max	C max	N max	O max	H max	Al max	V max
Grade 1	0.20	0.08	0.05	0.12	0.01	—	—
Grade 2	0.25	0.08	0.05	0.18	0.01	—	—
Grade 3	0.30	0.10	0.05	0.25	0.01	—	—
Grade 4	0.35	0.10	0.05	0.35	0.01	—	—
Ti6Al4V	< 0.25	< 0.08	< 0.05	< 0.13	< 0.012	5.5–6.5	3.5–4.5

Ti is now extensively accepted by medical professions as the metal of choice for prosthetics, internal fixation, inner body devices etc. Ti usage in body is shown in Figure 2.22 [29].

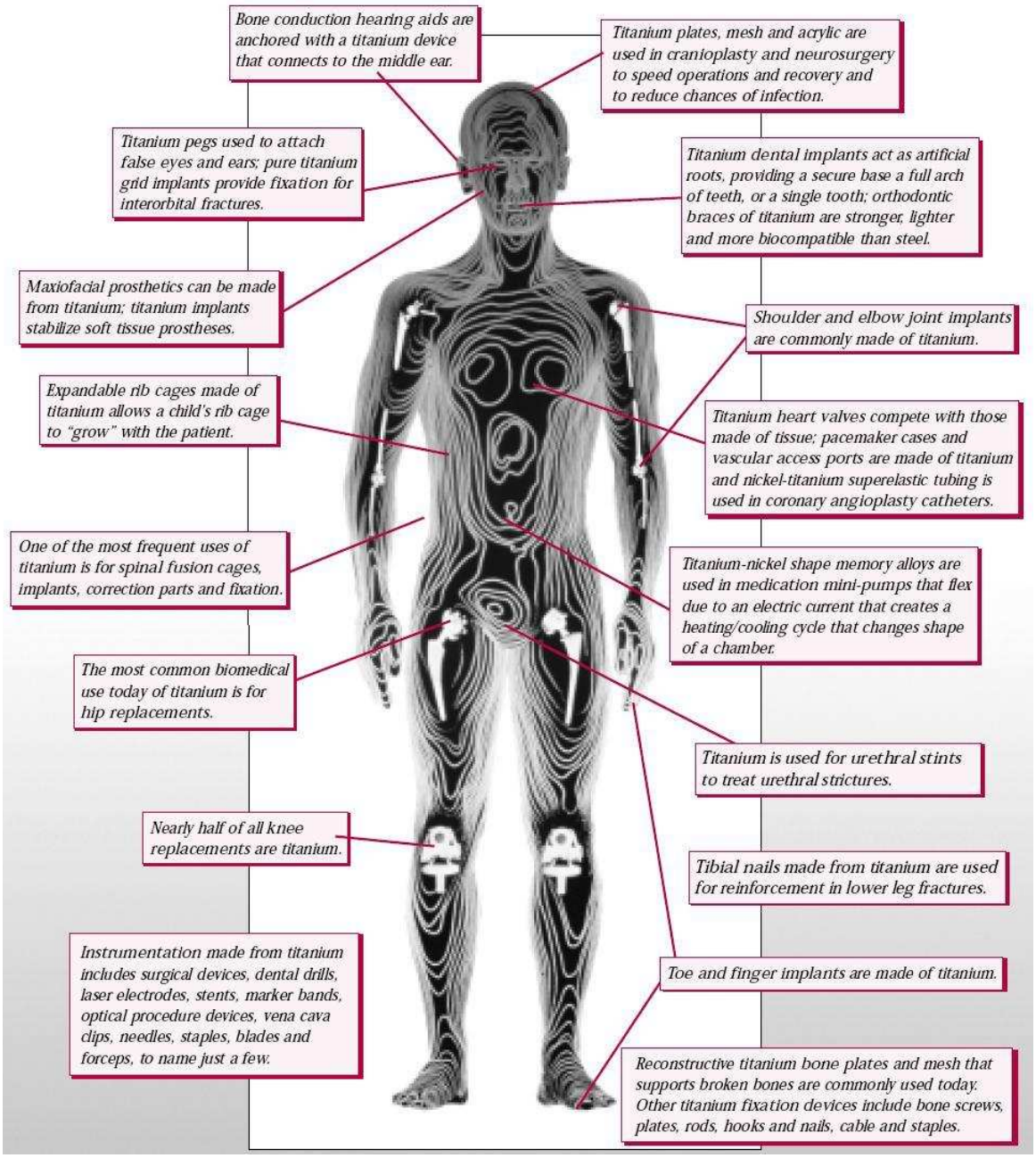

Figure 2.22. Titanium usage in body [29]

A Ti alloy hip is shown in Figure 2.23.

Figure 2.23. Titanium alloy hip [30]

2.1.7. Biocompatibility of Titanium

Biocompatibility can be defined as the ability of a material to perform with an appropriate host response in a specific application or the quality of not having toxic or injurious effects on biological systems. Osseointegration is the contact between the metallic implant and the living tissues. This contact is made through the oxide layer on the implant surface. The good corrosion resistance is due to this oxide layer. Ti is biocompatible, so osseointegration is seen between dental implant and the body. There are some studies about the biocompatibility of Ti [31, 32, 33].

Biocompatibility of lotus–type stainless steel and Ti in alveolar bone is studied by Higuchi *et al.* [34]. Their paper was about the biocompatibility of lotus–type porous stainless steel and Ti in alveolar bone in order to investigate the possibility of an implant by animal experiments.

As shown in Figure 2.24, lotus–type porous stainless steel and porous Ti of the specified pore size and porosity were fabricated by continuous zone melting technique. The metals were melted by high frequency induction heating and solidified by unidirectional solidification. During solidification from liquid phase to solid phase, gas phase separation evolves gas bubbles which grow in one direction [34].

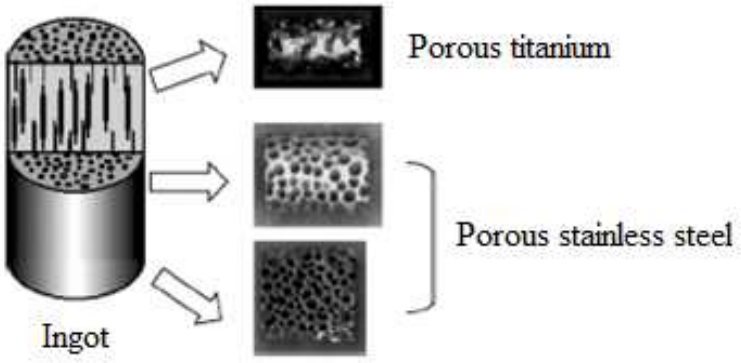

Figure 2.24. Production of lotus–type porous metals used for animal experiments [34]

The porous metals which were cut into 5 mm cubes (non–dehydrogenated) and 3.4 mmΦ × 5 mm cylinders (dehydrogenated) were implanted into the canine mandible alveolar bone for two, four and eight weeks for animal experiments. The changes in the tissues were observed using SEM.

For porous stainless steel, new formation of bones was observed around the sample in two weeks without any sign of bone ingrowth into the pores. The osteogenesis (growth of bone) was found in shallow areas in the pores in four weeks and deep in the pores in eight weeks. Porous Ti, on the other hand, showed deep ingrowth of new bones in four weeks. Osteogenesis for both materials is represented in Figure 2.25 and 2.26 respectively [34].

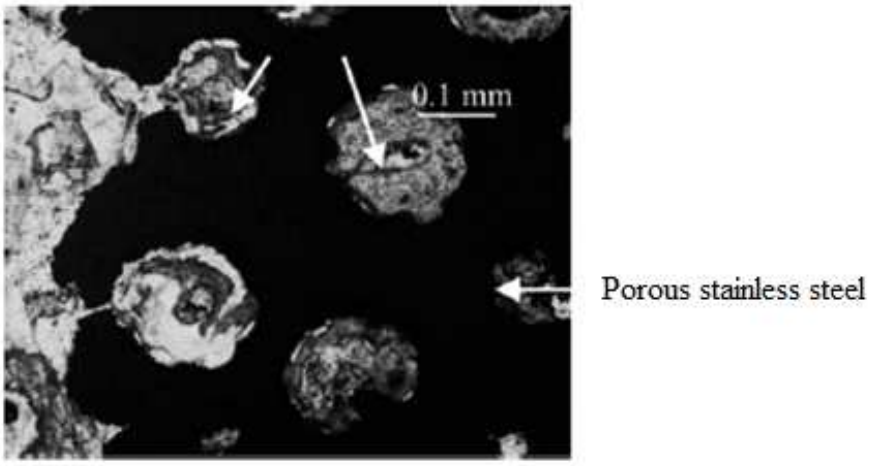

Figure 2.25. Osteogenesis in the porous stainless steel [34]

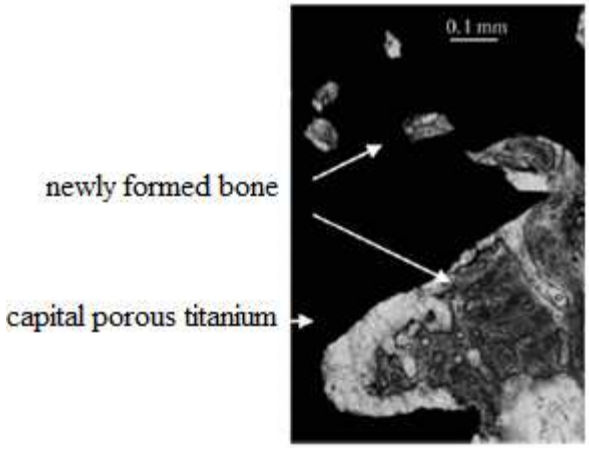

Figure 2.26. Osteogenesis in the porous titanium [34]

In the study of Wulf Braemer, the corrosion behavior of metallic dental materials with saliva in “in vitro” tests and the influence of alloy components on bacteria were discussed.

Metallic dental materials are tested to evaluate their corrosion behavior according to ISO/DIS 10271. Figure 2.27 shows a type of corrosion test method called static immersion test. In “static immersion test”, cast alloy samples should have a total surface area of at least 10 cm^2. The casting skin has to be removed with fresh abrasive paper for each alloy. The surface of the sample is cleaned ultrasonically for 2 minutes in ethanol or methanol and rinsed with distilled water. Each sample is placed in a separate glass container without touching the glass surface.

In solution preparation, 10.01 g lactic acid (90 per cent) $C_3H_6O_3$ and 5.845 g NaCl is dissolved in approximately 300 ml H_2O. Then, it is diluted to 1000 ml with H_2O: the pH value should be 2.3 ± 0.1. To prevent evaporation, the container has to be closed. The induction period is 7 days ± 1 hour at 37 ± 1°C.

Generally alloys in the cast conditions are tested. The cast objects are heat treated at the ceramic firing temperature of 900°C. The outer sheet of oxide is removed mechanically, simulating the polishing process of the dental technician. After polishing, the surface of the sample has a metallic brightness. Electroplated gold is deposited on a

smooth metallic object of 10 cm^2. The gold sheet is removed from the base material and can be used analogously to cast alloys in the corrosion test [35].

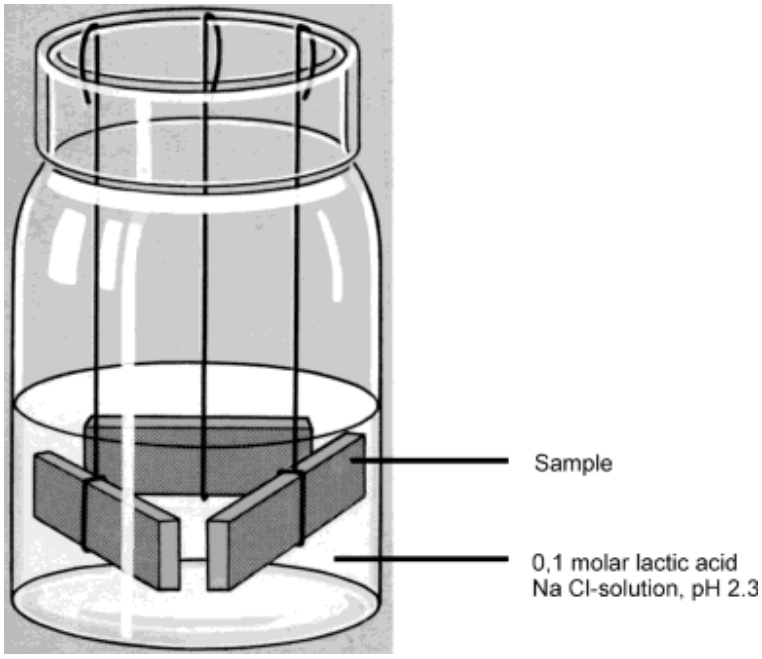

Figure 2.27. Static immersion test [35]

In vitro test samples are cast plates of Au Ag Cu and Au Pd Ag based alloys with 10 mm diameter and 1.5 mm thickness. The surface is ground with ceramic stones and sandblasted. By interaction with artificial saliva (ISO/DIS 10271), the natural conditions in the mouth are simulated. The samples are immersed in this solution for 30, 60, and 120 minutes. A modified “Agar diffusion test” is the basis of the bacteriological investigations. L. casei and S. mutans are test bacterias. After treatment in an autoclave, 8 ml of the relevant bacterial culture is pipetted onto the growth–sheet (Figure 2.28). The culture is incubated for 48 hours under anaerobic conditions at 37°C, then the zone of growth inhibition is measured [35].

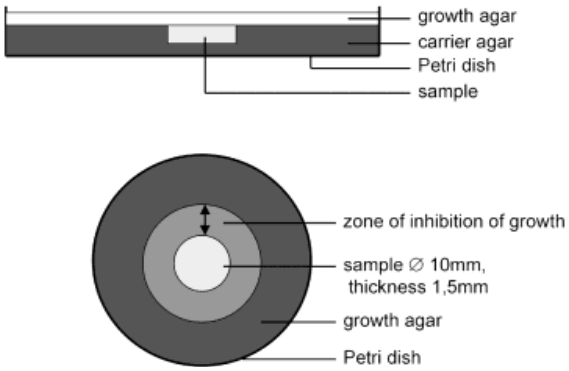

Figure 2.28. Testing of antibacterial effects of alloys [35]

The study showed that high gold dental alloys, Co Cr Mo alloys, and Ti have suitable corrosion behavior. The allergic potential of dental alloys should be considered and Ni containing alloys should be avoided. The alloying of indium and gallium with Co Cr Mo and Ni or Fe based alloys should be avoided. After all comparisons, he said that Grade 2 Ti is the best material for dental implants [35].

Kurt studied about finding the microstructure and surface topography of cast Ti as a dental material. In this study, experiments about the physical, chemical and mechanical properties of Ti and Ti casting technology were performed. Surface roughness with respect to different grinding levels, wear and general corrosion resistance of Ti in artificial saliva solution were tested. Vickers hardness values of dental materials were compared. Microstructure of cast Ti and other dental materials were investigated.

In the experiments, it was found that Ti had a problem about oxidation for casting, so it would be melted under high vacuum. The melt would also react with the crucible and mold material. The most important limitation was the time period that Ti was in contact with the crucible. Another problem which was internal porosity and it was solved by increasing the pressure of argon gas.

Ti and Co–Cr alloy were compared (microstructure). It was found that the cast Co–Cr had so much porosity. But Co–Cr alloys are cheaper than pure Ti and Ti alloys. However, Co reacts with the oral mucosa and causes allergic reactions. Ti has no toxic or allergic reactions and is the only metal that is not rejected by the human body [2].

As seen, biocompatibility of Ti was proved in many experiments and it is the material of choice for oral applications.

2.1.8. Heat Treatment of Titanium

Ti and its alloys are heat treated in order to:

- Reduce residual stresses developed during fabrication (stress relieving)
- Produce an optimum combination of ductility, machinability and dimensional and structural stability (annealing)
- Increase strength (solution treating and aging)
- Optimize special properties such as fracture toughness, fatigue strength, and high-temperature creep strength

The response of Ti and Ti alloys to heat treatment depends on the composition of the metal and the effects of alloying elements on the α–β crystal transformation of Ti. In addition, not all heat treating cycles are applicable to all Ti alloys, because the various alloys are designed for different purposes [13].

Oxygen and iron levels have significant effects on mechanical properties after heat treatment. It should be realized that:

- Oxygen and iron must be near specified maximums to meet strength levels in certain commercially pure grades
- Oxygen must be near a specified maximum to meet strength levels in solution treated and aged Ti–6Al–4V
- Oxygen levels must be kept as low as possible to optimize fracture toughness. However, the oxygen level must be high enough to meet tensile strength requirements
- Iron content must be kept as low as possible to optimize creep and stress–rupture properties. Most creep resistant alloys require iron levels at or below 0.05 weight per cent [13]

2.1.8.1. Stress Relieving. Ti and Ti alloys can be stress relieved without adversely affecting strength or ductility. Stress relieving treatments decrease the undesirable residual stresses that result from first, nonuniform hot forging or deformation from cold forming and straightening, second, asymmetric machining of plate or forgings and third, welding and cooling of castings. The removal of such stresses helps maintain shape stability and eliminates unfavorable conditions, such as the loss of compressive yield strength commonly known as the Bauschinger effect.

When symmetrical shapes are machined in the annealed condition using moderate cuts and uniform stock removal, stress relieving may not be required. Compressor disks made of Ti–6Al–4V has been machined satisfactorily in this manner, conforming with dimensional requirements. In contrast, thin rings made of the same alloy could be machined at a higher production rate to more stringent dimensions by stress relieving 2 hours at 540°C (1000°F) between, rough and final machining. Separate stress relieving may be omitted when the manufacturing sequence can be adjusted to use annealing or hardening as the stress-relieving process. For example, forging stresses may be relieved by annealing prior to machining [13].

Selected stress relieving heat treatment values for cp Ti (all grades) is 480 – 595°C and ¼ – 4 hours.

2.1.8.2. Annealing. Common annealing treatments are mill annealing, duplex annealing, recrystallization annealing and beta annealing.

Mill annealing is a general purpose treatment given to all mill products. It is not a full anneal and may leave traces of cold or warm working in the microstructures of heavily worked products, particularly sheet.

Duplex annealing alters the shapes, sizes and distributions of phases to those required for improved creep resistance or fracture toughness. In the duplex anneal of the Corona 5 alloy, for example, the first anneal is near the β transus to globularize the deformed α and to minimize its volume fraction. This is followed by a second, lower temperature anneal to

precipitate new lenticular (acicular) α between the globular α particles. This formation of acicular α is associated with improvements in creep strength and fracture toughness.

Recrystallization annealing and β annealing are used to improve fracture toughness. In recrystallization annealing, the alloy is heated into the upper end of the α–β range, held for a time, and then cooled very slowly. In recent years, recrystallization annealing has replaced β annealing for fracture critical airframe components.

Beta annealing is done at temperatures above the β transus of the alloy being annealed. To prevent excessive grain growth, the temperature for β annealing should be only slightly higher than the β transus. Annealing times are dependent on section thickness and should be sufficient for complete transformation. Time at temperature after transformation should be held to a minimum to control β grain growth. Larger sections should be fan cooled or water quenched to prevent the formation of a phase at the β grain boundaries [13].

Selected annealing treatment values for cp Ti (all grades) are 650 – 160°C and 0.1 – 2 hours. Cooling method is air cooling.

2.1.8.3. Solution Treating and Aging. A wide range of strength levels can be obtained in α–β or β alloys by solution treating and aging. With the exception of the unique Ti–2.5Cu alloy (which relies on strengthening from the classic age hardening reaction of Ti_2Cu precipitation similar to the formation of Guinier – Preston zones in aluminum alloys), the origin of heat treating responses of titanium alloys lies in the instability of the high temperature β phase at lower temperatures.

β alloys are normally obtained from producers in the solution treated condition. If reheating is required, soak times should be only as long as necessary to obtain complete solutioning. Solution treating temperatures for β alloys are above the β transus; because no second phase is present, grain growth can proceed rapidly.

Selection of a solution treatment temperature for α–β alloys is based on the combination of mechanical properties desired after aging. A change in the solution treating

temperature of α–β alloys alters the amounts of β phase and consequently changes the response to aging.

To obtain high strength with adequate ductility, it is necessary to solution treat at a temperature high in the α–β field, normally 25 to 85°C (50 to 150°F) below the β transus of the alloy. If high fracture toughness or improved resistance to stress corrosion is required, β annealing or β solution treating may be desirable. However, heat treating α–β alloys in the β range causes a significant loss in ductility. These alloys are usually solution heat treated below the β transus to obtain an optimum balance of ductility, fracture toughness, creep, and stress rupture properties [13].

2.1.9. Surface Treatment of Titanium

There are four types of surface treatments for Ti:

- Shot Peening
- Laser Shock Processing
- Chemical Milling
- Electrochemical Machining

In this section, most common method, chemical milling, will be explained.

Chemical milling is a common way to selectively remove material from the surface of a component to create an array of features. Chemical removal of material from the surface that has been contaminated by oxygen during processing uses the same chemical reactions, but is usually called pickling by analogy to the terminology used in the steel industry. An example of a compressor casing for an aircraft engine is shown in Figure 2.29 [9].

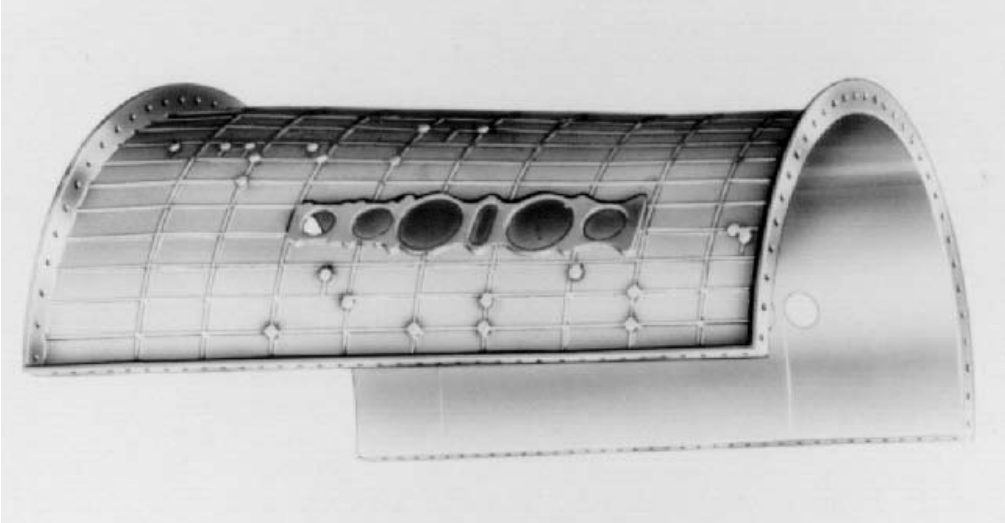

Figure 2.29. Ti–6Al–4V compressor casing (upper half) with features created by chemical milling [9]

Chemical milling is done using a mixture of HF and HNO_3 (generally 1 – 3 volume per cent HF and 10 – 30 volume per cent) acids in aqueous solution (distilled water). The acid concentration and the bath temperature control the rate of material removal. HF removes the surface oxide from titanium, allowing the metal to be dissolved. HNO_3 is an oxidizing acid and repassivates the titanium surface. This allows better control of the rate of metal removal during chemical milling [9].

The metal dissolution reaction is exothermic; consequently, provision for water cooling of the bath must be made for large parts or continuous use. If the rate of metal removal is too high, gas evolution occurs at the metal/bath interface and the gas bubbles can cause uneven material removal. If the HNO_3/HF ratio is not maintained at ≥ 5, and is not controlled, excessive hydrogen liberation occurs and the titanium absorbs hydrogen from the bath during processing. The Ti surface during chemical milling is free of oxide, and hydrogen entry is easy if the hydrogen potential in the bath favors this. The chemical milling reaction depletes HNO_3 and thus the bath chemistry must be monitored and the acid ratio adjusted regularly. Hydrogen pickup during processing is harmful to the properties of the material and must be avoided.

This hydrogen can be removed by vacuum annealing at temperatures of 600ºC or higher and at pressures of 10^{-4} torr or lower. For large parts this creates some obvious

issues regarding vacuum furnace size and availability and component distortion during annealing, but the capability of salvaging large, high value parts contaminated by hydrogen pick up is possible. Better management of bath temperature and composition makes this unnecessary [9].

2.1.10. Microindentation Hardness Test of Titanium

Hardness tests are very useful for materials evaluation, quality control of manufacturing processes and research and development efforts. Hardness, although empirical in nature, can be correlated to tensile strength for many metals, and is an indicator of wear resistance and ductility.

Microindentation tests extend hardness testing to materials too thin or too small for macroindentation tests. This test method covers determination of the microindentation hardness of materials, the verification of microindentation hardness testing machines, and the calibration of standardized test blocks.

Calibration is very important for optimum testing. Calibration is defined as determining the values of the significant parameters by comparison with values indicated by a reference instrument or by a set of reference standards.

In the microindentation tests, indentations are made with Knoop and Vickers indenters are pressed into test specimen surface under an applied force in the range from 9.8×10^{-3} to 9.8 N (1 to 1000 gf) [36]. Vickers hardness is used commonly.

Vickers indenter is a square based pyramidal–shaped diamond indenter with face angles of 136°. Vickers hardness number (HV) is an expression of hardness obtained by dividing the force applied to a Vickers indenter by the surface area of the permanent impression made by the indenter [36]. Figure 2.30 shows Vickers indenter.

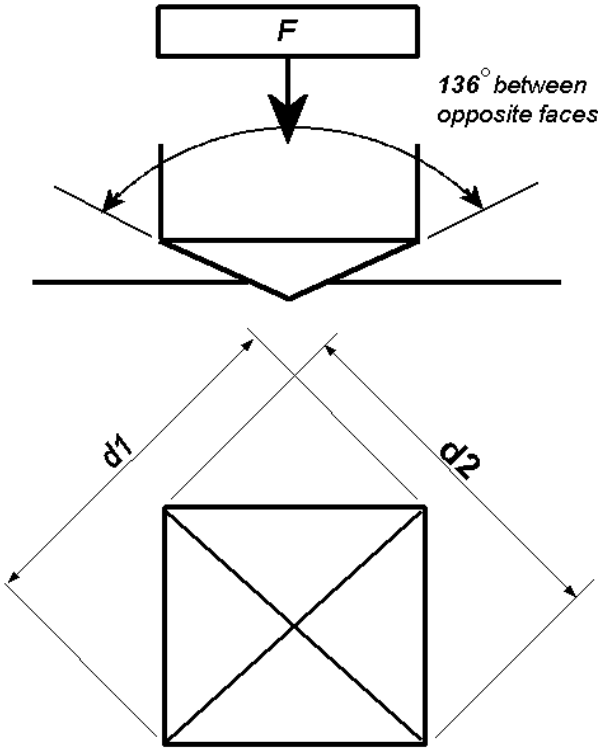

Figure 2.30. Vickers indenter [37]

HV can be found by:

$$HV = 1854,4\frac{P}{d^2} \tag{2.8}$$

where:

P = force, gf

d = mean diagonal length of the indentation, μm [36]

There are some studies about microhardness of Ti and its alloys, also including heat treatments on the material.

Rocha *et al.* [38] made a study about Vickers hardness of cast commercially pure titanium and Ti–6Al–4V alloy submitted to heat treatments. Six mm diameter cylindrical specimens were cast in a Rematitan System. Commercially pure Ti and Ti–6Al–4V alloy specimens were randomly assigned to 3 groups (n=10) that received the following heat

treatments: control (no heat treatment); treatment 1 (T1): heating at 750ºC for 2 hours and treatment 2 (T2): annealing at 955ºC for 1 h and aging at 620ºC for 2 h. After heat treatments, the specimens were embedded in acrylic resin and their surface was ground and polished and hardness was measured.

Table 2.4 shows Vickers hardness means (± SD) for each experimental condition and metal. For cp Ti, VHN means of T2 group was significantly higher than those of the other groups. VHN means of control and T1 groups did not differ statistically to each other. Regarding Ti–6Al–4V alloy, statistically significant difference was observed among the three groups (T2>T1>control) [38].

Table 2.4. Vickers hardness means (± SD) for each experimental condition [38]

Materials	Control	T1	T2
Cp Ti	200,26 ± 5,43	202,23 ± 10,69	259,90 ± 23,26
Ti–6Al–4V	340,51 ± 6,20	351,94 ± 7,85	369,08 ± 10,37

Trillo *et al.* [39] studied about evaluation of mechanical and corrosion biocompatibility of TiTa alloys. As received and heat treated Ti40Ta and Ti50Ta alloys were evaluated to determine their corrosion as well as mechanical performances and compared to Ti–6Al–4V, a common material utilized for orthopedic (surgical) implants.

Four different heat treatments were carried out on all three materials. Set one was heat treated to 1000°C for 1 hour and then water quenched. Set two was carried out at the same temperature and time but furnace cooled. Set three was aged at 400°C for 3 hours and then water quenched. Set four was aged at 400°C for 10 hours and then water quenched. All heat treatments were carried out in an argon atmosphere. Table 2.5 illustrates Vickers microhardness values translated to tensile strength.

Table 2.5. Vickers microhardness values translated to tensile strength [39]

Sample	Vickers	Brinell	TS, ksi/MPa
Ti–6Al–4V – AR	306	287	100/689
Ti40Ta – AR	348	327	114/786
Ti50Ta – AR	320	300	105/724
Ti40Ta – Q	265	256	90/620
Ti50Ta – Q	278	265	93/641
Ti40Ta – FC	370	349	122/841
Ti50Ta – FC	386	365	128/882
Ti40Ta – 3h	394	373	131/903
Ti50Ta – 3h	469	449	156/1075
Ti40Ta – 10h	358	337	118/813
Ti50Ta – 10h	475	452	158/1089

The estimated tensile strengths of these Ti–Ta alloys look quite promising for most of the heat treatment conditions. The quenched samples did not produce an increase in the tensile strengths the furnace cooled samples did. The Ti40Ta increased nearly 7 per cent in estimated strength in the furnace cooled state over the as received state. The Ti50Ta furnace cooled material increased 21.8 per cent from the as received condition. They show an improvement of 22 per cent and 28 per cent in tensile values over the Ti–6Al–4V material. It may be that the α phase is much harder than the martensite phase, which is what predominated at the furnace cooled state. The aging experiments have shown that the enhanced α phase produces higher tensile strengths for all cases when comparing it to the as received and Ti–6Al–4V materials.

The aging experiments produced a change in precipitate morphology to a more elongated a microstructure, which could certainly have affected the hardness. Thus this enhanced a microstructure not only improved the strength of the material but often resulted in better corrosion resistance [39].

A comparison of the hardness of different types of Ti and conventional metal ceramics was studied by King *et al.* This study compared the surface hardness of machine milled Ti and cast Ti and the surface hardness profile of a gold–palladium alloy, a nickel chromium alloy, milled and cast Ti.

For each group, 15 discoid specimens, 10 mm in diameter and 5 mm thick were fabricated by either casting or milling. Five specimens of each group underwent one of three treatments: (1) no heat treatment, (2) a standard heat treatment, or (3) an extended heat treatment. Knoop hardness values were determined.

Results indicated that the Knoop hardness of cast Ti was less than that of the cast Ti standard treatment group, which was less than the Knoop hardness of the cast Ti extended treatment group. Knoop hardness of milled Ti was less than that of the milled Ti standard treatment and milled Ti extended treatment groups. For the surface hardness profile, cast Ti showed a decreasing surface hardness as the distance from the surface of the specimen increased [40].

2.2. Centrifugal Casting

Centrifugal casting is a process where the mould is rotated rapidly about its central axis as the metal poured into it. Because of the centrifugal force, a continuous pressure will be acting on the metal as it solidifies. The melt is thrown out by the centrifugal force under sufficient pressure to assure better die filling. Solidification occurs from outer surface to the inside [6, 41].

2.2.1. Centrifugal Casting Types

2.2.1.1. True Centrifugal Casting. In true centrifugal casting, a permanent mold is rotated about its axis at high speeds as the molten metal is poured. Centrifugal speed can be adjusted from the buttons on the machine. The molten metal is centrifugally thrown towards the inside mold wall, where it solidifies after cooling. The casting is usually a fine grain casting with a very fine grained outer diameter. The casting is resistant to atmospheric corrosion, a typical situation with pipes. The inside diameter has more impurities and inclusions, but it can be machined away. True centrifugal casting process is illustrated in Figure 2.31 and 2.32 respectively [42].

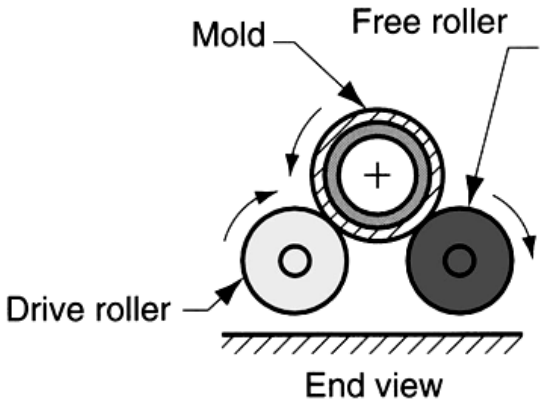

Figure 2.31. End view of true centrifugal casting [43]

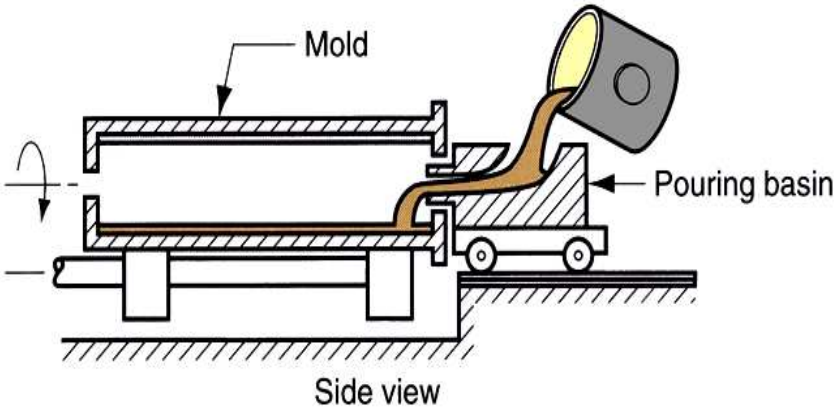

Figure 2.32. Side view of true centrifugal casting [43]

2.2.1.2. Semi–Centrifugal Casting. In semi–centrifugal casting, a central core is used to allow for shapes other than a true cylinder to be produced on the inside surface of the casting. In this method, centrifugal force is used to produce solid castings rather than tubular parts. Density of the metal in the final casting is greater in the outer sections than at the center of rotation. The process is used on parts in which the center of the casting is machined away, such as wheels and pulleys. Figure 2.33 shows semi–centrifugal casting [44, 45].

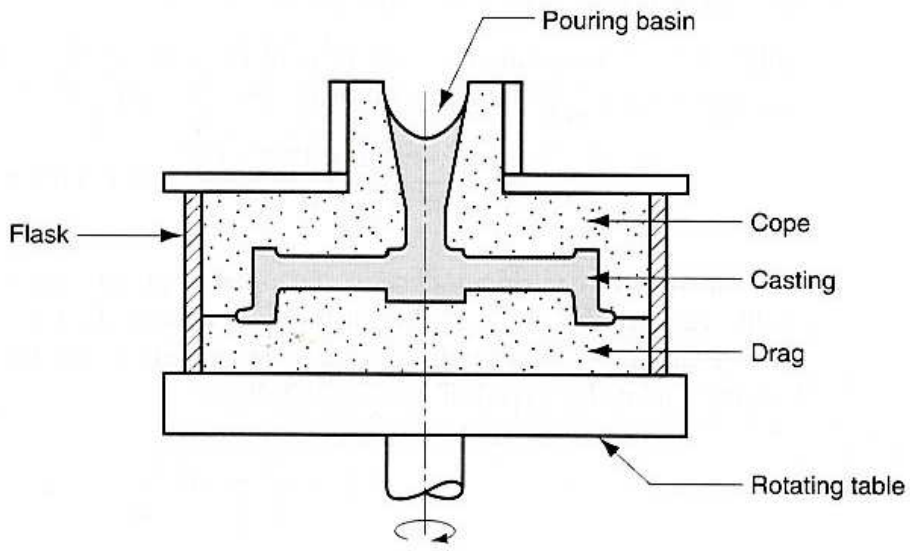

Figure 2.33. Semi–Centrifugal Casting [45]

2.2.1.3. Centrifuging. In the method, the molds are placed a distance from the center of rotation. Thus, when the poured metal reaches the molds, there is a high pressure available to completely fill the cavities. The distance from the axis of rotation can be increased to change the properties. This process is used for production of jewelry and dental bridge work [46, 47]. Figure 2.34 illustrates centrifuging.

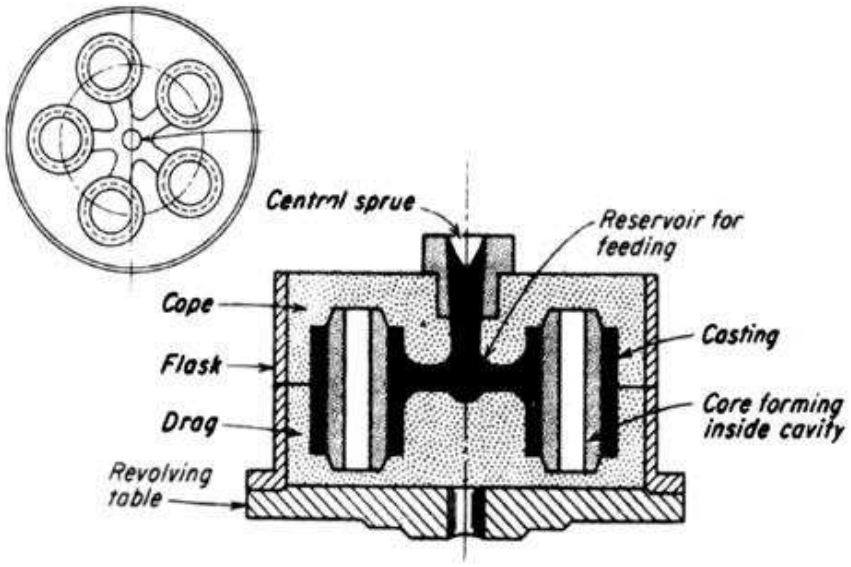

Figure 2.34. Centrifuging [48]

2.2.2. The Advantages of Centrifugal Casting

Wang *et al.* [49] studied about in situ surface composites of (Mg2Si+Si)/ZA27 fabricated by centrifugal casting. In situ composites of Zn–27Al–6.3Mg–3.7Si alloy have been fabricated by centrifugal casting using the heated permanent mold. In situ composites fabricated by centrifugal casting have lots of advantages, because they overcome the interface problem in the artificial composites and have a lot of advantages such as clean interface between reinforced phase and matrix, excellent properties, simple fabrication technology, easiness to control technology parameters, small investment and adaptability to large-scale industry production.

In the study of Chirita *et al.* [50], the mechanical properties advantages of using the vertical centrifugal casting technique were discussed for the production of structural components when compared to traditional gravity casting. A comparison of mechanical properties of specimens obtained by both centrifugal casting technique and gravity casting technique is made.

The material used for castings was an aluminum alloy AS12UN with the following composition: Fe–0.75 per cent, Si–(11.50–13.00) per cent, Zn–0.20 per cent, Mg– (0.75–1.30)per cent, Ni– (0.80–1.30) per cent, Pb–0.10 per cent, Sn–0.05 per cent, Ti–0.20 per cent.

The material was melted at 670ºC and poured into the permanent mould which was preheated at 130ºC. A high frequency induction centrifugal casting furnace (Titancast 700 mP Vac, from Linn High Term, Germany), equipped with a vacuum chamber, was used for melting and casting the samples. A charge of ≈140 grams of material was used in each experiment, which was always performed under vacuum.

For centrifugal casting while the mould was rotating around the central axis of the casting machine, the molten aluminum was poured into the mould cavity. For gravity casting was used the same induction vacuum melting equipment used in centrifugal casting, but in this case the melt was poured into the mould manually. Three tensile specimens from each casting were cut in order to compare the mechanical properties of the

aluminum alloy in different places of the ingot. Rupture strength, rapture strain (per cent) and young modulus results are shown in Figure 2.35, 2.36 and 2.37 respectively.

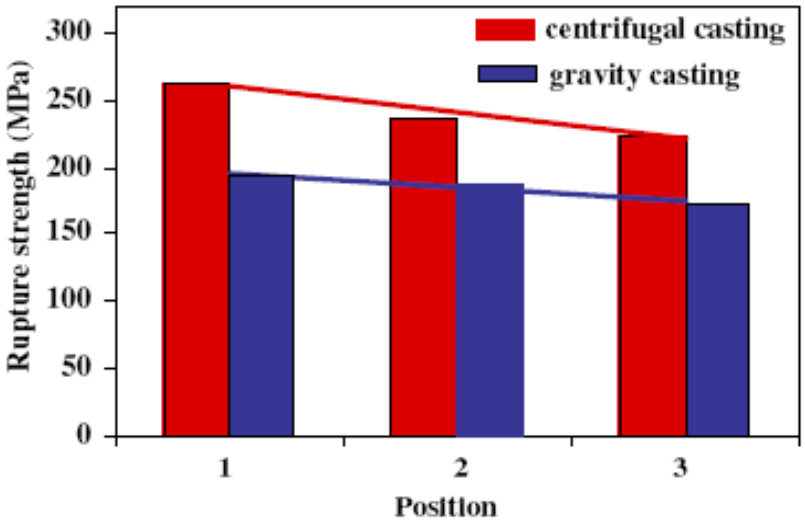

Figure 2.35. Rupture strength results for both centrifugal and gravity castings in different positions of the casting [50]

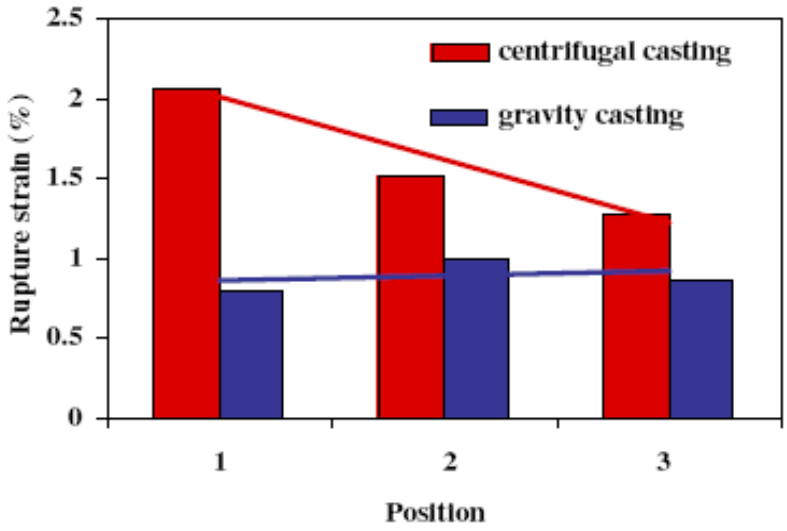

Figure 2.36. Rupture strain results for both centrifugal and gravity castings in different positions of the casting [50]

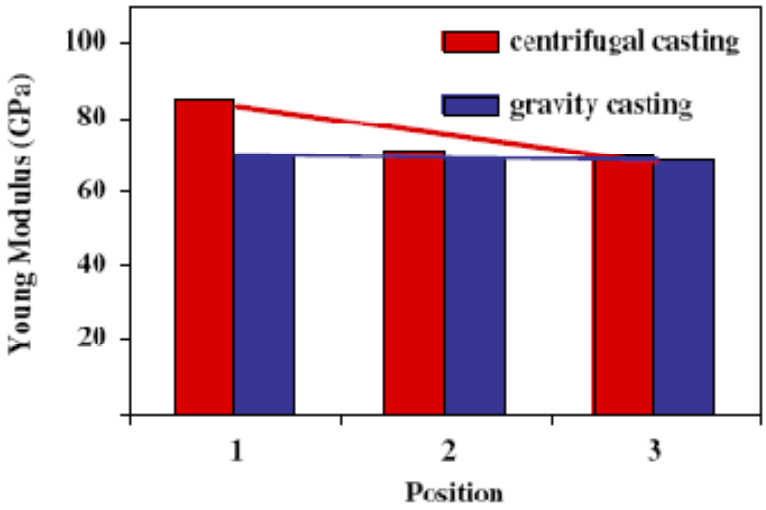

Figure 2.37. Young's modulus results for both centrifugal and gravity castings in different positions of the casting [50]

It is observed that the centrifugal force may increase rupture strength in ≈35 per cent, and rupture strain in about 160 per cent over the gravity casting technique. The Young modulus also increases in about 18 per cent. The fatigue life experiences an increase of about 1.500 per cent and the fatigue limit increases in about 45 per cent. The centrifugal casting process is, therefore, much more effective in terms of obtained mechanical and fatigue properties as compared to gravity casting [50].

The objectives of the study of Watanabe *et al.* [8] were to examine the castability of cp Ti using an ultra high speed centrifugal casting machine and a pressure difference type casting unit and to compare the castability of Ti with conventional dental casting alloys. To determine castability, two types of patterns were used: a commonly used mesh pattern and Meyer's remodeled Asgar Arfaei saucer shaped pattern.

Three metals were used: cp Ti, a commercial ADA Type IV gold alloy (Au 68 per cent; Ag 10 per cent; Pt 4.5 per cent; Pd 3 per cent; Cu 12.5 per cent; other 2 per cent) and a Ni–Cr alloy (Ni 60 ± 76 per cent; Cu, 12 ± 21 per cent; Mo 4±14 per cent; Ti 4 ± 6; Be 52 per cent) [8].

Two types of casting equipment were employed to cast the cp Ti. The first was a commercial centrifugal Ti casting machine. When casting with this machine, a 30 gram cp Ti piece (12 mm high and 30 mm in diameter) was placed on a graphite crucible. A burn out mold was placed close to the periphery of the turntable by weight-balancing it. The chamber was first evacuated to approximately $5x10^{-4}$ torr and high purity argon gas was introduced into the chamber until the pressure level was set at 200 torr (26.3 kPa). This procedure was repeated twice to reduce the amount of residual air. The Ti ingot was then arc-melted (230 A, DC 45 V) over a period of 55 seconds. The crucible holding the molten Ti was then tilted toward the inlet located at the center of the turntable. The turntable had a designed full rotation speed of 3000 rpm when the molten metal was poured. Figure 2.38 shows centrifugal casting machine [8].

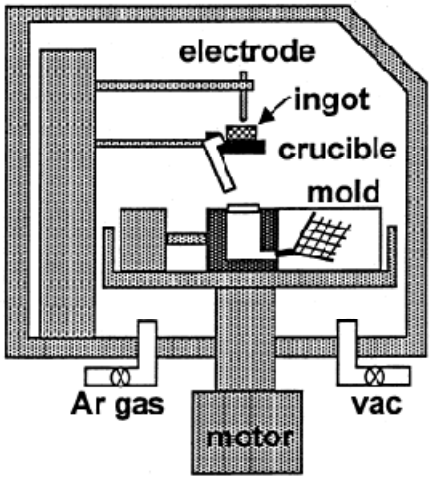

Figure 2.38. Ultra High Speed Centrifugal Titanium Casting Machine [8]

Experimental pressure difference type casting consists (Figure 2.39) of an upper melting chamber and a lower mold chamber. After placing a piece of Ti (30 grams) in the upper melting chamber, the upper chamber and the lower chamber (under which the mold was attached) were evacuated to a vacuum level of approximately $6x10^{-2}$ torr. Then high purity argon gas was introduced into the melting chamber until the argon pressure difference between the two chambers became almost 150 torr (20.0 KPa). The Ti was melted by an electric arc (200 A, DC 60 V) over a period of approximately 60 seconds, after which the molten Ti dropped by itself into the mold as a result of the argon gas pressure difference [8].

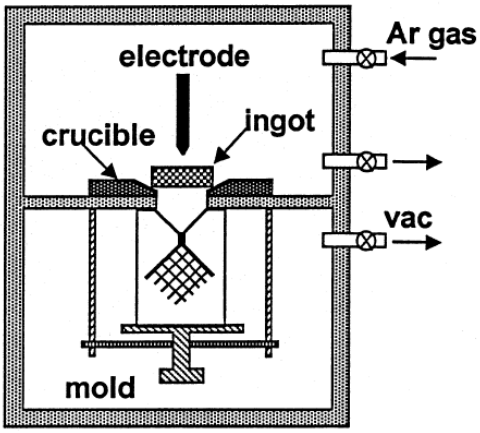

Figure 2.39. Pressure Difference Casting Unit [8]

To determine castability, used patterns are shown in Figure 2.40 and Figure 2.41 respectively.

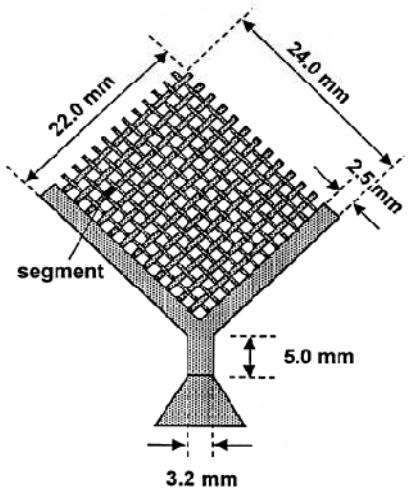

Figure 2.40. Mesh Pattern [8]

The castability index for the mesh pattern can be found as

$$\text{Castability Index (CI)} = \frac{\text{Cast Segments}}{264} \times 100(\%) \qquad (2.9)$$

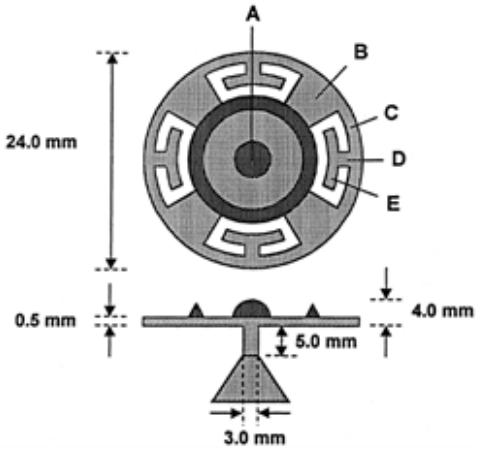

Figure 2.41. Saucer Pattern [8]

The castability index for the saucer pattern can be found as

$$\text{Castability Index (CI)} = \frac{\text{Counting Points}}{25} \times 100(\%) \qquad (2.10)$$

Total counting points for the pattern is 25:

- 1xA = 1
- 4xB = 4
- 8xC = 8
- 4xD = 4
- 8xE =8

The internal porosity of the cast Ti specimens (both cast mesh and saucer pieces) was examined radiographically using a conventional dental X–ray unit.

Castability indices are summarized in Figure 2.42. The castability indices obtained from both patterns of cp Ti cast in the centrifugal casting machine were significantly greater than the indices for the pressure difference casting unit. The values for the mesh patterns of the cp Ti cast in the pressure difference casting unit were significantly lower (20 per cent), compared to the values obtained in the ultra high speed centrifugal casting machine [8].

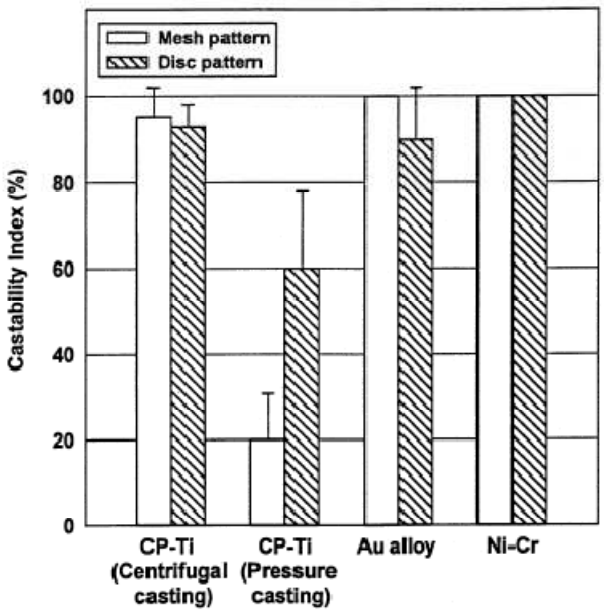

Figure 2.42. Castability Indices [8]

Representative radiographs of both patterns cast in the pressure difference casting unit and the centrifugal Ti casting machine are shown in Figure 2.43 and Figure 2.44, respectively. There were much larger pores in both cast patterns made in the pressure difference casting unit. The results of the castability indices and radiographic evidence indicated that the centrifugal Ti casting machine produced a much sounder casting than did the two-chamber pressure difference casting unit [8].

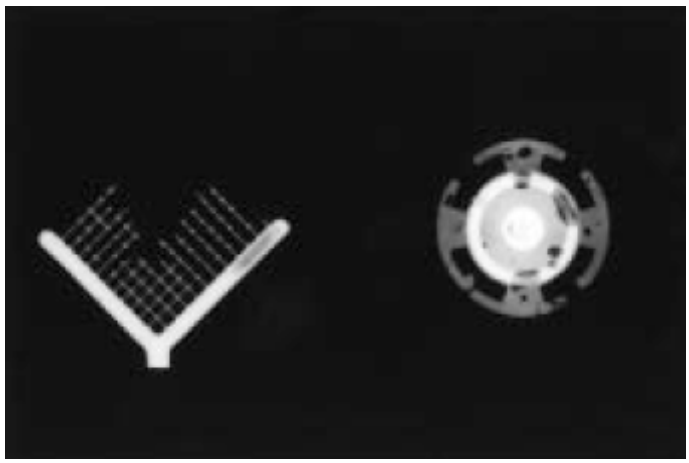

Figure 2.43. Representative radiographs of both patterns cast in the pressure difference casting unit [8]

Figure 2.44. Representative radiographs of both patterns cast in the centrifugal casting unit [8]

2.2.3. Casting Parameters for Centrifugal Casting

Alam and Marshall [5] studied about a novel centrifugal casting method which allows gunmetal bushes, within a restricted size range, to be cast simultaneously. The method involves the incorporation of sodium silicate bonded and segmented sand moulds in a conventional die. A range of centrifuging speeds was employed to study the effect on microstructure and properties.

A number of trial castings were made at speeds of rotation ranging from 90 to l000 revolutions per minute. In all cases molten alloy was introduced into the pouring basin at a low spinning speed and when full the mould was rapidly accelerated to the desired speed.est specimens. Plain bushes were divided into four sections with respect to the position of the runner in order to assess the homogeneity of the properties at different casting speeds and in different relative positions. Test pieces were taken at angles of 0, 50, 90 and 135 degrees.

At low casting speeds the alpha dendrites formed were fine and uniform in size and levels of porosity and solidification shrinkage were also reduced. An improved distribution of spherical lead particles was also evident at low RPM (Figure 2.45). As casting speed increased voidage also increased, but some decrease in the size of the alpha dendrites was

noticed at these higher speeds of rotation. It is possible that the greater levels of hydrostatic pressure developed at increased casting speed led to an increase in turbulence which caused dendritic breakdown (Figure 2.46 and 2.47) [5].

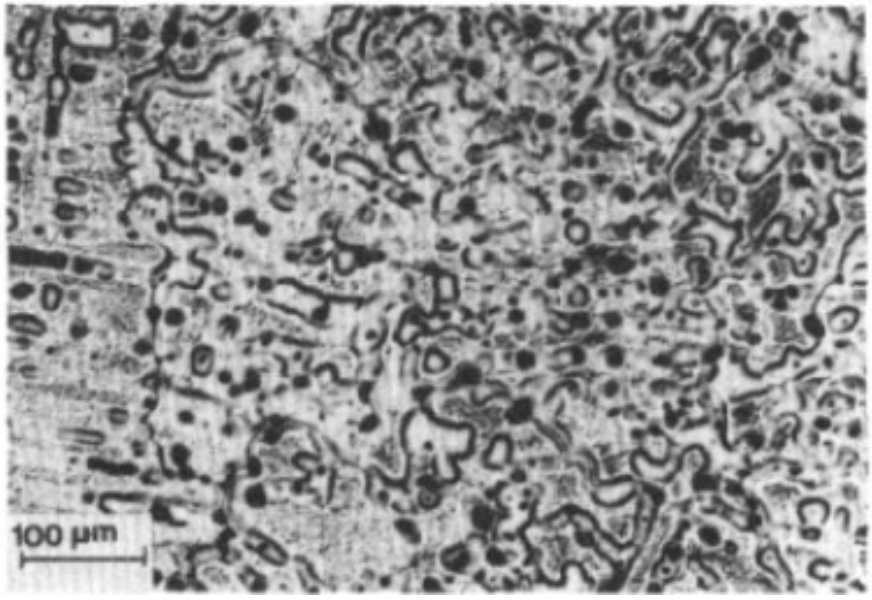

Figure 2.45. Microstructure of centrifuged casting at 90 RPM [5]

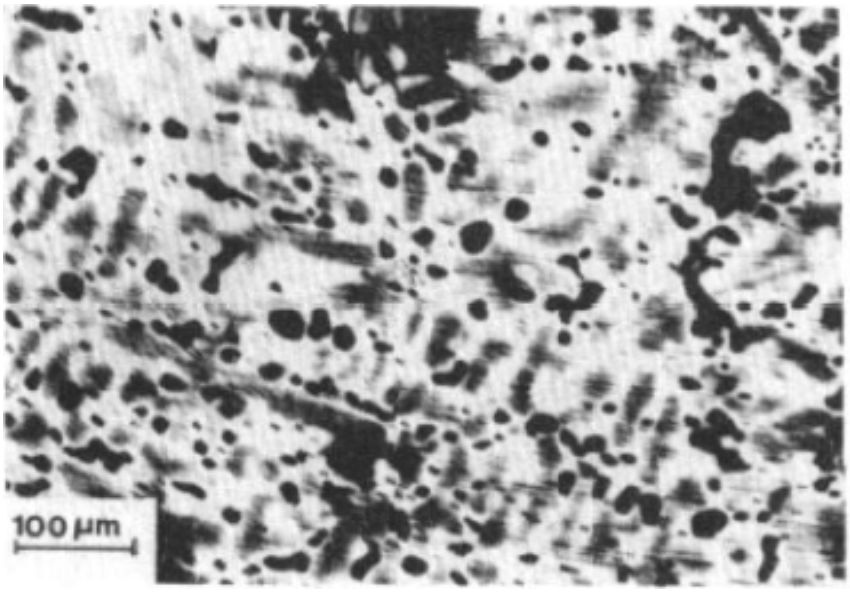

Figure 2.46. Microstructure of centrifuged casting at 650 RPM [5]

Figure 2.47. Microstructure of centrifuged casting at 1000 RPM [5]

Higher speeds of rotation resulted in high outward lead segregation to the periphery of the casting and random microporosity probably caused by increased splashing and vibration causing an irregular metal flow.

Vickers hardness measurements were made on all test specimens from top to bottom and at intervals of 10 mm using a machine test load of 5 kg. The results obtained from the bushes cast at low speeds were more consistent due to the lower levels of porosity and shrinkage present in these castings. The results obtained from the castings made at high speed showed inconsistencies associated with the greater levels of random microporosity.

The bushes cast at the lowest rotational speed showed the greatest consistency in density and were denser than the other materials tested by as much as 2.2 per cent.

The results obtained show that it is possible to make centrifugally cast plain bushes in gunmetal which are superior in mechanical properties and performance to bushes made by conventional static casting. It is important however to minimize the rotational speed of the casting machine, as high speeds lead to turbulence which gives rise to increased levels of porosity, and the higher centrifugal forces developed encourage outward segregation of heavy elements, particularly lead [5].

Pathak *et al.* [51] investigated centrifugal casting of leaded aluminium alloys. Hollow cylindrical castings (90 mm outside diameter, 80 mm internal diameter and 150 mm length) of leaded aluminium alloys (Al–4·1Cu–15,20,25Pb) were prepared by vertical centrifugal casting technique. Operational parameters such as mould speed and pouring temperature were optimized for 20 weight per cent lead alloys. These casting parameters (mould rotation speed 1600 rev min^{-1} and pouring temperature 900°C) were found to be suitable for 15–25 weight per cent Pb alloys.

Jovanović *et al.* [52] studied about the microstructure and mechanical properties of precision cast TiAl turbocharger wheel. The goal of the results described in the paper was to develop a prototype of a γ–TiAl turbocharger wheel via vacuum centrifugal casting process with cost that could be low enough to be applicable in automobile industry. The results concerning technology of precision casting, as well as microstructural and mechanical properties of a TiAl turbocharger wheel prototype developed at "Vinča" Institute were described.

In the present work, a conventional "lost wax" procedure was used to fabricate ceramic shell molds. Conditions during melting and casting were as follows: pouring temperature was varied in the range between 1550 and 1650°C, preheated temperature of ceramic shell mold was varied between 400 and 800°C, speed of mold rotation: 200 rpm, vacuum during processing: 1 Pa.

Mold preheat temperature is one of the most important casting parameters. Higher preheat not only improves fill and feeding but also reduces thermal gradient and cooling rates. However, higher preheating may lead to severe mold/metal reaction and may increase the propensity for surface-connected porosity. Slower cooling rates may induce coarser grain size and inferior mechanical properties.

The first castings showed defects, such as a misrun, when the preheat temperature was below 500°C. In the case when the preheating was too high (above 800°C), rough surface and macroporosity as well as microporosity were observed. Pouring temperature above 1600°C also causes a significant extent of microporosity. Applying higher preheat temperature (between 750 and 800°C), many of these defects were successfully eliminated

and a smooth surface together with thin and sharp blade edges were obtained. Macro and micro defects caused by inadequate mold preheat or pouring temperature and correctly cast turbocharger wheel are shown in Figure 2.48 and 2.49 respectively [52].

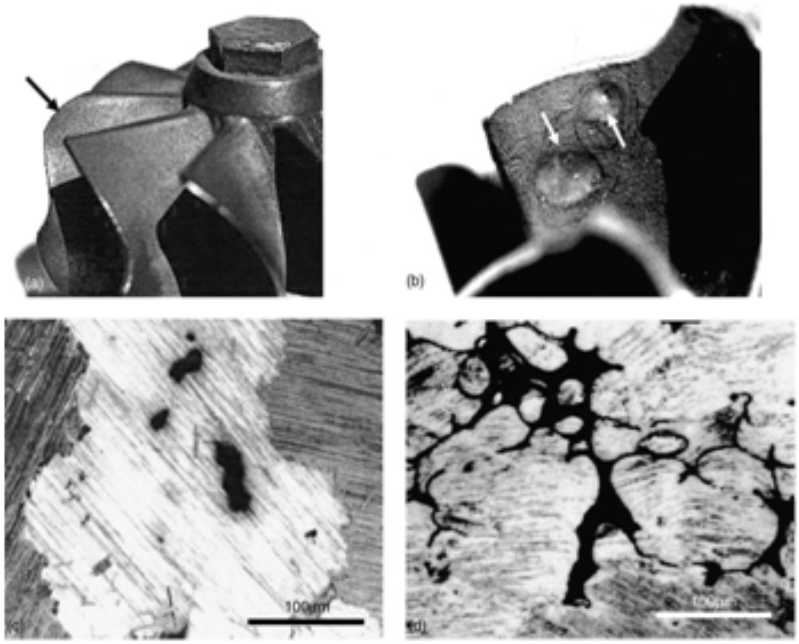

Figure 2.48. Macro and micro defects caused by inadequate mold preheat or pouring temperature a) misrun b) rough surface and macropores (arrows) c) micropores d) extensive microporosity [52]

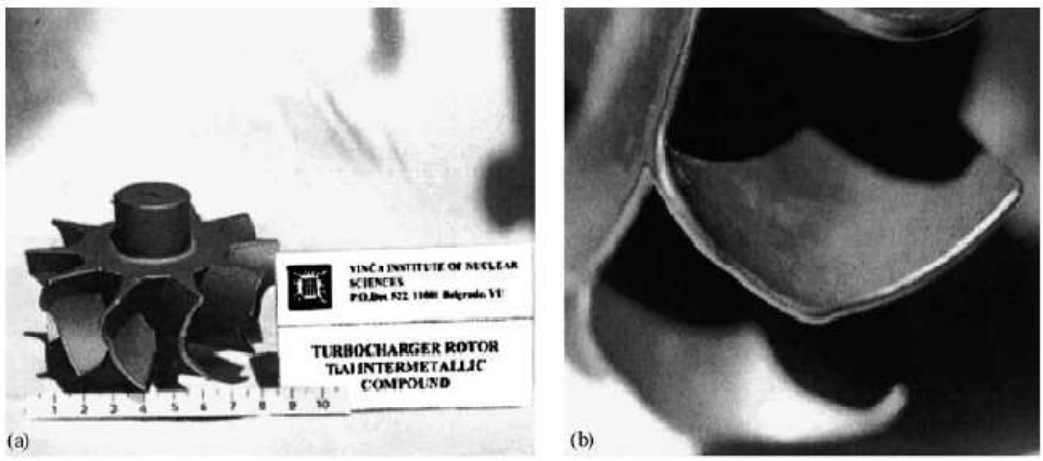

Figure 2.49. Correctly cast turbocharger wheel and assembly of specimens for tensile testing a) general look of wheel b) detail showing blade edge [52]

Higher cooling rate (mold was preheated at 500°C) yielded grains between 100 and 300 µm in size, whereas lower cooling rate (mold temperature was around 800°C) produced rather coarse (between 300 and 600 µm) grains. Lamellar spacing was found to depend on cooling rate, i.e. in coarse grains (slower cooling rate) this spacing was somewhat larger than in smaller grains (higher cooling rate). The effect of smaller grain size on mechanical properties is evident, i.e. higher strength and hardness, but lower elongation showed specimens solidified under higher cooling rate. Light microscope view for the as cast (AC) microstructure can be seen in Figure 2.50 [52].

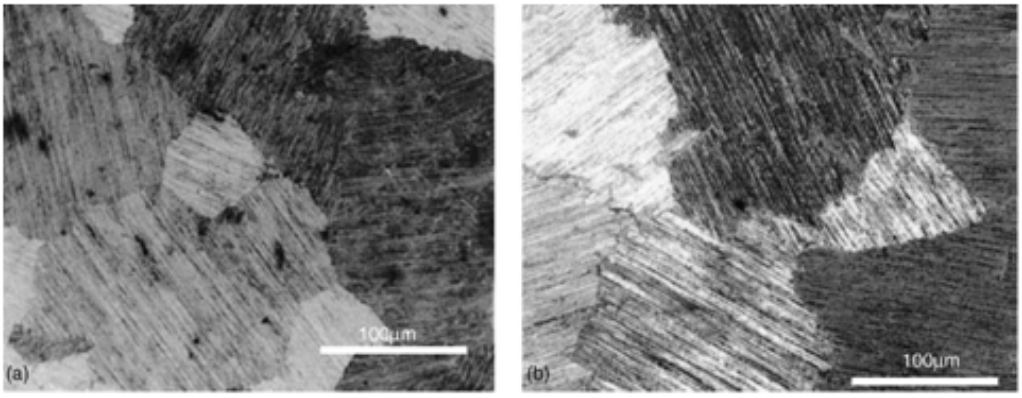

Figure 2.50. Light microscope AC microstructure a) mold preheated at 500°C b) mold preheated at 800°C [52]

Jing *et al.* [53] investigated the technology of centrifugal casting for titanium alloy. The investment technologies of preparing wax moulds, mould shells and technology of centrifugal casting for titanium alloys were studied. Low priced refractory and binder materials were used in the process of preparing shell moulds, the parameters of preparing wax moulds, mould shells were optimized and the titanium components were cast successfully using low priced shell mould materials by the centrifugal technology, in which the preheat temperature of the mould was 300°C and the centrifugal speed was 280r/min.

Liua *et al.* [54] aimed to produce TiAl automotive valves by single step centrifugal casting. They looked at the effects of the casting conditions, including superheat, rotation speed at one mould temperature have been investigated in terms of the product integrity and porosity and the microstructure of the valves.

The nominal composition Ti45Al8Nb alloy with different boron additions was selected as the cast valves material and the feedstocks including sponge Ti, industrial pure aluminum, metal niobium and Al–B (boron addition in this form) were melted in the vacuum induction furnace using the CaO crucible. There were three dimension valves:

- Type–a with the small head dimension, the diameter 31 mm, edge thickness 2.0 mm and stem Φ7x100 mm.
- Type–b with the head diameter 44 mm, edge thickness 5.7 mm and stem Φ8.2x100 mm.
- Type–c with the head diameter 45 mm, edge thickness 4.7 mm and stem Φ9 mm x 100 mm have been cast.

The ceramic mould used in this research project was Al_2O_3 mould. Cast parameters selected in this study are:

- liquid superheating from 140 to 180ºC;
- rotation speed 420, 500 r/min;
- preheated mould temperature 900ºC.

To reduce the cost of the cast valves, the one step melting and centrifugal casting process was adopted. X–ray inspected the porosity in the cast valves. Microstructure examination was carried out using a scanning electron microscope (SEM). Tensile test pieces from the cast valves stem were machined to have a diameter of 5 mm and a 30 mm gauge length. Tensile tests were performed at room temperature.

The fullfilling quality of three dimension cast valves was first examined after cleaning the Al_2O_3 shell. At the low superheating of 140ºC, about 50 per cent cast valves head edge fully filled, when alloy liquid superheating increased to 160ºC, this fullfilling rate definitely got 80 per cent and reached the maximum 90 per cent yield at 180ºC. The higher the superheat, the higher the fully filling rates. When increased the centrifugal turning speed from 420 to 500 r/min at the same superheating (160ºC) and mould temperature (900ºC), the filling rate did not improve, which means that speeds of mould have no definite effect on the filling-rate at a certain superheat.

Compared to the small dimension Type–a cast valve, the full-filling head rate of Type–b and Type–c valves with big head dimension have been significantly improved. The effects of superheat of the molten liquid on cast valve O contents indicated that the higher of superheating, the higher of the O contents it was. Results demonstrated that the O increase vertically came from the interaction of the higher superheated liquid with CaO crucible.

X–ray test (Figure 2.51) inspected the internal porosity of the three type cast valves. Type-a valve have a few porosities existed in the centerline of the cast valve stem [54].

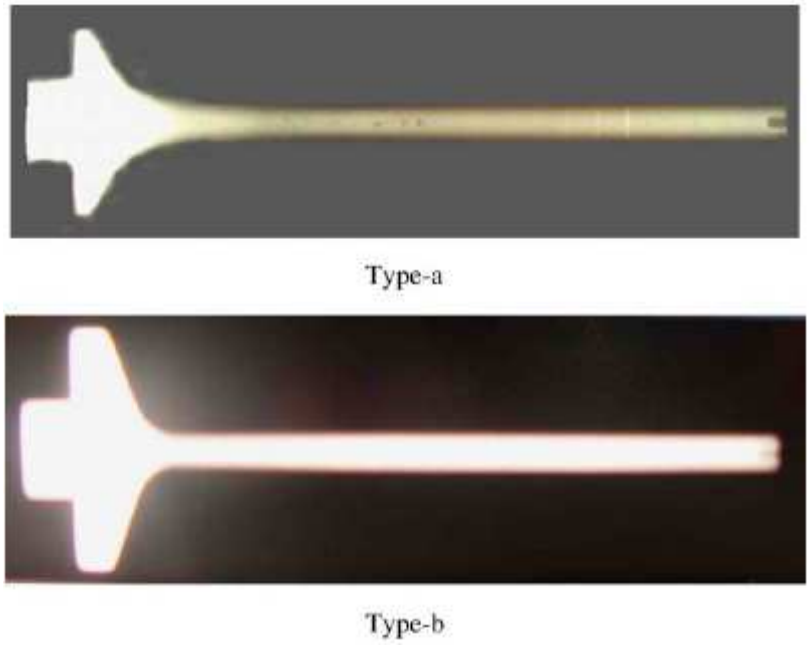

Figure 2.51. The X–ray photographs of two type valves [54]

SEM microstructure of the valves was shown in Figure 2.52. It could be found that cast valves got the near-fully lamellar structure and the refined grain size with two boron contents. Grain size of Type–a valve with 1 at. per cent B addition was about 50 µm, a bit finer than Type–b valve with 0.8 at. per cent B content [54].

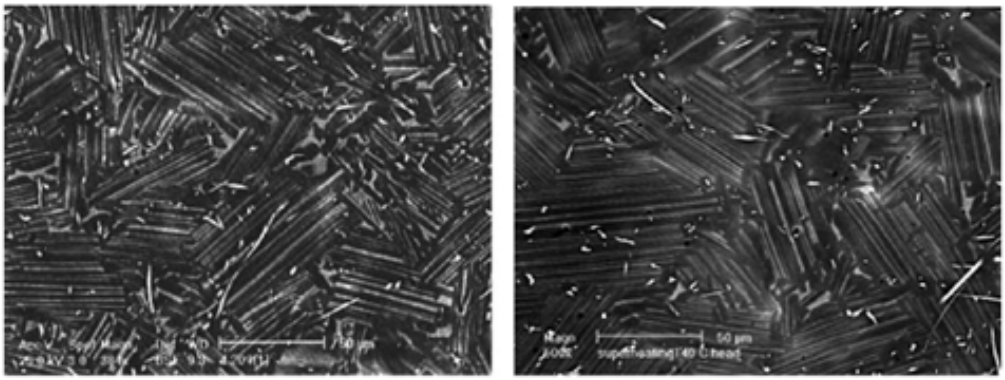

Figure 2.52. SEM images of the centrifugal valves with two boron additions of a) 1 at. per cent B and b) 0.8 at. per cent B [54]

The statistic results of the ultimate tensile strength can be seen in Figure 2.53. There is some variation in strength, and variation is related to the cast valve size. Type–a valves, the porosities still existed in the centerline of the stem. The strength variation was big, within 150 MPa. The Type–b valve with improved porosity, the variation was controlled within 100 MPa. The stable tensile strengths appeared in Type–c valves with the appropriate head and stem size, most of them were around 500 MPa and the variation of the strengths were limited. Such results revealed that the tensile properties are mainly affected by the porosity are existed in the cast stems [54].

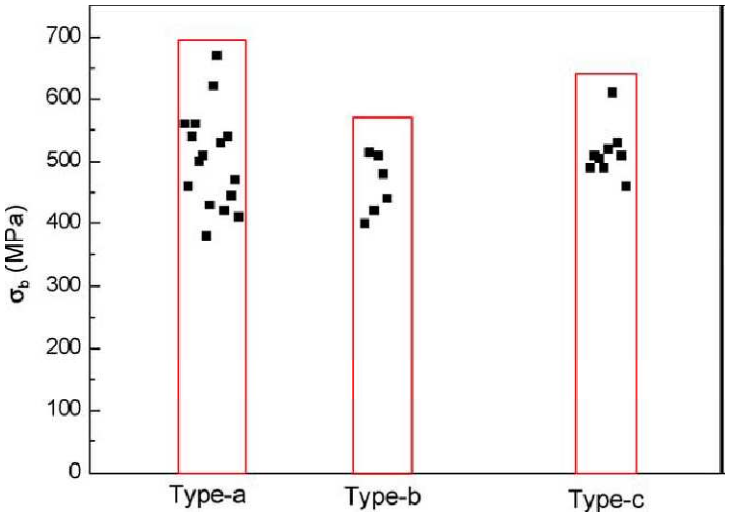

Figure 2.53. Tensile strength of three types of the valves [54]

To sum up, in Liua and co–workers' study, it is explained that TiAl automotive valves could be cost-effective made by the developed single step induction melting using CaO crucible and centrifugal casting techniques and the cast valve has the following characteristics:

- The sufficient high superheat is needed to get the good cast quality valves and the O contents could be mainly controlled less than 1500 wt ppm.
- The as-cast valves under the developed process possess the near-fully lamellar microstructure and less than 100 mm refined grain size.
- Some low and scattered tensile properties of the cast valves still exist at AC condition [54].

Halvaeea and Talebib [55] studied about the effect of process variables on microstructure and segregation in centrifugal casting of C92200 alloy. In their research, effect of process variables including pouring temperature, mould rotation speed and mould cooling rate on microstructure and segregation of lead and tin have been investigated.

Melting operations were carried out in a crucible furnace. The metal surface was covered by Cuprex 16 and charcoal granules, respectively. Deoxidation was performed using Cu–15P hardener out of the furnace. The liquid metal was poured into the moulds preheated up to 150ºC. Below is the dimensions and pouring conditions of bushings are: (1) thickness, 20 mm; (2) length, 20 cm and (3) external diameter, 17 cm.

In Figure 2.54 and 2.55, it can be seen that at a constant temperature, concentration of lead and tin firstly drop sharply from external to internal casting wall but then raise slowly. Also raising the pouring temperature from 1040 to 1230ºC, the amount of lead and tin increase at external wall and decrease at internal wall. Difference in concentration of these elements between maximum and minimum increases as the pouring temperature raises. Because the solubility of lead in copper is zero and its density is higher than the density of copper (11.3 vs. 8.9 g/cm^3), lead moves towards the mould external wall due to a higher centrifugal force. Raising the pouring temperature elongates the time of solidification, so the centrifugal force causes higher difference between the maximum and the minimum concentration of lead. Segregation of tin occurs during solidification [55].

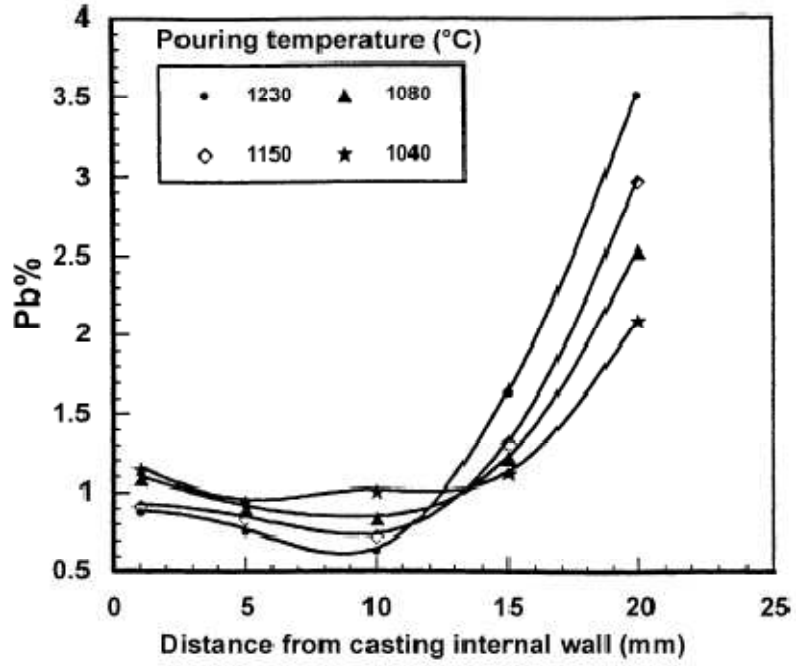

Figure 2.54. Lead percent vs. distance from casting internal wall at different pouring temperatures [55]

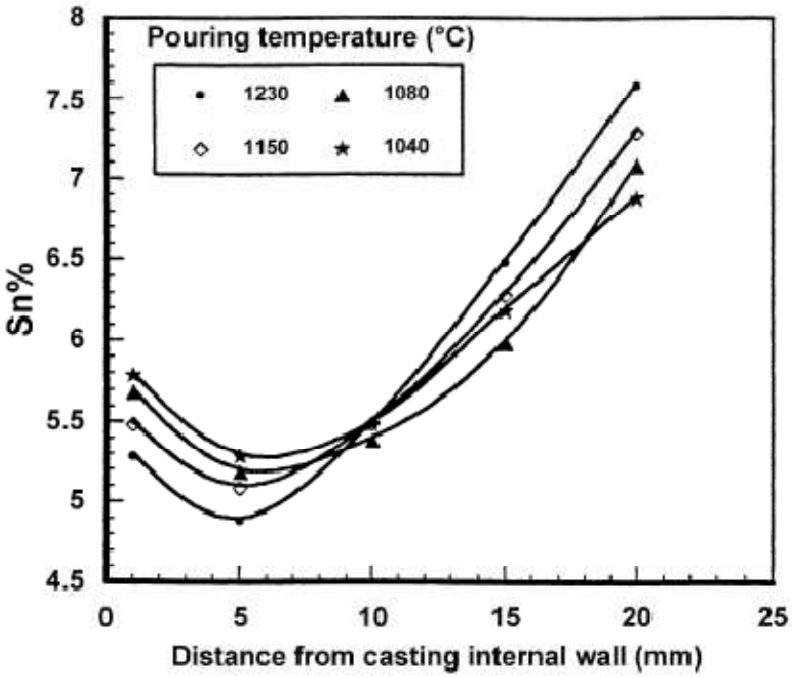

Figure 2.55. Tin percent vs. distance from casting internal wall at different pouring temperatures [55]

Due to a wide solidification range (about 160ºC), solidification of C92200 alloy is mushy, i.e. alpha dendrites poor in tin nucleate and grow, rejecting liquid metal rich in lead and tin. Figure 2.56 shows that phases formed at pouring temperature 1040ºC are finer than those formed at 1230ºC. This is due to decrease in nucleation and solidification rates and increase in thermal gradient. At lower pouring temperatures, fine equiaxed grains are formed and at higher pouring temperatures coarse columnar grains are formed [55].

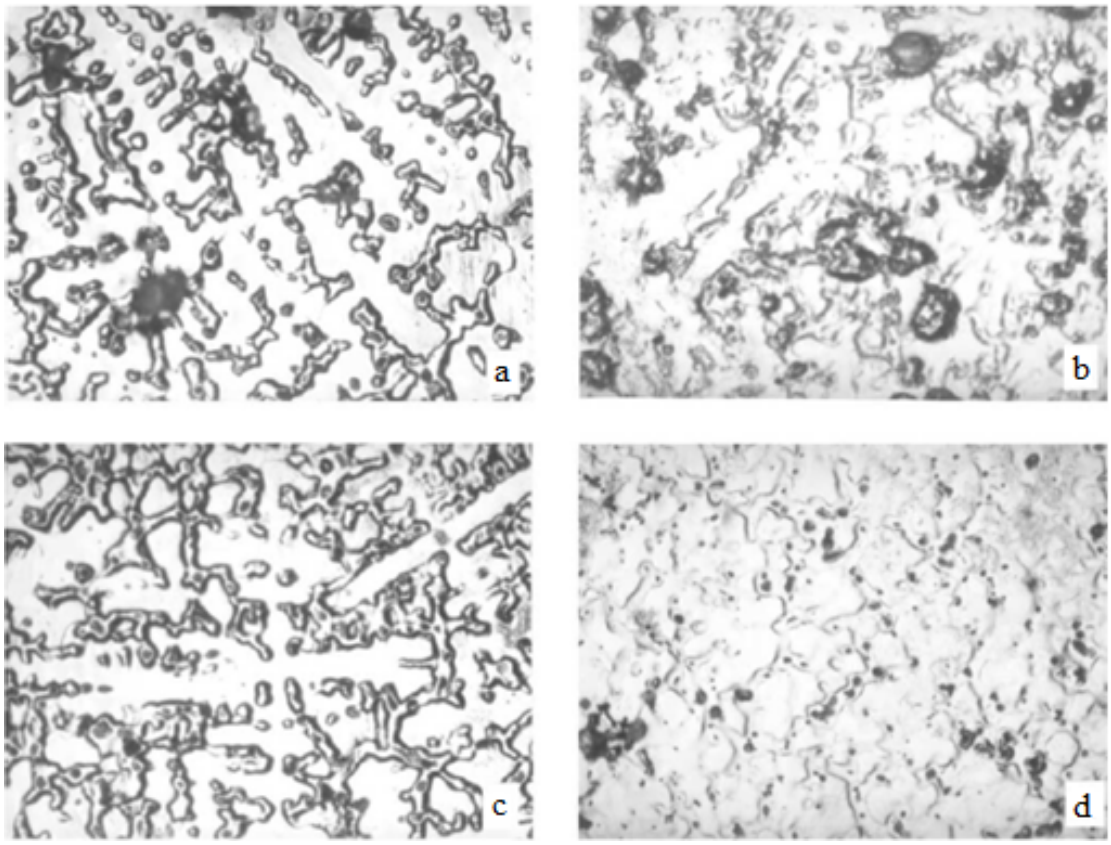

Figure 2.56. The microstructure of C92200 alloy at different pouring temperatures: a) 1040ºC, b) 1080ºC, c) 1150ºC and d) 1230ºC; Etchant–ammonium hydroxide plus hydrogen peroxide [55]

When the thermal gradient between the mould and the liquid metal is very high, the solidification time decreases leading to smaller DAS. As solidification continues, the mould become hotter and thermal gradient decreases at solidification front. Hence, solidification rate and time reduce, primary dendrites grow and DAS increases [55].

As the pouring temperature increases, the rate of nucleation and solidification decreases due to slower heat transfer. In this situation, dendrites grow and DAS increases.

As the mould cooling rate directly affects the solidification rate, it affects the grain size. As the cooling water flow increases, finer microstructure is formed. If the water flow rises, the thermal gradient between liquid metal and mould wall increases, reducing the solidification range and time. In this case, primary solid nuclei cannot grow and a fine columnar grain structure is formed and DAS is reduced.

As the thermal gradient between the cooled mould surface and the molten metal is high, solidification of very fine grains occur. As solidification proceeds, the mould become hotter, the thermal gradient falls and the solidification rate reduces. In this case, dendrites grow and DAS increases.

If the mould rotation speed raises, the centrifugal force more acting on heavy particles intensify segregation of lead in casting section. Severe segregation of tin at higher rotation speeds is due to rejecting the liquid metal rich in tin from dendrites.

DAS increases when the mould rotation speed is higher. In fact, it is supposed that increasing rotation speed and consequent mould cooling rate and also more possibility of dendrites to be broken can cause DAS to reduce.

To sum up, it can be said that:

- Raising the pouring temperature causes grain size and DAS to increase and segregation to intensify.
- Increasing the mould cooling rate, diminishes the segregation of lead and tin and reduces grain size and DAS.
- Raising the mould rotation speed leads to high segregation of lead and tin and increases the grain size and DAS [55].

In the study of Ping *et al.* [12], a multiscale model is developed for simulating the microstructure evolution during solidification processes of Ti–6Al–4V alloy in vertical

centrifugal casting, which combines the 3D finite difference method (FDM) at the macroscale with a 2D cellular automaton (CA) model at the microscale. With the proposed model, numerical simulations are performed to investigate the influences of mould rotation speed, superheat, and mould material on microstructure formation.

Calculated results reveal that the equiaxed zone is found to expand with increasing the mould rotation speed, as well as decreasing melt superheat and heat diffusivity of mould. The role of rotation speed is much greater than that of superheat and mould material in centrifugal casting.

Vaidyanathan *et al.* [56] studied about correlation between macroscopic porosity location and liquid metal pressure in centrifugal casting technique. A review of the literature indicates several sources of porosities and defects in dental castings. The most important of them are:

- Shrinkage porosity
- Porosities due to occluded gases
- Porosities and/or defects due to "back pressure" of gases in the mold
- Porosities due to inclusion of investment
- Incomplete filling of the mold prior to solidification onset
- Incomplete filling of the margins due to surface tension effects
- Suckback porosities

Ryge *et al*. characterized the porosities in dental castings into two distinct groups:

- porosities caused by cooling and solidification (i.e., shrinkage, subsurface and microscopic porosities) [56]
- porosities caused by gas (pinhole porosities and gas inclusions)

A total of 300 castings was made using a Howmedica "Electromatic" Induction casting machine. All castings were cylinders (0.25-0.3" in diameter and 1-1.5" long), so that macroscopic porosity could be detected and analyzed without introducing the geometrical variables of the sections cast.

All castings were made from a non–precious alloy, Dentillium. The casting temperature of the melt was 2800°F for all castings. Similarly, the centrifugal rotation speed was maintained constant at 400 rpm. Burnout temperature for wax elimination was 2100°F. All patterns were painted with a Howmedica protective coating prior to investment. VR investment for Vitallium processing was used.

Preliminary tests were carried out using different diameters of sprues 12, 10, 8, and 6 gauges, corresponding to diameters of 0.055, 0.095, 0.128, and 0.182" respectively (Figure 2.57) [56].

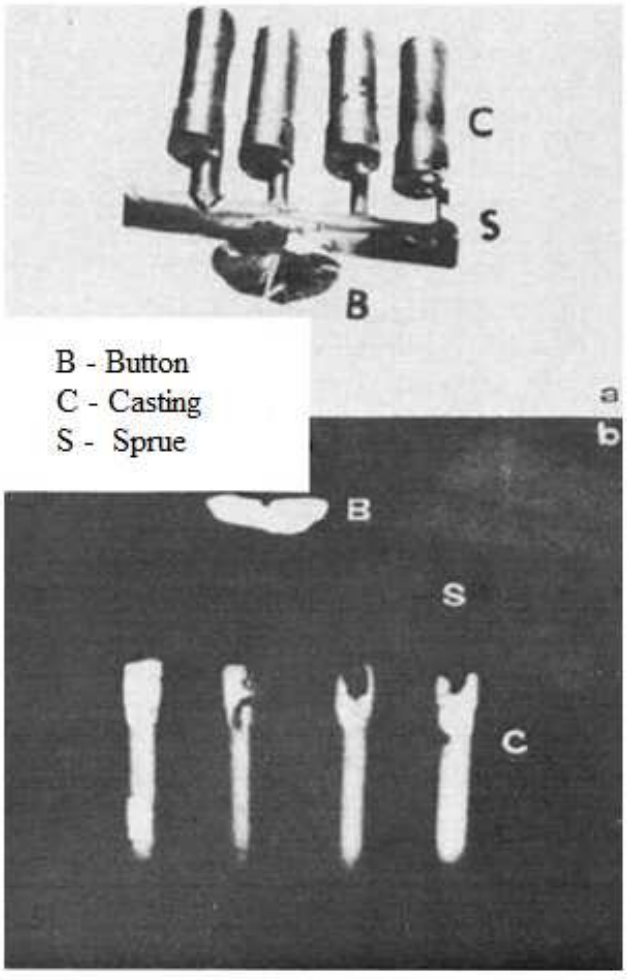

Figure 2.57. Four unit casting with different sprue diameters (12, 10, 8, and 6 gauges) a) macrophotograph, b) radiograph [56]

Five different sprue casting combinations were then studied extensively. These included different sprue locations on the castings with respect to the position of the button and minor additional variations. The different combinations studied were:

- direct spruing to casting near the button, as used conventionally;
- indirect spruing to the portion of the casting away from the button;
- same as in second, but with an L shaped sprue
- indirect spruing to one side of the casting with the longitudinal section of the casting oriented parallel to the free surface of the button
- same as in fourth, but sprues were attached to both sides of the casting (Figure 2.58)

For each type, at least 20 castings were fabricated and analyzed in the study [56].

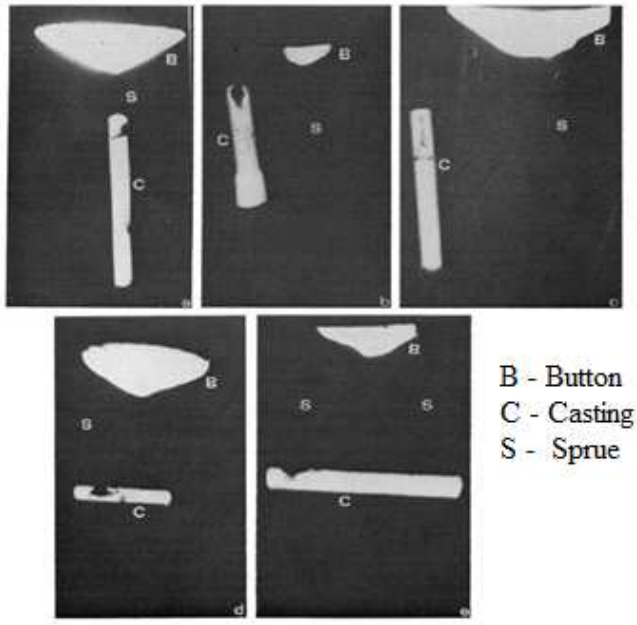

Figure 2.58. Radiographs of cylindrical castings with different sprue locations [56]

The relationship between the free surface of the button and the macroscopic porosity can be rationalized by the pressure differences at different points in the liquid metal. Nielsen1 utilized a section of the free surface of the button as part of a reference parabola and stated that the pressure at any point along the sprue axis in the liquid metal of a mold in the horizontal centrifugal casting technique is given by:

$$P_i = \frac{\omega^2}{2g}(X_i^2 - X_1^2)d \qquad (2.11)$$

P_i: Pressure at any point i along the sprue axis in the liquid metal

ω: The angular velocity of rotation

g: The acceleration due to gravity

d: The weight density of the liquid

X_i: The distance of the point i from the axis of rotation along the sprue axis

X_1: The distance of the free surface of the button at point 1 from the axis of rotation

When $X_i = X_1$,

$$P_1 = \frac{\omega^2}{2g}(X_1^2 - X_1^2)d = 0 \qquad (2.12)$$

Figure 2.59 illustrates liquid metal pressure at different points of the cylindrical casting.

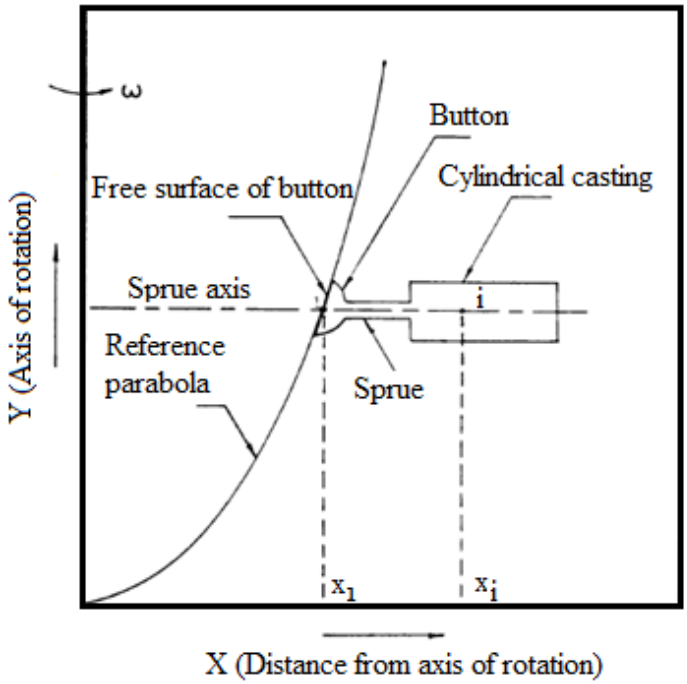

Figure 2.59. Liquid metal pressure at different points of the cylindrical casting [56]

It is easily seen that by considering different axes parallel to the sprue axis, the free surface of the button becomes a zero pressure surface in the liquid metal. For a given angular velocity of rotation, the pressure at any point in the liquid metal will be determined by the term $(X_i^2 - X_1^2)$ and therefore, the pressure difference with distance will be dramatic. This leads to a pressure gradient in the liquid metal with much higher pressures developing at points farthest from the free surface of the button and lower pressures developing at points close to the free surface of the button. The effect of this pressure gradient is to introduce directional solidification from the points of high pressure to those of lower pressure in the liquid metal because of significant differences in the heat transfer with pressure differences. The rate of solidification at the points of higher pressure in the liquid metal will be higher because of increased heat transfer with higher pressure.

In the study, it has been found that macroporosity is primarily shrinkage porosity but the portion of a cylindrical casting which solidifies last is the low pressure side of the liquid metal close to the free surface of the button, and, therefore, the macroporosity always appears in this portion of the casting. It was observed that this porosity can be reduced or eliminated by providing a reservoir contiguous or close to the low pressure end of the liquid metal. This displaces the shrinkage porosity to the reservoir. In addition, the macroporosity may be affected by the closeness of the individual units in a multiple-unit casting [56].

2.3. Rapid Prototyping

Rapid prototyping is the automatic construction of physical objects using solid freeform fabrication. The first techniques for rapid prototyping became available in the late 1980s. Today, they are used for a much wider range of applications and are even used to manufacture production quality parts in relatively small numbers.

3D printing is a category of rapid prototyping technology. A three dimensional object is created by layering and connecting successive cross sections of material. 3D printers are generally faster, more affordable and easier to use than other additive fabrication technologies [57].

In Boğaziçi University Materials Laboratory, there is a “ZPrinter 310 Plus” machine which is used for rapid prototyping. ZPrinter 310 Plus (Figure 2.60) is used with a program called ZPrint. There are generally three material options for Z310 Plus: zp®130, zp®131 and zp®140. In Boğaziçi University Materials Laboratory, zp®131 is used as a material in ZPrinter 310 Plus.

Figure 2.60. ZPrinter 310 Plus [58]

Figure 2.61 shows a city model printed by ZPrinter 310 Plus.

Figure 2.61. A city model printed by ZPrinter 310 Plus [59]

Before starting 3D printing, “Z310 Plus” needs to be prepared for the printing operation. First, the feed box must be filled with powder (zp®131). Powder is pressed to hinder the printing failures (Figure 2.62) [60].

Figure 2.62. Pressing powder [60]

Then, powder must be spread over the build area. For this, there are two techniques. One of them is manual spreading; the other one is software aided spreading (ZPrint Sofware).

Bond material (binder) is the second material used directly at 3D printing. This binder is actually used to bind the powders to gather at necessary forms. That’s why, checking the binder level and filling it, if it is necessary is critical. The binder fluid is filled till the neck of the tank (Figure 2.63). Checking the waste bottle is also important. It must be empty [60].

Figure 2.63. Adding bond material [60]

After preparation, ZPrint Software is opened for printing. Model is opened in the program. 3D Print Setup is adjusted. Checking powder level is important.

Z Corporation 3D Printer processes are based on the Massachusetts Institute of Technology's patented 3DP™ (Three Dimensional Printing) technology [61]. Printing steps of the machine is shown in Figure 2.64.

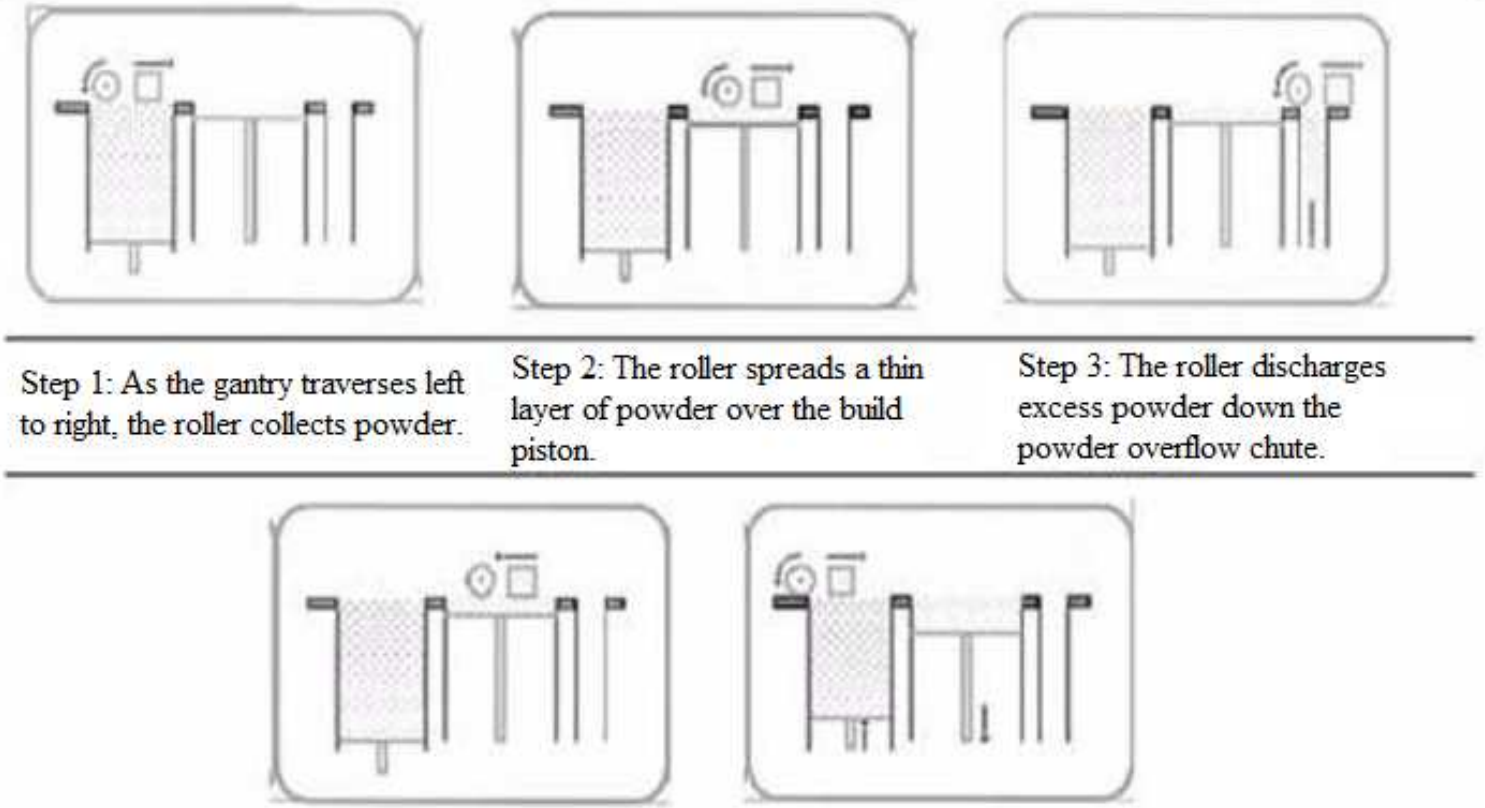

Figure 2.64. Printing steps [60]

First of all the printed part should be removed from the build (Figure 2.65). To do that, the excess powder is removed gently by using brushes and vacuuming etc. Before doing that one should wait till the part is dries enough. Then, the part is depowdered at the recycling station. For this, the part is put on a tray. By using vacuum and especially air compressor, the part is depowdered. Vacuum can be connected to the recycling room, so; powders streaming in the recycling room are vacuumed. Cleaning instruments are illustrated in Figure 2.66 [60].

Figure 2.65. Removing the part from the machine and cleaning with compressed air [60]

Figure 2.66. Cleaning instruments [60]

2.4. Investment Casting

Investment casting is a very old casting method that is known for centuries. The principle of investment casting is heating of molds which are prepared by using wax or alike models and forming the mold cavity by flowing out the melted model material from the mold.

Investment casting methods are basically two types:

- Investment Shell Casting
- Investment Flask Casting

In this study, first four steps of investment flask casting (to make mould) will be used. So, it will be briefly explained. In investment flask casting technique, the entire volume in a pot, except the mold cavity, is filled with ceramic/plaster material.

Investment flask casting technique includes seven steps:

- Wax models are pasted on the model tree by melting.
- A cylindrical sleeve (fanus) is placed around the model tree.
- Plaster/ceramic mixture is poured into all of the cavities between the sleeve and the model tree.
- By heating in the furnace, the mixture is dried and the mold is reversed in order to let the wax models in the mold to melt and flow.
- The hot mold is filled with melted metal. Casting can be eased by vacuum or centrifugal force.
- The mold material is cleaned by spraying pressurized water.
- The components detached from the casting tree are made ready for after casting usage by cleaning the material entrance burrs [62].

Figure 2.67 shows investment flask casting technique.

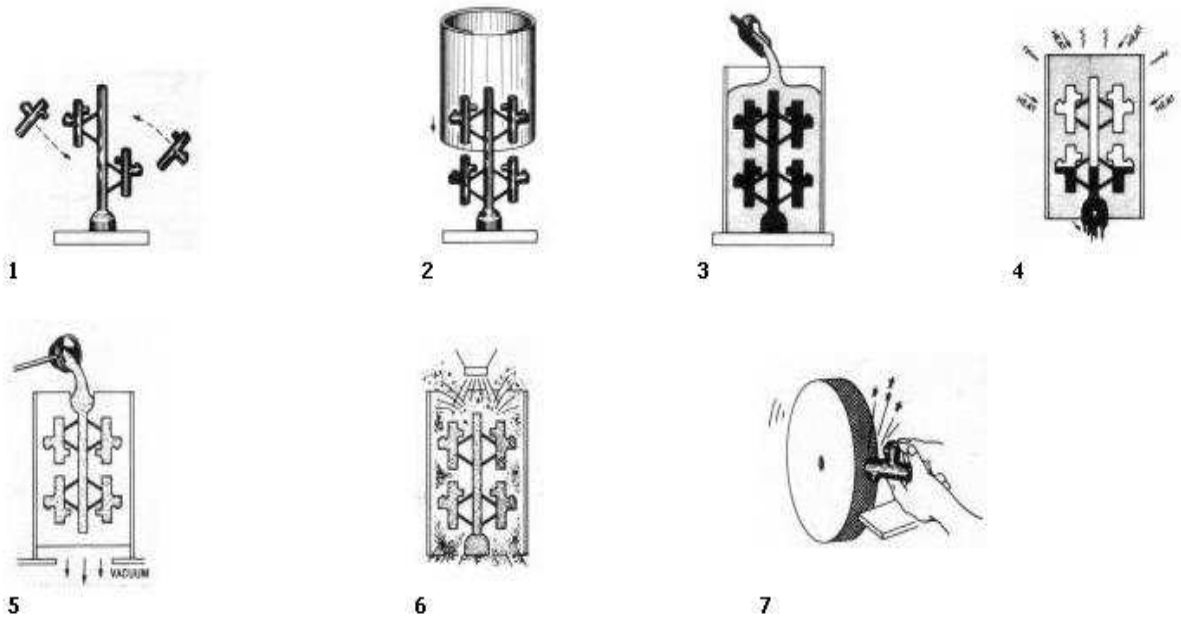

Figure 2.67. Investment flask casting [63]

2.5. Dental Implants

2.5.1. Review on Dental Implants

Dental implants are artificial substitutes of teeth. These include cylindrical screws that are implanted in the maxillary. Biomaterials in the dental material area require a recovery with mechanics characteristics compatible with the human body. Biomaterials must simultaneously satisfy many requirements and possess properties such as non-toxicity, corrosion resistance, thermal conductivity, strength, fatigue durability, biocompatibility, and sometimes aesthetics [64, 65].

Great effort has been made over the last few decades in searching for suitable biomaterials for medical applications. Most work has been focused on the biocompatibility of materials (metals, ceramics and polymers) in contact with blood or tissue. In the dental area, Ti and Ti based alloys are the materials of choice used in most surgical implant operations in recent years. Ti has advantageous bulk properties, such as low modulus of elasticity, light weight, poor heat conduction, and high strength to weight ratio [66].

The surface properties of Ti are particularly relevant as the first contact of the body with the artificial material is through the surface. In particular, Ti implants are known to interact with bone tissue so that a large percentage of the implant surface will finally be in close contact with the newly formed bone tissue.

In 1952 Per–Ingvar Brånemark used a titanium implant chamber to study blood flow in rabbit bone and noted that the chambers could not be removed at the end of the experiment. He called the discovery “osseointegration” (as told before). That is important for the long-term stability and success of permanent implants [67, 68].

A dental implant consists of three parts:

- the implant, which replaces the root. The implant is placed in the bone of the upper or lower jaw and allowed to bond with the bone and serve as an anchor for the replacement tooth.
- the abutment, which serves as a connector between the implant and the crown.
- the crown or tooth, placed by a restorative dentist and attached to the abutment.

Dental implants can be used to replace a single lost tooth or many missing teeth. Parts of a normal tooth and a dental implant are shown in Figure 2.68 [69].

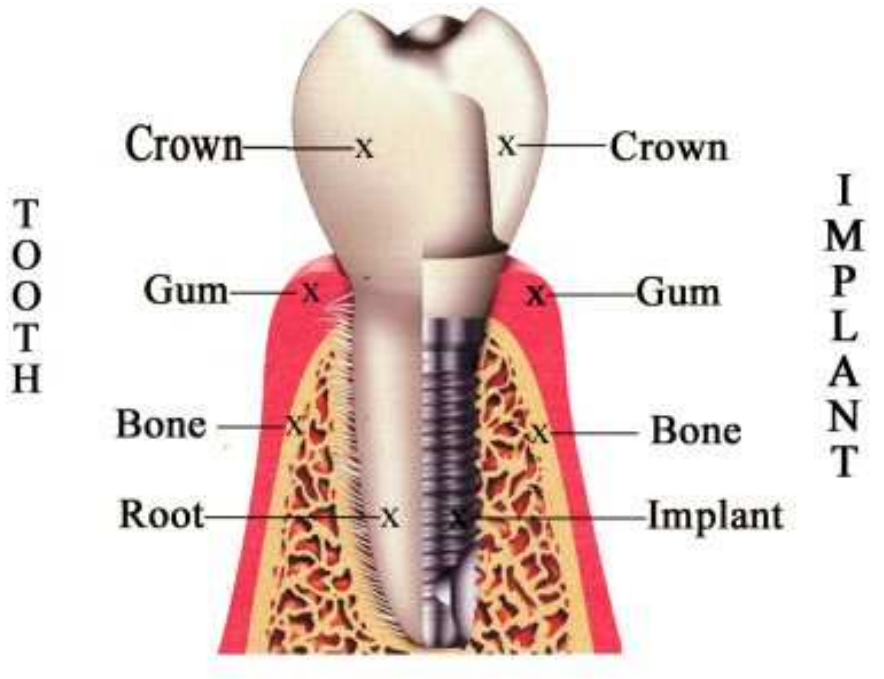

Figure 2.68. Parts of a normal tooth and a dental implant [69]

2.5.2. Dimensions of Dental Implants

There isn't any standard for dental implant dimensions, so there are some experimental and commercially used dimensions today in the world of medical dental implants.

Simunek *et al.* [70] studied on the hydroxyapatite (HA) coated root-form dental implants. The endosseous implants were cylindrical, smooth or threaded rootform HA coated. The implant diameter was 3.6 mm with lengths of 8, 10, 12 or 14 mm (Figure 2.69). The thickness of the HA coating was 50 μm, and was formed by spraying HA particles. 56 – 162 μm in size, on a core of Ti6AI4V (90 per cent Titanium, 6 per cent Aluminum and 4 per cent Vanadium) titanium alloy in plasma flame.

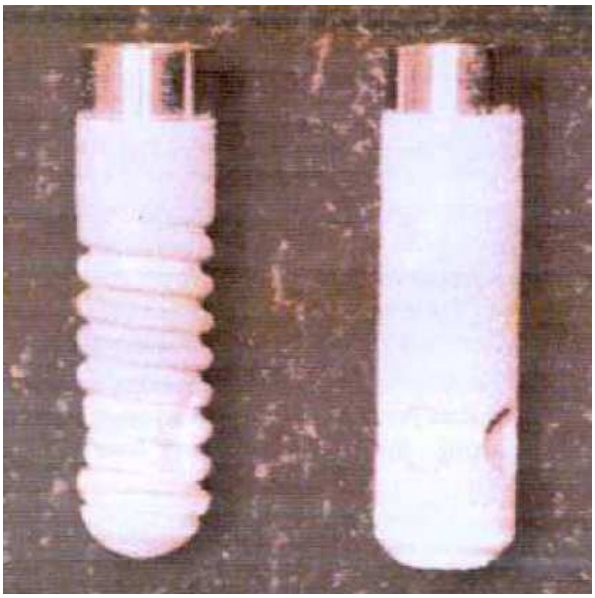

Figure 2.69. Hydroxyapatite coated dental implants [70]

The fatigue properties of rods of HA coated, titanium alloy implant material after it was exposed to a periodontal pathogen, Actinobacillus actinomycetemcomitans (Aa) was studied by Mukherjee *et al.* [71]. They used Ti6Al4V rods 4 mm in diameter and 19.67 mm in length. 50 microns of HA have been coated onto the titanium alloy. Titanium alloy rod can be seen in Figure 2.70.

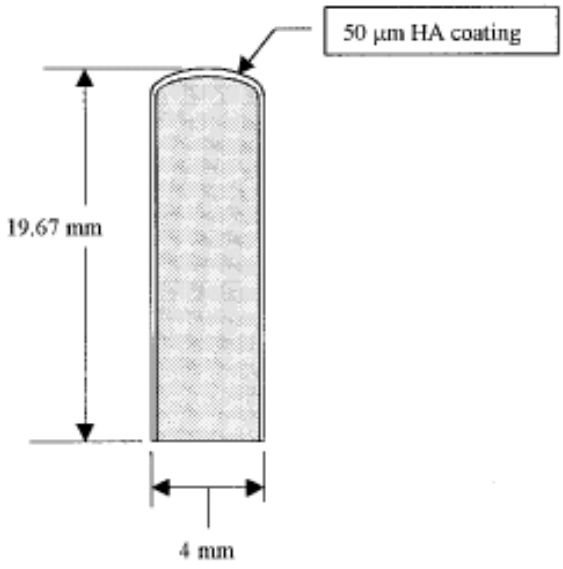

Figure 2.70. Titanium alloy rod [71]

Bozkaya and Muftu [72] studied about the mechanics of the tapered interference fit in dental implants. Bicon implant – abutment attachment method was used in the study. The properties of the implant – abutment system is shown in Table 2.6.

Table 2.6. The Bicon implant – abutment system used in the study [72]

Bicon	Size	Length	Material
Implant	3.5 mm	11.12 mm	Ti6Al4V ELI
Abutment	4 x 6.5 mm 0°	N/A	Ti6Al4V ELI

Some implant – abutment attachment methods are shown in Figure 2.71. Astra and Nobel Biocare use a screw, Ankylos and ITI use a screw with an interference fit and Bicon uses only-interference fit [72].

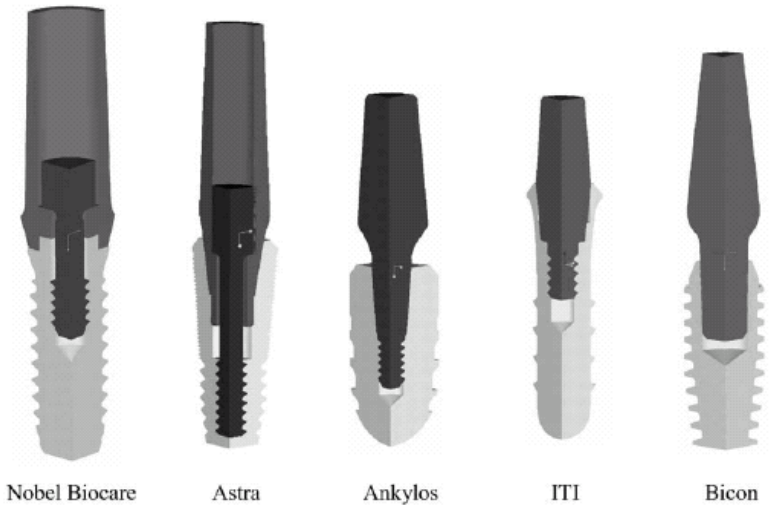

Figure 2.71. Different implant – abutment attachment methods [72]

Zimmer Dental Company Spline Implant System models can be seen on Figure 2.72.

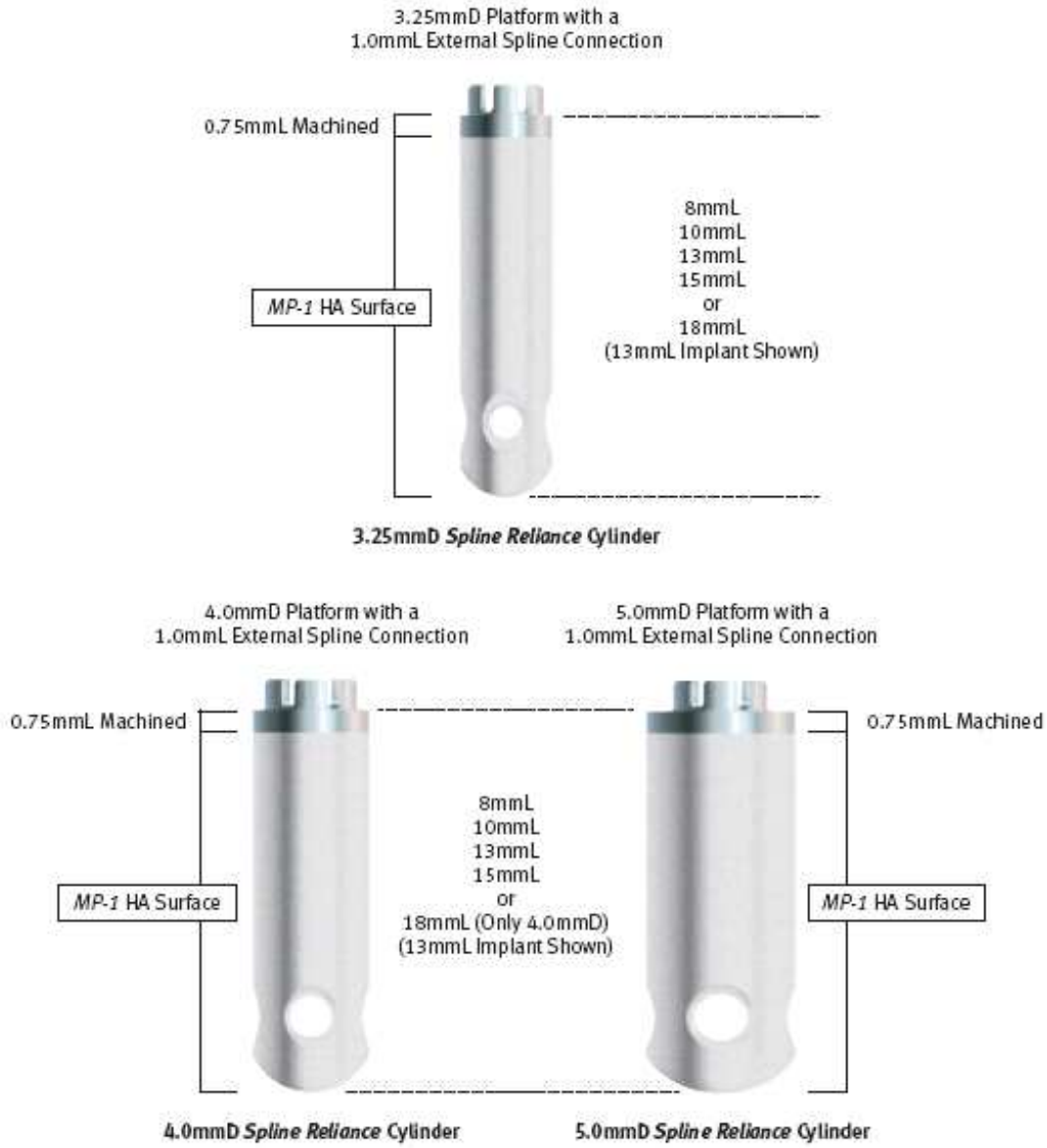

Figure 2.72. Zimmer Dental, Spline Implant System models [73]

Oal's work focuses on the stresses on the implant. For this, an implant model with different diameters and lengths was used (3.3 mm, 3.8 mm, 4.3 mm, 5.0 mm and 6.0 mm as diameters for a 13 mm length dental implant and 4.3 mm diameter for 9 mm, 11 mm, 13 mm and 16 mm lengths). As an abutment length, 9 mm was selected. Implant without abutment and implant and abutment are shown in Figure 2.73 and Figure 2.74 respectively [74].

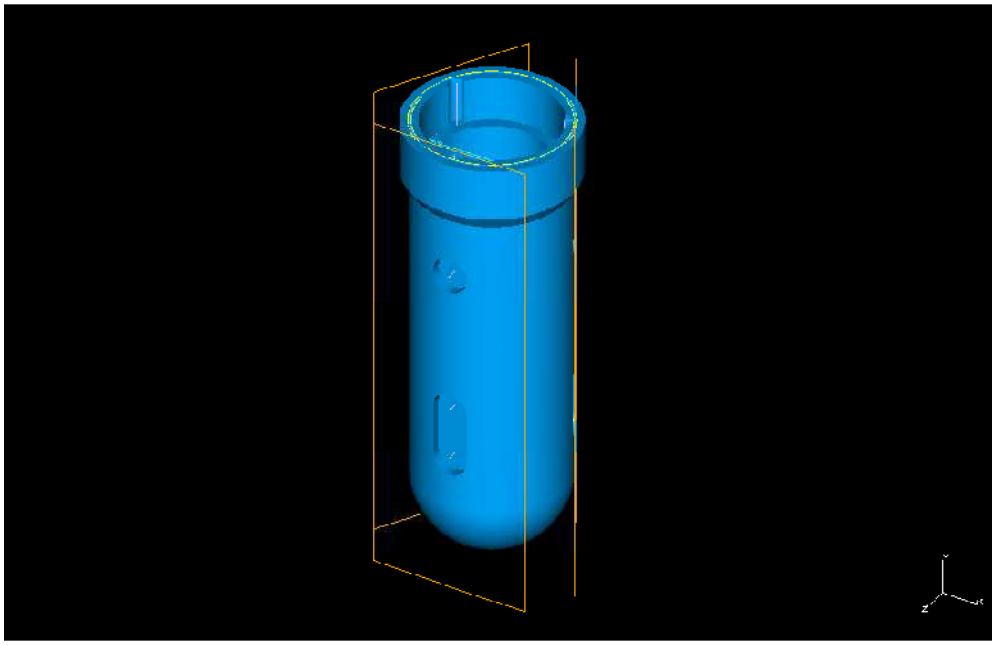

Figure 2.73. An implant model without abutment [74]

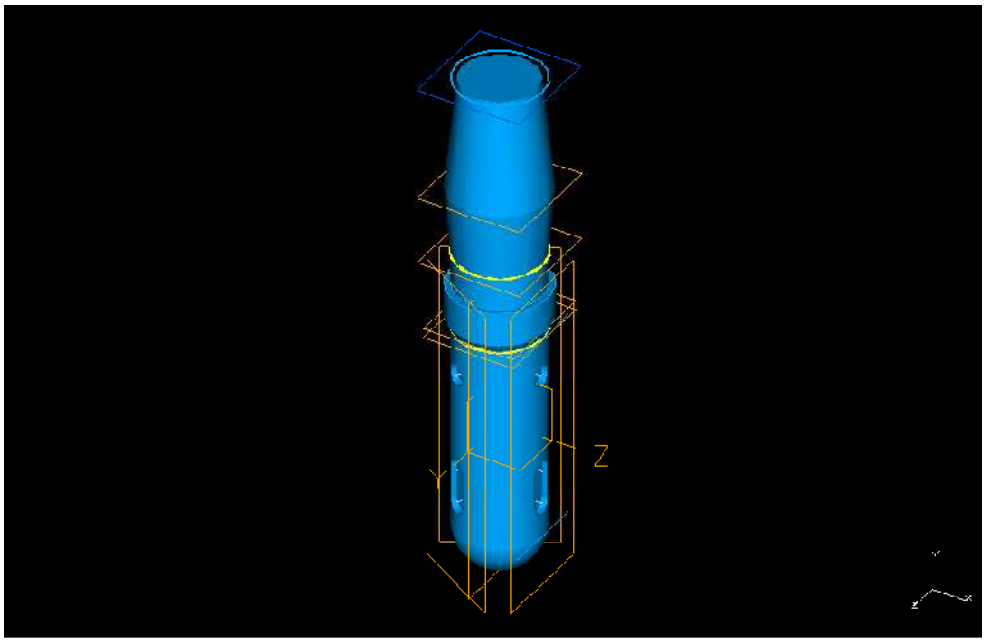

Figure 2.74. Implant and abutment [74]

3. EXPERIMENTAL WORK

An experimental approach is presented in this chapter which includes the manufacturing of the centrifugal casting mould and the production of Ti Grade 4 dental implant specimens.

3.1. Manufacturing of the Mould

3.1.1. Dental Implant Model

A model with two implants (with its sprue and gating) was drawn by using Solidworks 2009 software. Solidworks dental implant model is illustrated in Figure 3.1, Figure 3.2 and Figure 3.3 respectively. Technical drawing of the implant is shown in Figure 3.4.

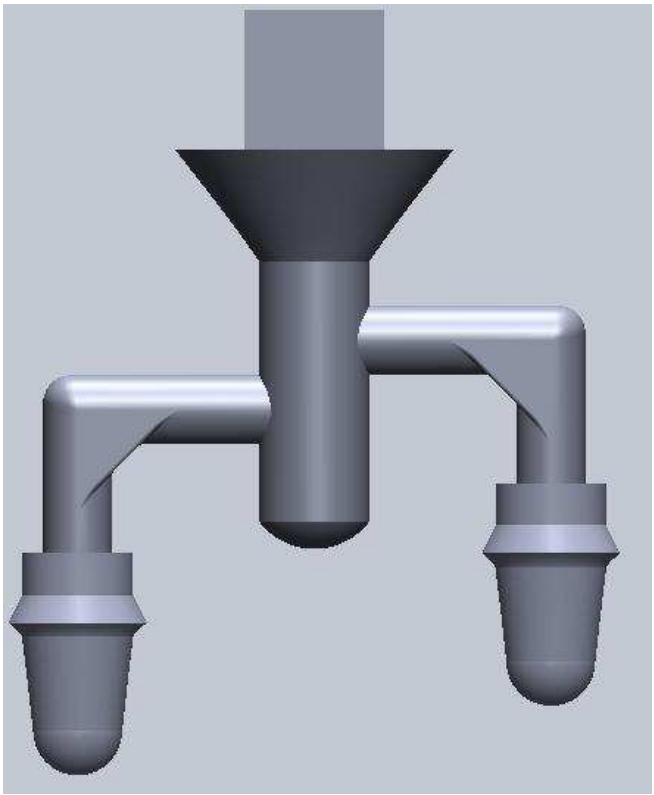

Figure 3.1. Front view of the model

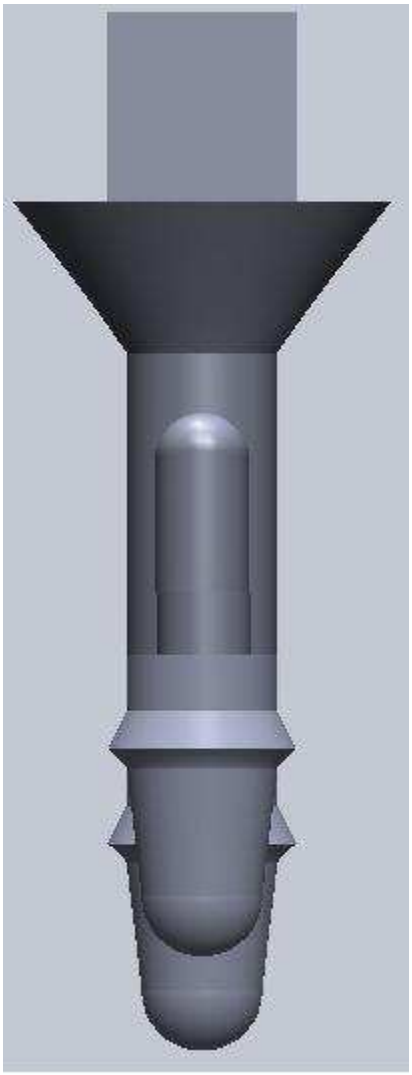

Figure 3.2. Right view of the model

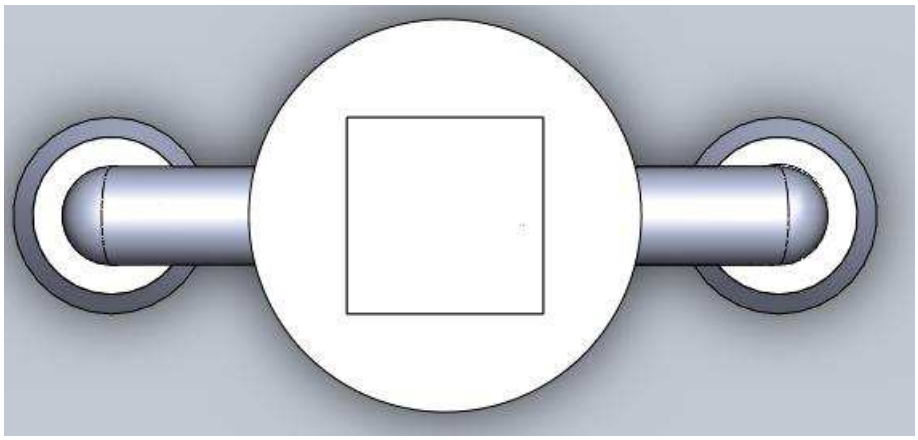

Figure 3.3. Top view of the model

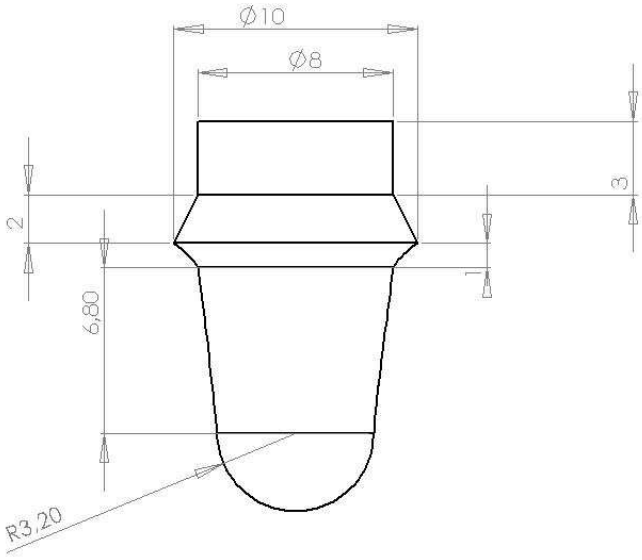

Figure 3.4. Technical drawing of the implant

3.1.2. Rapid Prototyping Procedure

Zprint software is used to generate rapid prototyping model. ZPrinter 310 Plus is the rapid prototyping machine. Figure 3.5 shows rapid prototyping model in Zprint software.

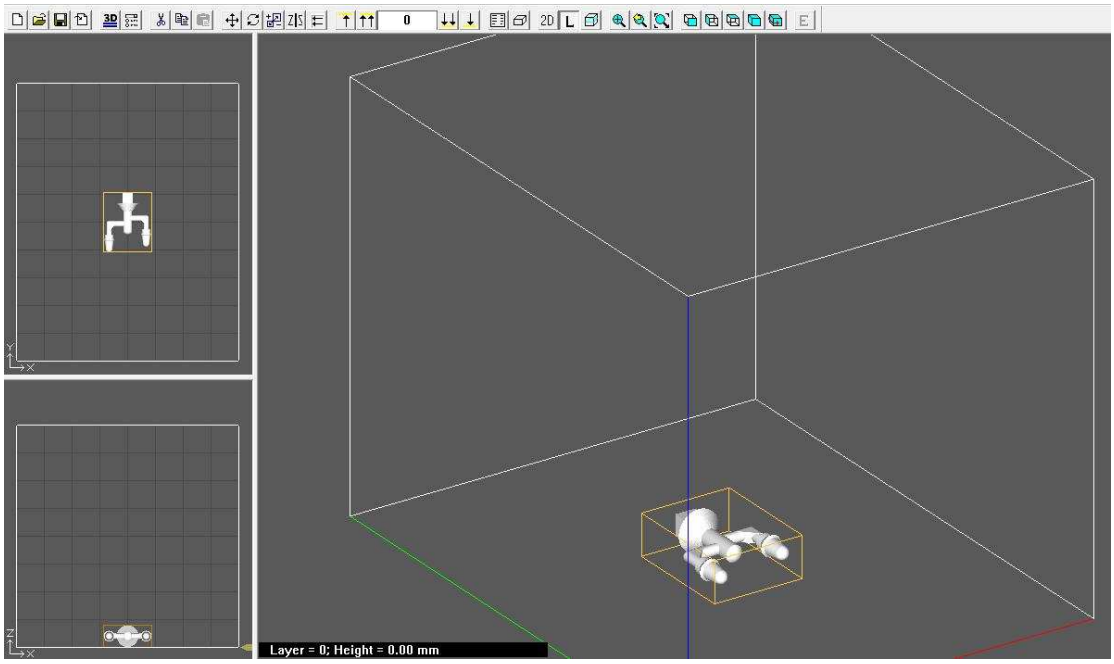

Figure 3.5. Rapid prototyping model in Zprint software

Rapid prototyping finished model (by using zp®131 powder, a high performance composite) is shown in Figure 3.6 and Figure 3.7.

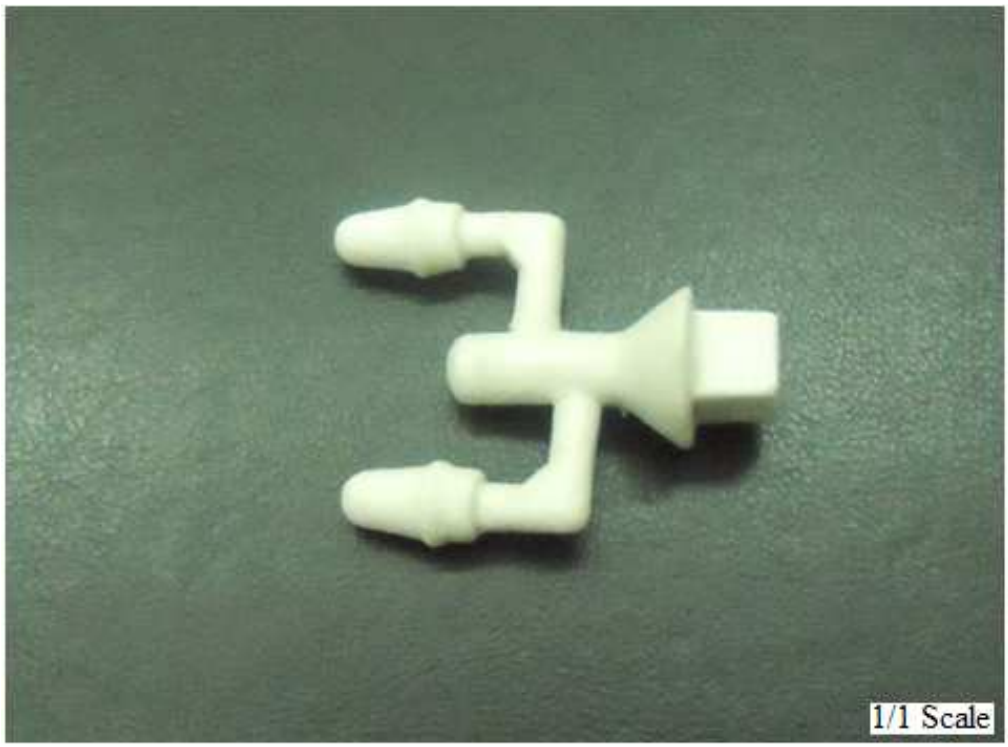

Figure 3.6. Rapid prototyping model, first view

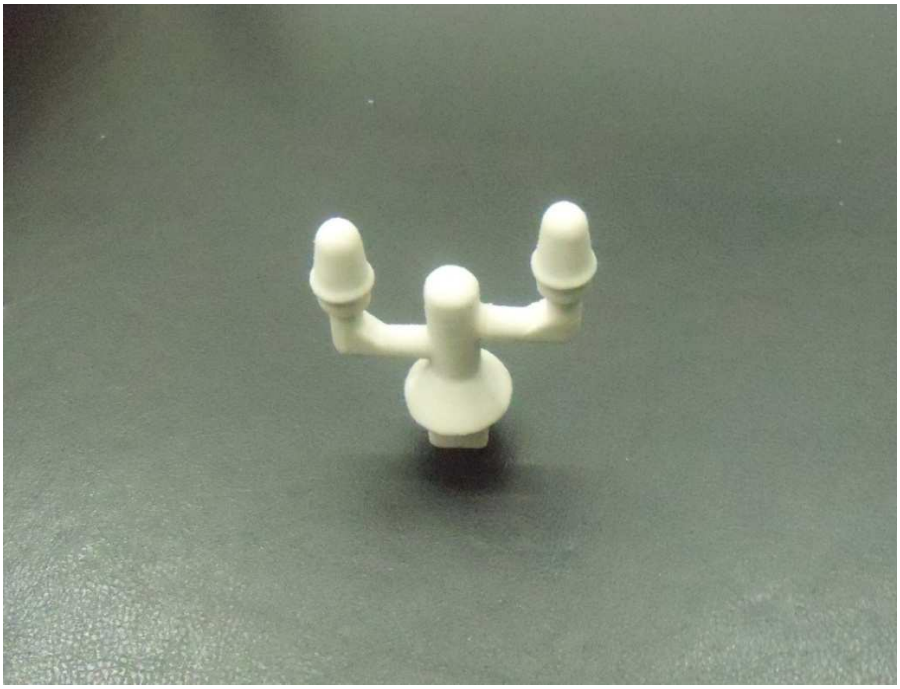

Figure 3.7. Rapid prototyping model, second view

3.1.3. Silicone Moulding

After rapid prototyping, the model is put in a cylinder like in the investment casting. Then, silicone is mixed with hardener. After 5 minutes, silicone is poured into the model surrounded with cylinder. Silicone mould is shown in Figure 3.8.

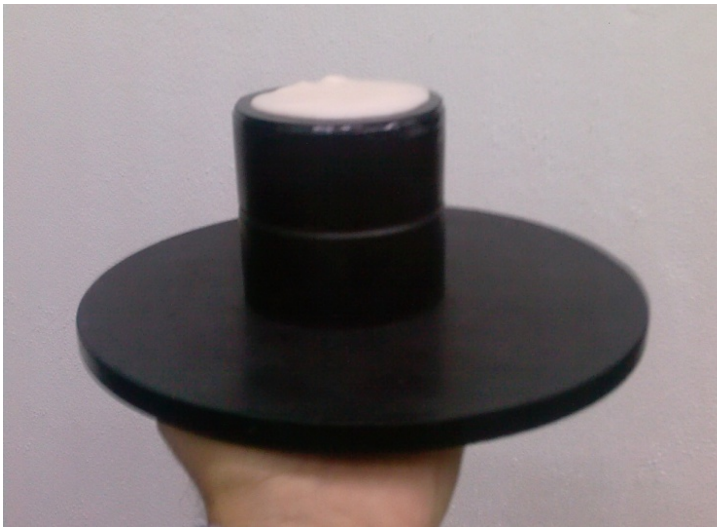

Figure 3.8. Silicone mould

After one day, cylinder is removed and silicone mould is cut into two parts. Rapid prototyping model is removed from silicone mould. Silicone mould and the rapid prototyping model are illustrated in Figure 3.9.

Figure 3.9. Silicone mould and rapid prototyping model

3.1.4. Wax Modelling

Wax is used in silicone moulds to make wax implant models. Wax model is shown in Figure 3.10.

Figure 3.10. Wax model

Wax model and silicone mould is illustrated in Figure 3.11.

Figure 3.11. Wax model and silicone mould

Figure 3.12 shows wax model and its main rapid prototyping model.

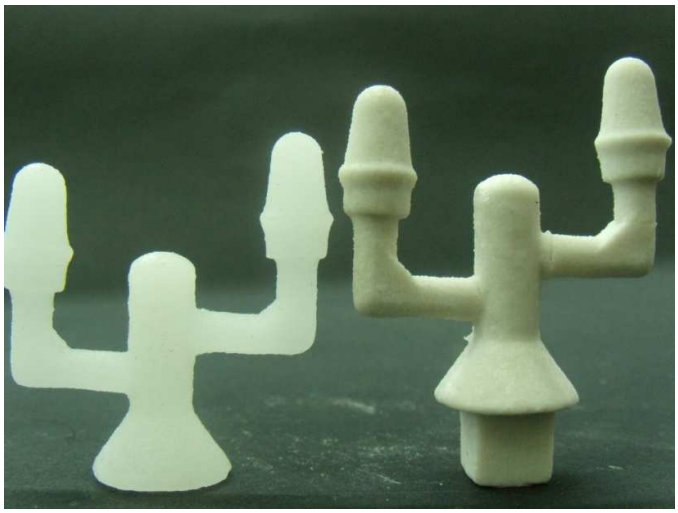

Figure 3.12. Wax model and its main rapid prototyping model

3.1.5. Centrifugal Casting Mould

For titanium casting, Rematitan® Plus (the DENTAURUM Group, Germany) is used as an investment material. For 250 grams of Rematitan Plus, 40 ml mixing liquid is used to prepare one mould. Rematitan® Plus and its mixing liquid is shown in Figure 3.13.

Figure 3.13. Rematitan® Plus and its mixing liquid

By using the purest fire proof components (purity > 99%) and special additives in the Rematitan® Plus investment, the reaction between forming material and molten titanium is widely minimized [75].

For making mould, first of all, implant wax model attached to a clean surface. Then a muffle is attached to that area. That provides Rematitan® Plus slurry a certain shape (Figure 3.14).

Figure 3.14. Wax and muffle on the clean surface

After then, slurry is poured into the muffle. For one day, wax and slurry stays inside the muffle. At last, muffle is put into a furnace for evaporating wax inside the mould and making the mould ready for centrifugal casting. Figure 3.15 and 3.16 show final mould (wax and the investment material) before entering the furnace.

Figure 3.15. Final mould, first view

Figure 3.16. Final mould, second view

Drying procedure for Rematitan® Plus is shown in Figure 3.17.

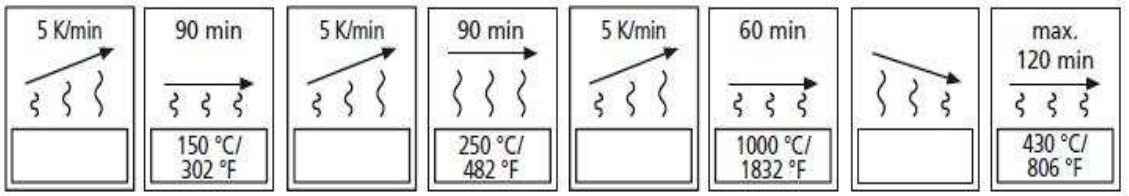

Figure 3.17. Drying procedure for Rematitan® Plus [76]

All the moulds are dried and they are ready for centrifugal casting (Figure 3.18).

Figure 3.18. Dried moulds

3.2. Centrifugal Casting Process

In Boğaziçi University Materials Science and Manufacturing Technologies Laboratory, High Frequency Casting Unit ”VACUTHERM 3,3 TITAN” exists as a centrifugal casting machine.

Its centrifugal speed is between 0 – 500 rpm. Maximum permissible water pressure for the machine is 5 bar. Protective gas flow is max. 1,5 l/min and maximum permissible protective gas pressure is about 2,5 bar. Cooling water rate is minimum 6 l/min. Maximum 80 g. Co, Cr and 40 g. of Ti can be melted in the machine. Ceramic and ceramic with graphite insert can be used as a crucible material. In the production of Ti, Ti should be pre-heated for 20 – 30 seconds in step 1 (67 per cent power). Then Step 2 (100 per cent power) must be used [77].

Figure 3.19 shows “VACUTHERM 3,3 TITAN” machine and Figure 3.20 is its casting arm [78].

Figure 3.19. VACUTHERM 3,3 TITAN [78]

Figure 3.20. Casting arm [78]

For Ti casting, ceramic crucible is used. Mould is put inside the casting arm of the machine and crucible is put (Figure 3.21 and Figure 3.22). Then the arm is closed. In all castings, mould preheat temperature is 500°C. For production, vacuum is done for some time and after that argon gas is given inside of the casting arm to purge it. Vacuum operation and argon gas purging is done for several times to make casting environment better (to have a suitable vacuum environment). There is an induction coil under the crucible and the casting machine works according the principle of a transformer, the induction melting process. This process is used for melting of Ti inside the crucible [77].

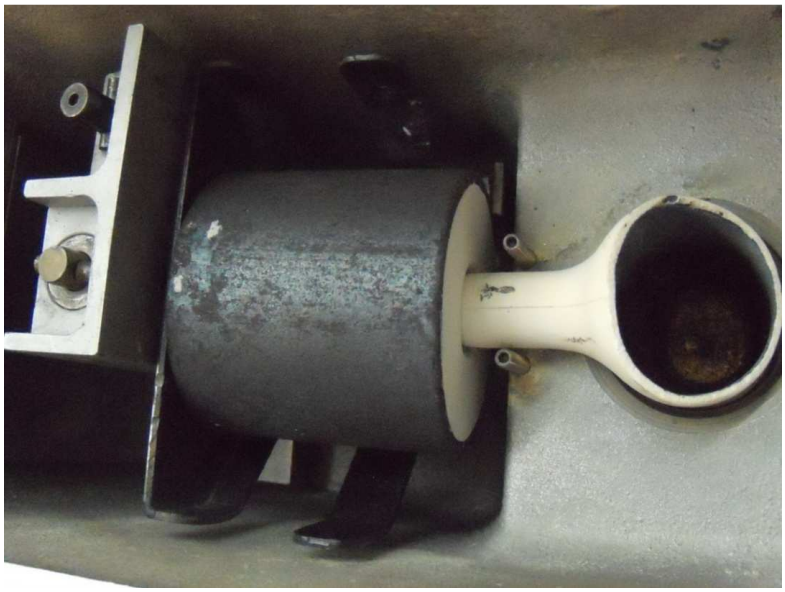

Figure 3.21. Mould and crucible

Figure 3.22. Mould and crucible inside the casting arm

Closed position of the casting arm can be seen in Figure 3.23.

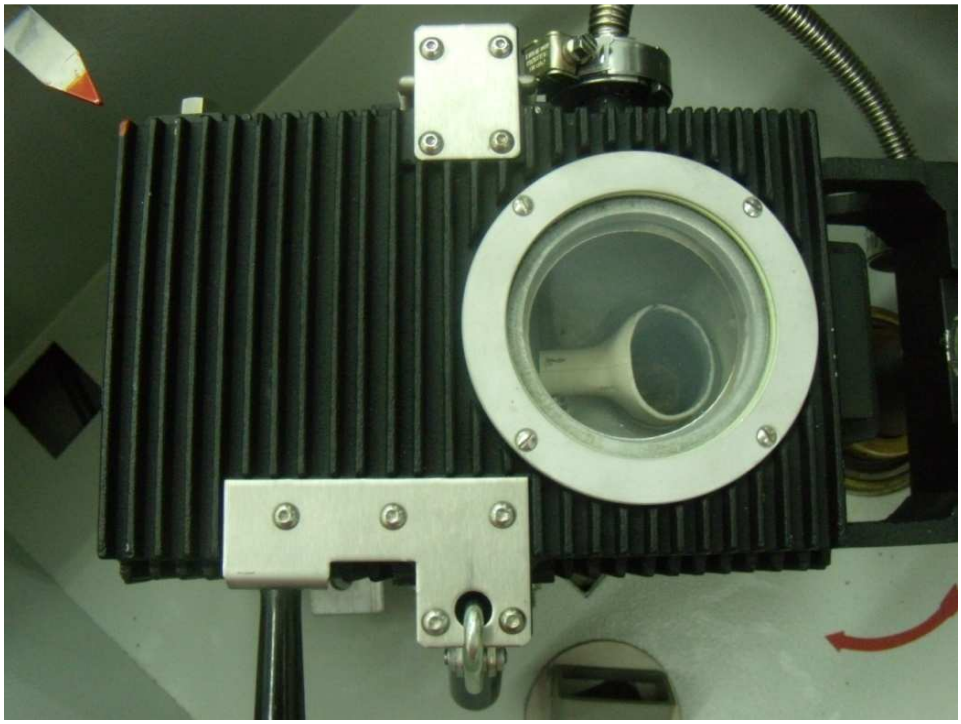

Figure 3.23. Closed casting arm

Casting is done with three different casting speeds and two different raise times: 500/1, 300/1, 200/2. Raise time is the parameter of reaching centrifugal speed in requested time. For example, 500/1 means that centrifugal speed of 500 RPM is reached in one second.

Cp Ti Grade 4 is used in the experiments. Of the four unalloyed grades, Grade 4 is the highest in oxygen content (0,4 weight per cent) and iron content (0,5 weight per cent) [13].

3.3. Dental Implant Specimens

“200 rpm and raise time 2” (200/2) casting parameters are not adequate enough to make casting and molten metal cannot go inside the mould. Molten metal stayed on the entrance of the crucible. The last condition of crucible after 200/2 casting can be seen in Figure 3.24.

Figure 3.24. Crucible after 200/2 casting condition

For 300/1, an empty muffle after casting, broken investments and the product is shown in Figure 3.25.

Figure 3.25. An empty muffle after casting, broken investments and the product (300/1)

Uncleaned and cleaned final products (300/1) are shown in Figure 3.26, 3.27 and 3.28 respectively.

Figure 3.26. Final product 300/1 (uncleaned)

Figure 3.27. Final product 300/1 (cleaned, front view)

Figure 3.28. Final product 300/1 (cleaned, top view)

The crucible used in 300/1 experiment can be seen in Figure 3.29.

Figure 3.29. The crucible after casting (300/1)

500/1 mould after casting is illustrated in Figure 3.30. Investment before breaking and the product inside of the investment are seen.

Figure 3.30. 500/1 mould after casting

Cleaned final product (500/1) is shown in Figure 3.31.

Figure 3.31. Final product 500/1 (cleaned)

3.4. Annealing Process

Implants were cut by using “Metkon Finocut Low Speed Precision Cutter” (manufactured in Bursa, Turkey). Sliced product (500/1) can be seen in Figure 3.32.

Figure 3.32. Sliced product (500/1)

Four sliced implants are obtained (two from 300/1, two from 500/1). One specimen from each casting operation (300/1 and 500/1) is taken for annealing process. Two

implants are annealed for an hour in 700°C. Then, all four specimens (300/1 as cast (AC), 300/1 annealed (AN), 500/1 AC and 500/1 AN) were metallographically prepared to see microstructure and to determine microhardness values. Table 3.1 shows process conditions of all specimens.

Table 3.1. Process conditions of all specimens

Specimen	Centrifugal Speed (RPM)	Anneal	Annealing Temperature (°C)	Annealing Time (h)
1	300	No	-	-
2	300	Yes	700	1
3	500	No	-	-
4	500	Yes	700	1

3.5. Metallographic Preparation of Titanium

Quality control of titanium production is extremely important. This is why metallography of titanium is an integrated part of quality control of titanium, from monitoring the initial production process, to porosity checks on cast parts and controlling heat treatment processes [79].

3.5.1. Mounting

For smaller manufactured parts that need to be mounted, such as wires or fasteners, hot compression mounting with phenolic resin or cold mounting with slow curing epoxy are recommended [79]. Four implant specimens are mounted by using hot compression mounting method in the study.

3.5.2. Grinding and Polishing

The first step is grinding with silicon carbide paper. The grit depends on the surface roughness and size of the samples to be prepared. For Ti, 240, 600 and 1200 grit silicon carbide papers were used. Grinding is followed by polishing step on a hard surface. 3 μm and 1 μm polish cloth were used respectively while polishing [79].

3.5.3. Etching

The most common chemical etchant for titanium is Kroll's reagent:

- 100 ml water
- 1-3 ml hydrofluoric acid
- 2-6 ml nitric acid

This etchant colors the β phase dark brown [79]. It is used on the four specimens of the study.

4. RESULTS AND DISCUSSION

4.1. Microstructure Examination

4.1.1. 300/1 As Cast Specimen

Figure 4.1 shows microstructure of 300/1 AC specimen (optical microscope – Nikon Eclipse LV150).

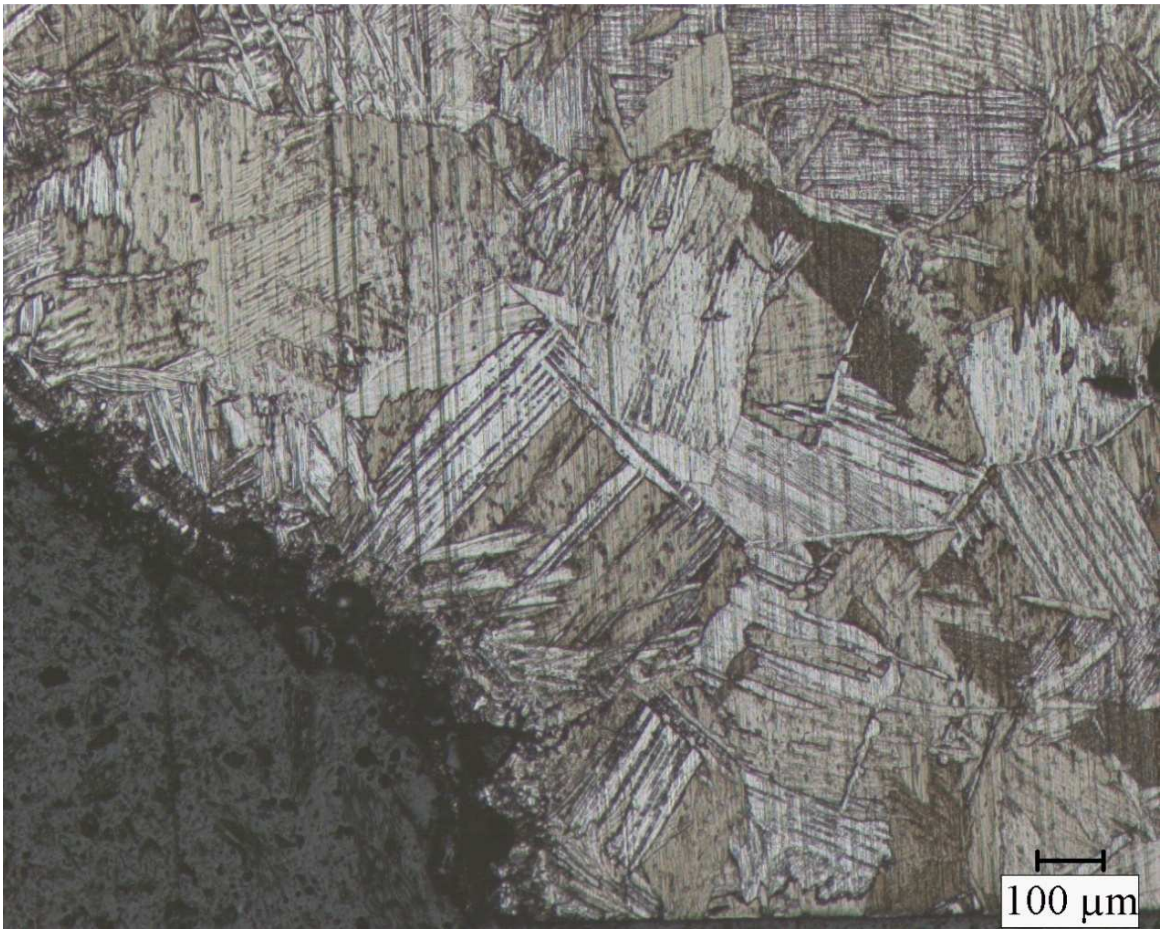

Figure 4.1. Microstructure of 300/1 AC specimen

From Figure 4.1, it can be seen that the microstructure of 300/1 AC specimen are composed from α grain structure and lamellic structure that is the α formed from β which is called Widmanstätten structure.

This lamellic α structure is acicular formed α. Because of rapid cooling, this metastable feather like acicular α structure forms.

β structure cannot be formed fully, rapid cooling occurs and α structure starts to grow. So, there are some acicular structures between the full growth α structures.

α grain boundary between two α grains is illustrated in Figure 4.2. Black arrow shows the grain boundary.

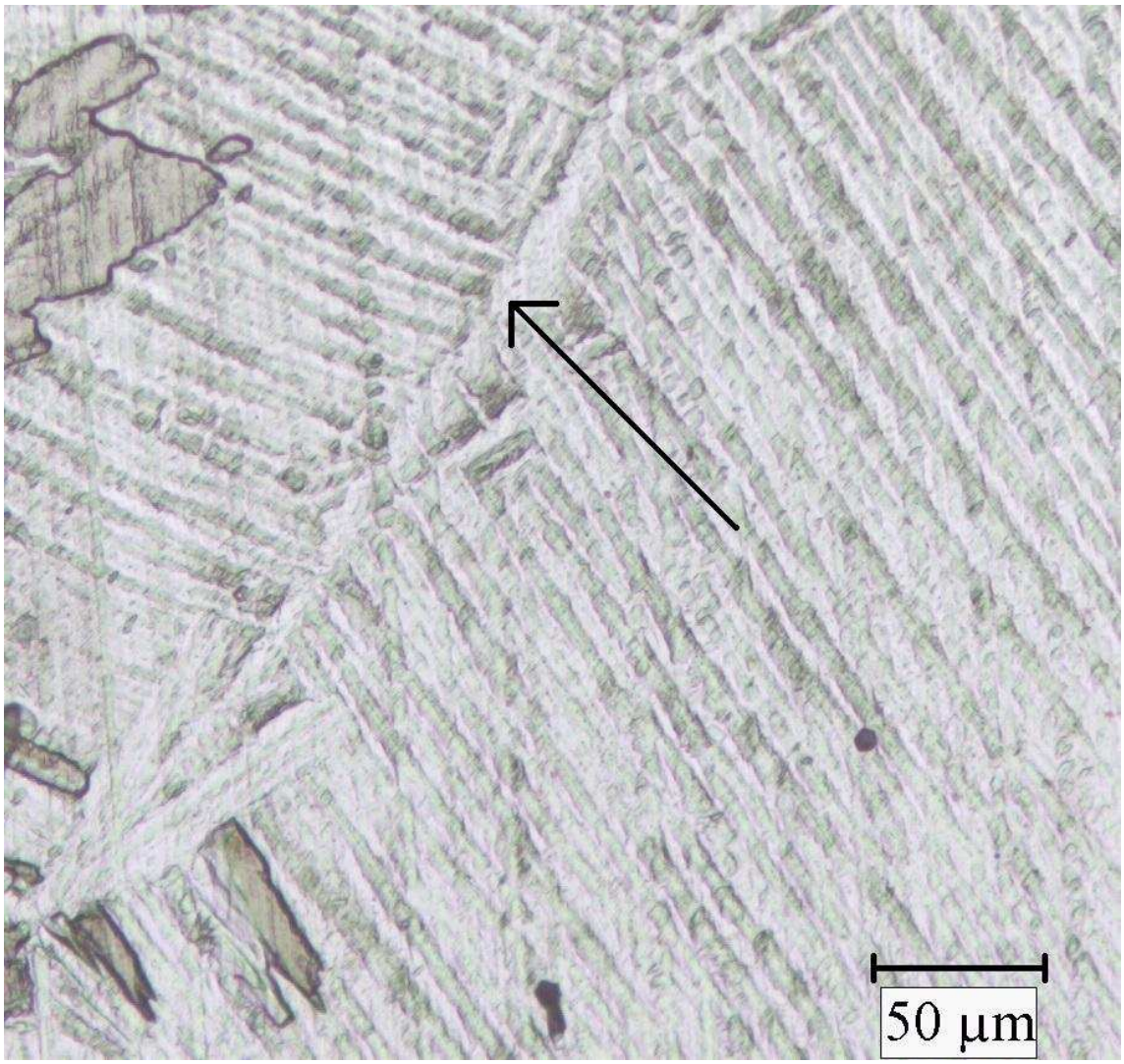

Figure 4.2. α grain boundary between two α grains

In the center part of the specimen, more equiaxed α grains are seen because of slower cooling. Amount of the acicular α structure is lower in this part (Figure 4.3).

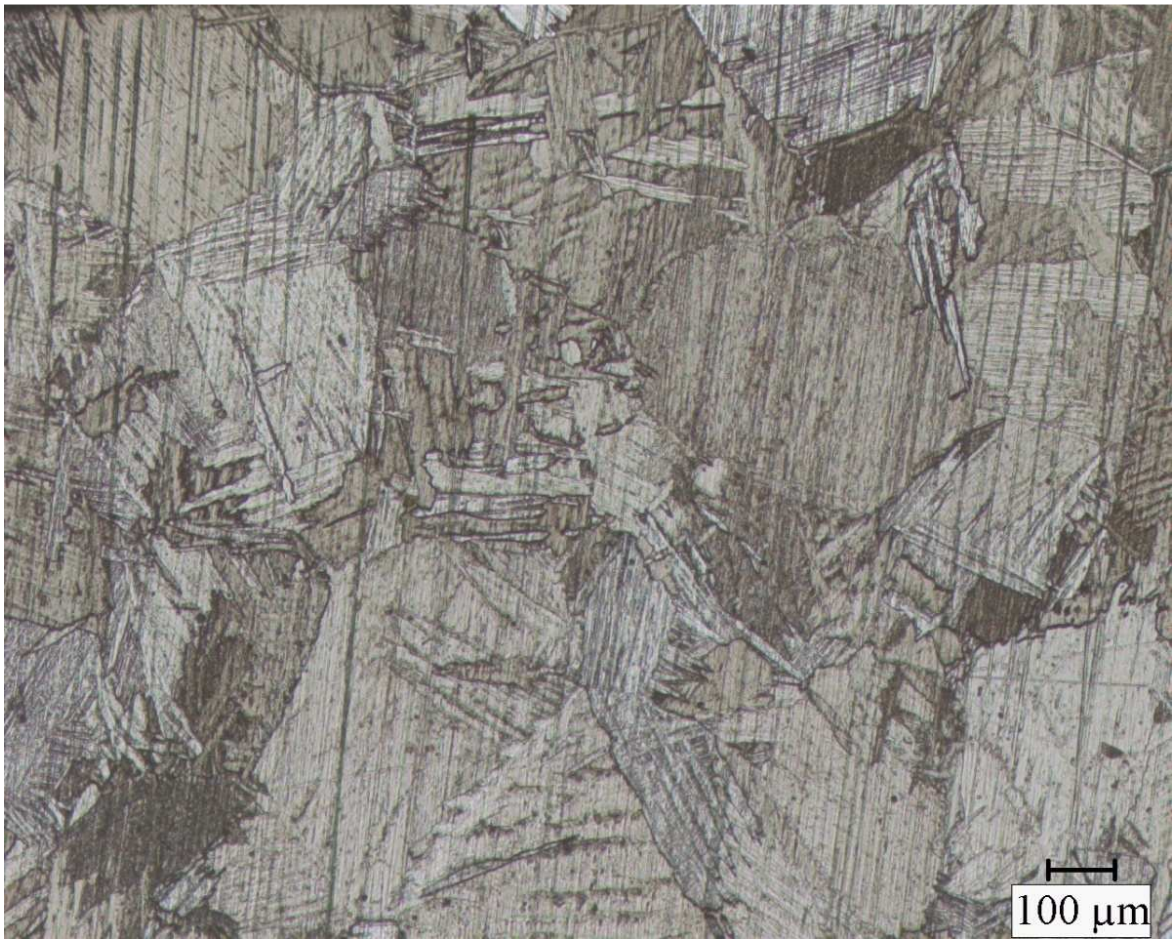

Figure 4.3. Microstructure of the center part of the specimen

The results agree with the results from the literature [13, 14, 15].

4.1.2. 300/1 Annealed Specimen

Annealing is done at 700°C for 1 hour. 300/1 annealed (AN) specimen is illustrated in Figure 4.4.

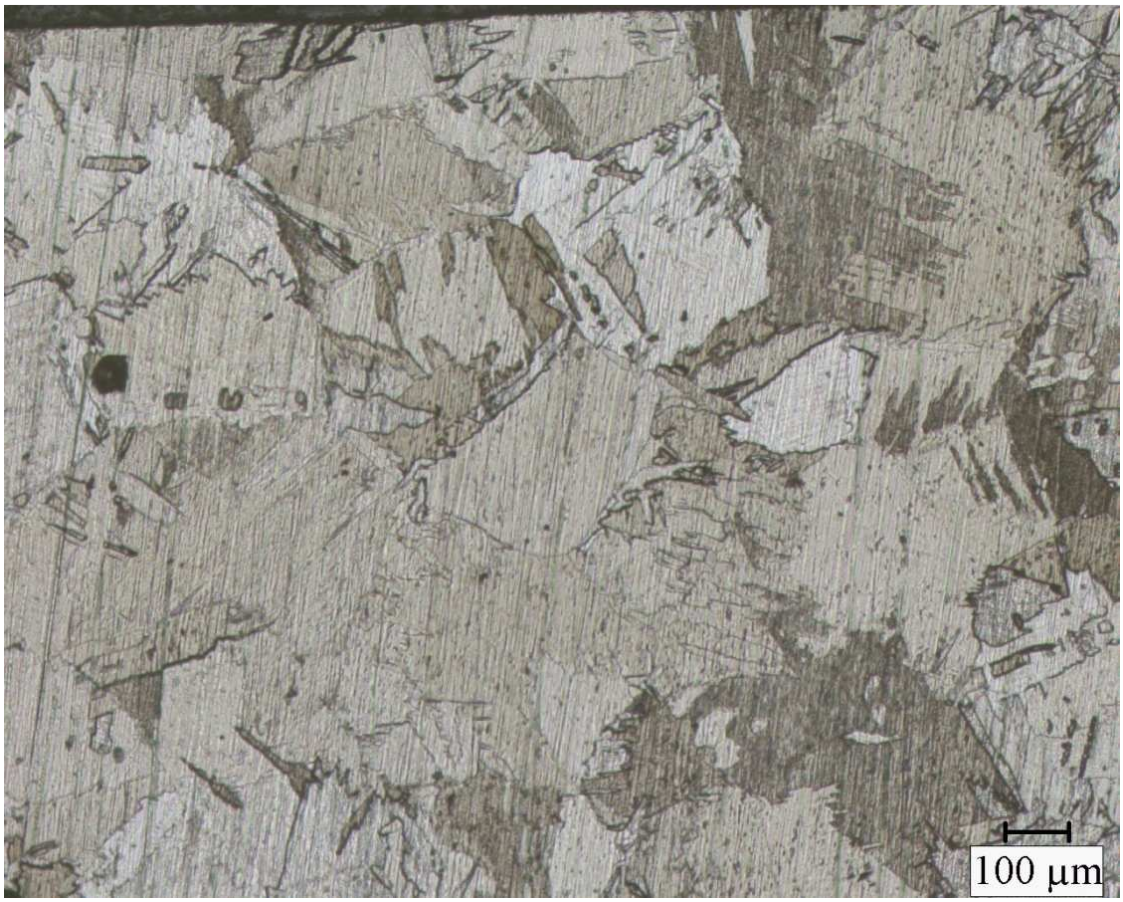

Figure 4.4. 300/1 AN specimen

After annealing, more equiaxed grains are seen in the microstructure of the specimen. Acicular α phases transformed to α phase in the annealing process. A small amount of porosity is also seen in the figure.

Figure 4.5 shows microstructure near the surface of the annealed specimen. It can be seen that most of the acicular α phase is changed. α grains are formed.

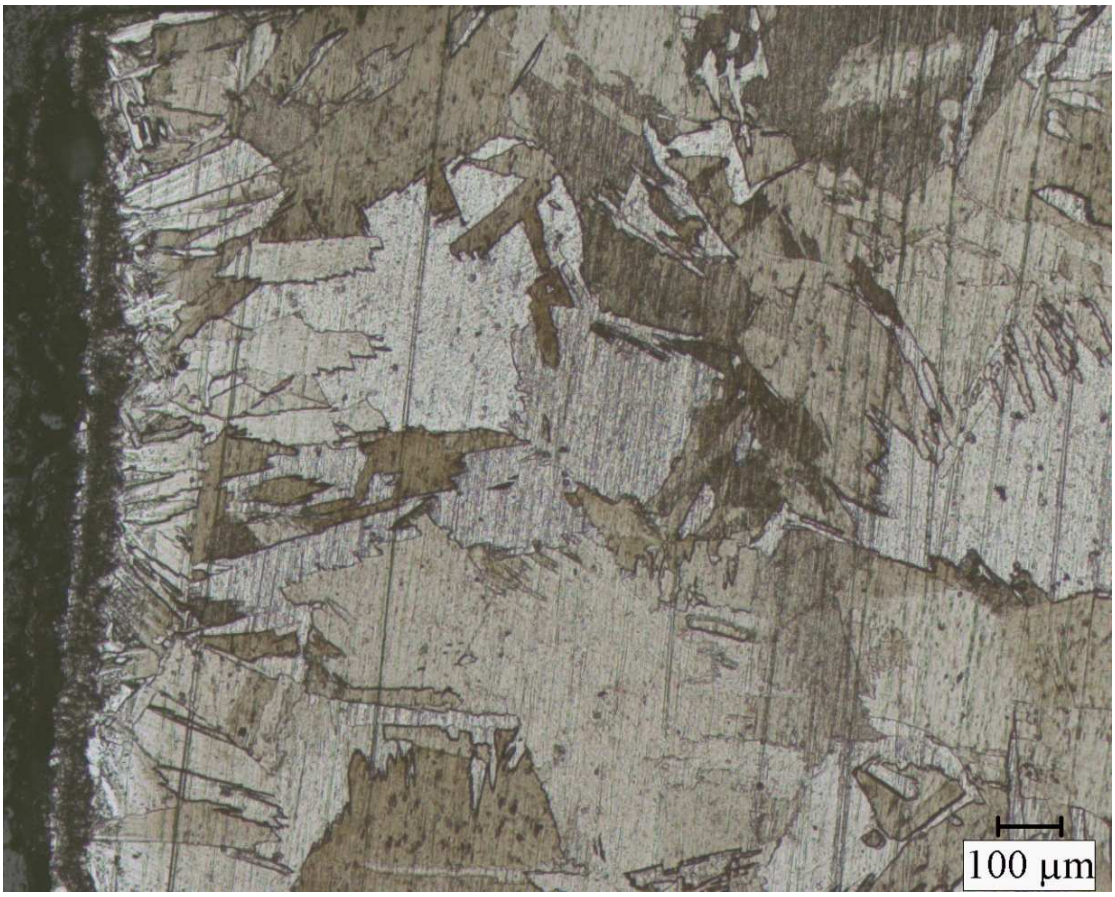

Figure 4.5. Microstructure near the surface of the annealed specimen

The findings agree with results from the literature [13].

4.1.3. 500/1 As Cast Specimen

Like 300/1 AC specimen, 500/1 AC specimen are composed from α structure and acicular plate–like α structure. This structure is also formed because of rapid cooling (Figure 4.6). Acicular α is also seen near the surface (Figure 4.7).

The results agree with the results from the literature [13, 14, 15].

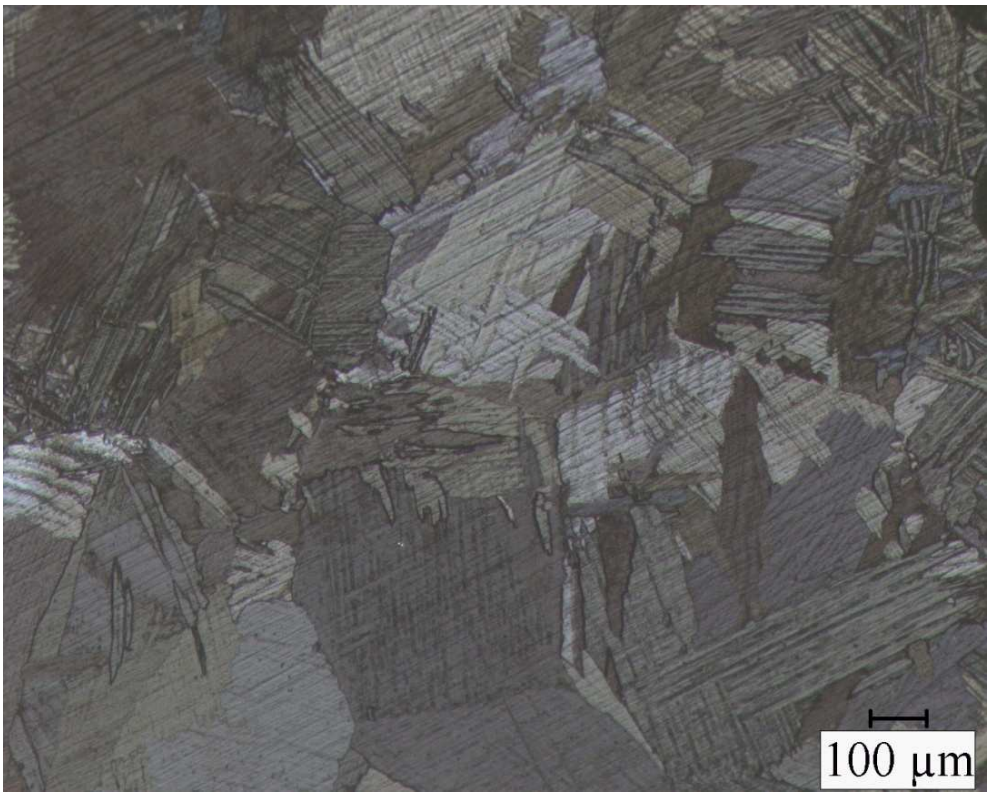

Figure 4.6. Microstructure of 500/1 AC specimen

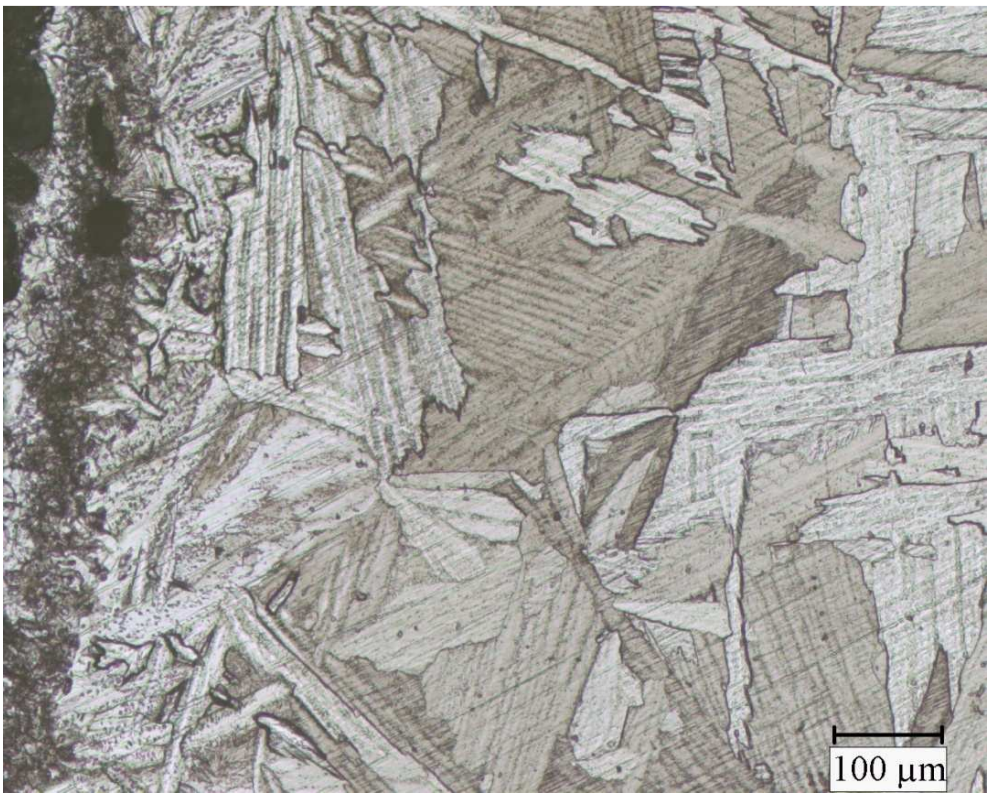

Figure 4.7. Microstructure near the surface of the specimen

4.1.4. 500/1 Annealed Specimen

Like 300/1 AN specimen, after annealing at 700°C (1 hour), 500/1 AN specimen has equiaxed α microstructure (Figure 4.8).

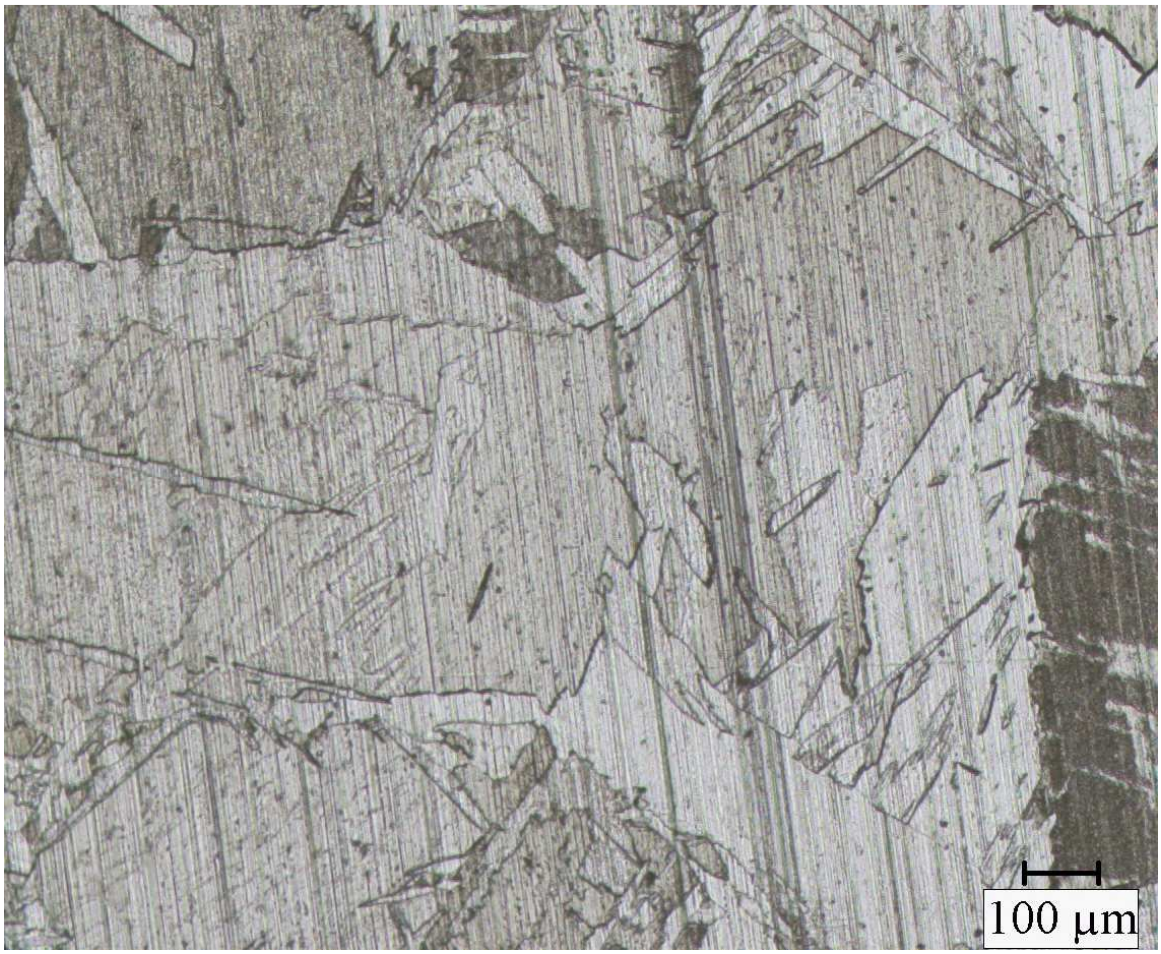

Figure 4.8. 500/1 AN specimen

Near the surface, most of the acicular α structure changed to α structure (Figure 4.9). The results agree with the findings from the literature [13].

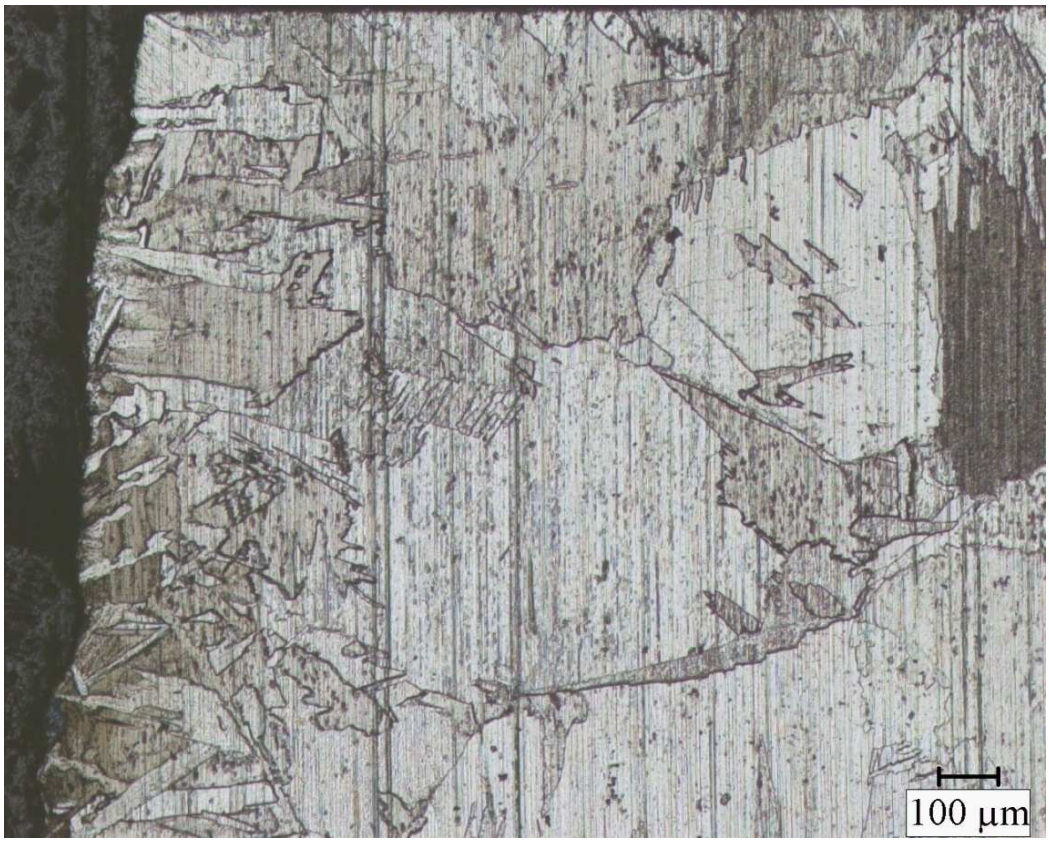

Figure 4.9. Microstructure of the 500/1 AN specimen near the surface

4.2. Microhardness Test

Microhardness test is done for each specimen in Shimazdu Microhardness Tester. Vickers test method is used. The distance between each indentation is 500 μm. If there is any defect, measurement is done a bit far from the defect. 200 gf is used as force. 8 tests are done on three different areas for every specimen (Upper part, largest diameter and bottom part). Each implant is compared in itself and then all implants are compared.

Microhardness test is done under ASTM Standard E 384 – 99. Hardness test areas can be seen in Figure 4.10.

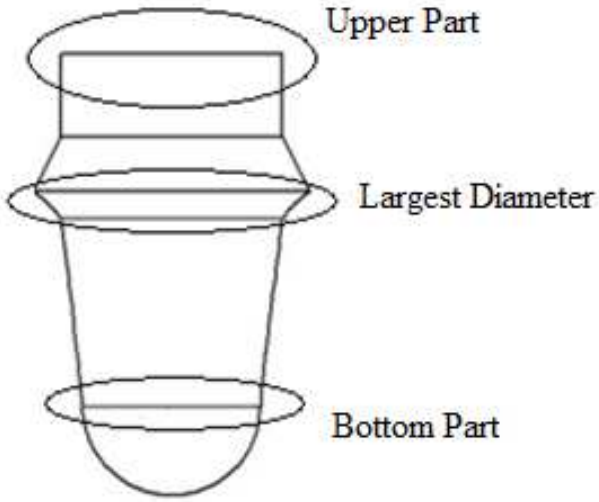

Figure 4.10. Hardness test areas

4.2.1. 300/1 As Cast Specimen

As mentioned before HV can be calculated by Equation 2.8.

8 results are taken from each of three hardness test regions. Figure 4.11 shows microstructure of indentation in 300/1 AC specimen. Results for 300/1 AC specimen are illustrated in Table 4.1.

Table 4.1. Results for 300/1 AC specimen

300/1 AC	Maximum HV	Minimum HV	Average HV	SD
UP	337,80	266,14	301,79	23,30
LD	337,09	270,18	304,24	21,51
BP	332,06	236,15	283,24	31,65

As seen from results, average HV for BP is slightly lower than other parts. There isn't any significant HV change between LD and UP. It can be said that there is a significant change between the HV values for BP (worst SD). Figure 4.12 illustrates HV results for 300/1 AC specimen.

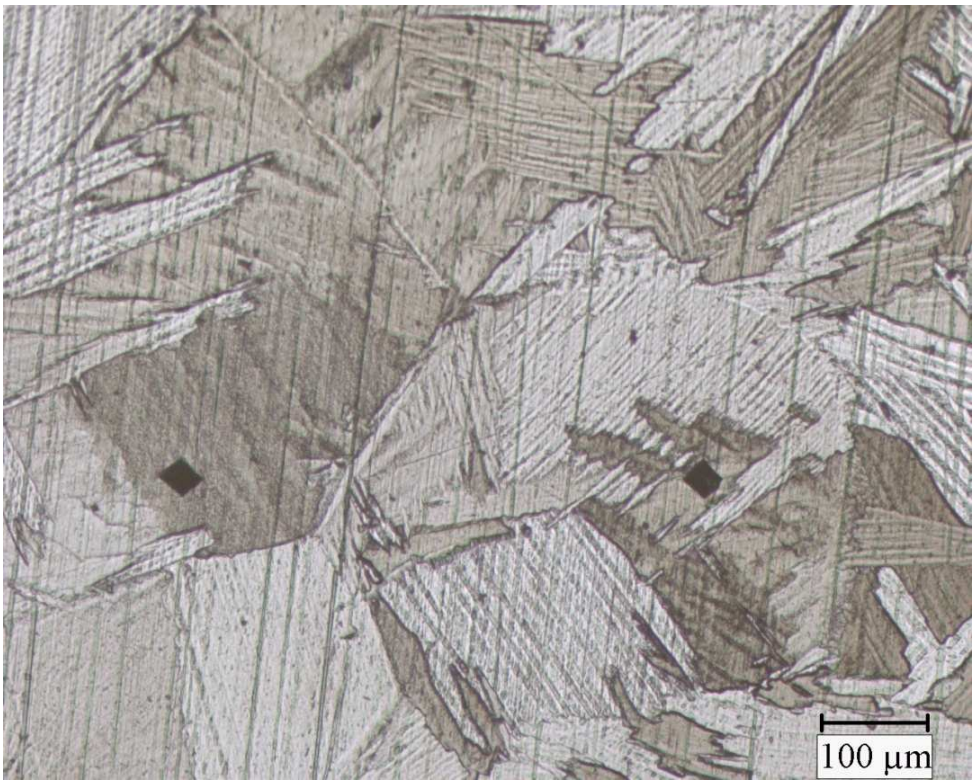

Figure 4.11. Microstructure of indentation in 300/1 AC specimen

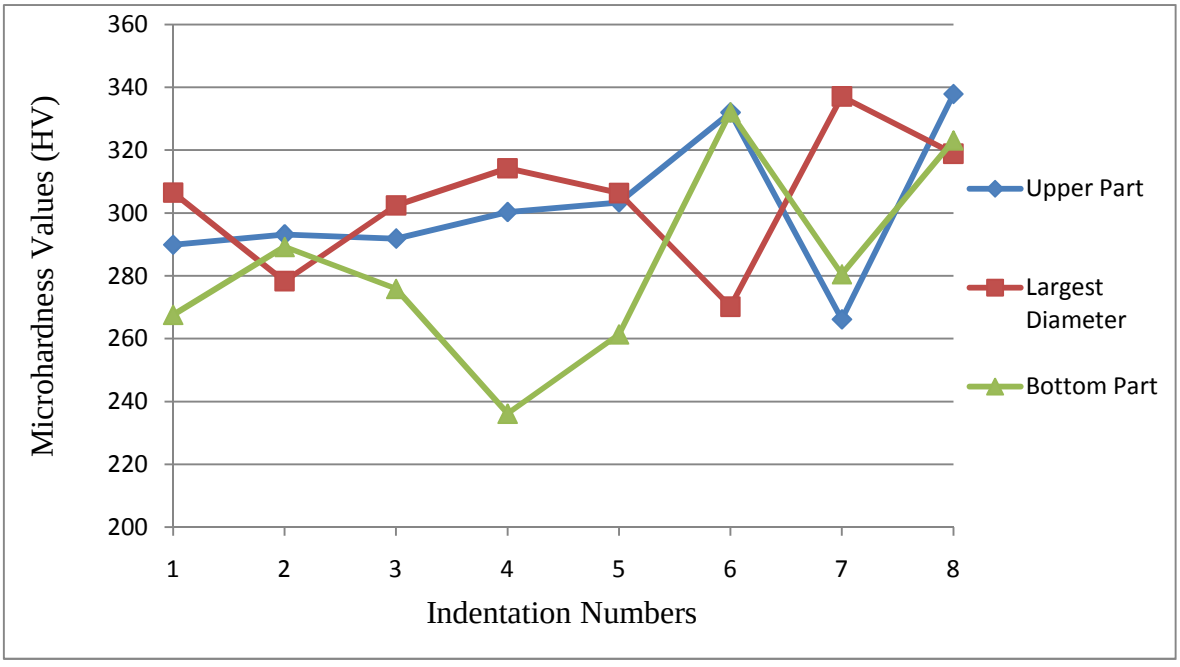

Figure 4.12. HV results for 300/1 AC specimen

4.2.2. 300/1 Annealed Specimen

Results for 300/1 AN specimen are illustrated in Table 4.2.

Table 4.2. Results for 300/1 AN specimen

300/1 AN	Maximum HV	Minimum HV	Average HV	SD
UP	382,35	288,41	326,42	34,03
LD	320,36	256,44	293,27	22,76
BP	300,35	283,41	292,60	5,63

As seen from results, HV for UP is higher than other parts. There isn't any significant HV change between LD and BP. BP has good HV distribution (best SD). There is an important change in the HV values for UP (worst SD). Figure 4.13 shows microstructure of indentation in 300/1 AN specimen and Figure 4.14 illustrates HV results for 300/1 AN specimen.

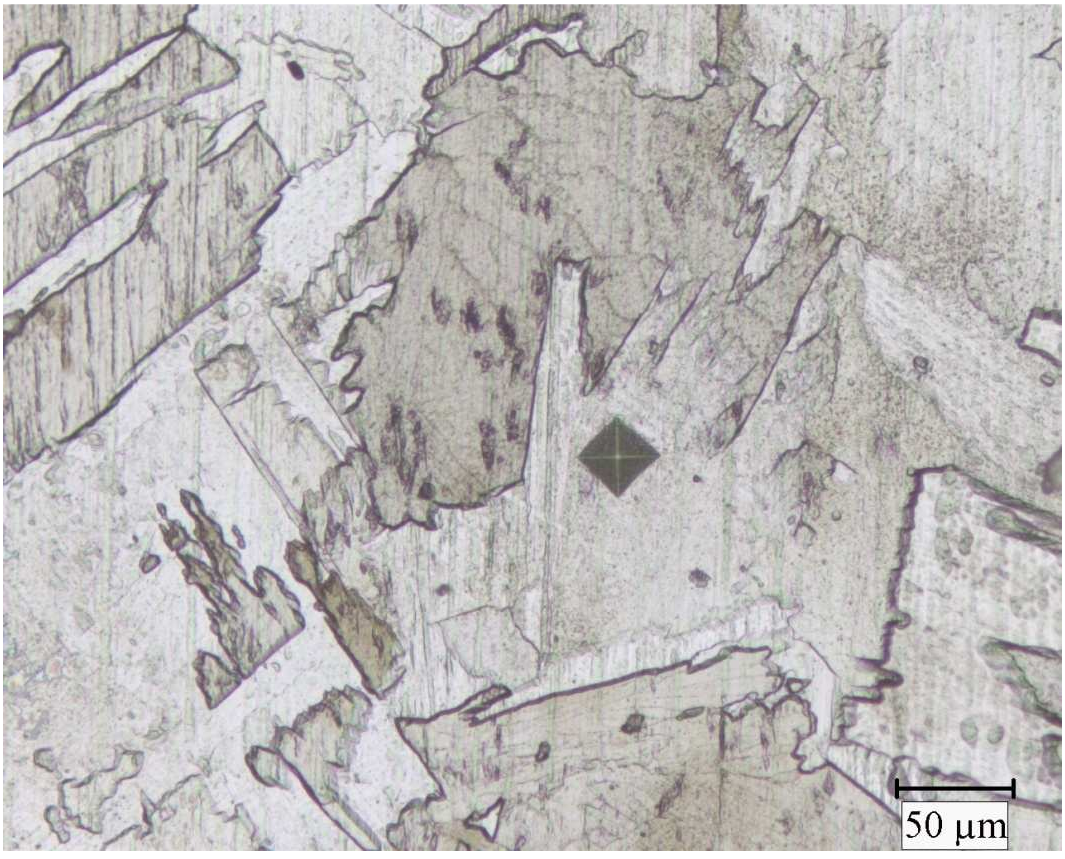

Figure 4.13. Microstructure of indentation in 300/1 AN specimen

Figure 4.14. HV results for 300/1 AN specimen

4.2.3. 500/1 As Cast Specimen

Results for 500/1 AC specimen are shown in Table 4.3.

Table 4.3. Results for 500/1 AC specimen

500/1 AC	Maximum HV	Minimum HV	Average HV	SD
UP	288,41	230,53	261,51	26,36
LD	306,16	266,14	288,02	14,36
BP	297,38	246,11	275,33	18,29

Average HV for LD is higher than other parts in this specimen and also this part has the best HV distribution. UP has the lowest average and also worst SD. Figure 4.15 illustrates microstructure of indentation in 500/1 AC specimen and Figure 4.16 shows HV results for 500/1 AC specimen.

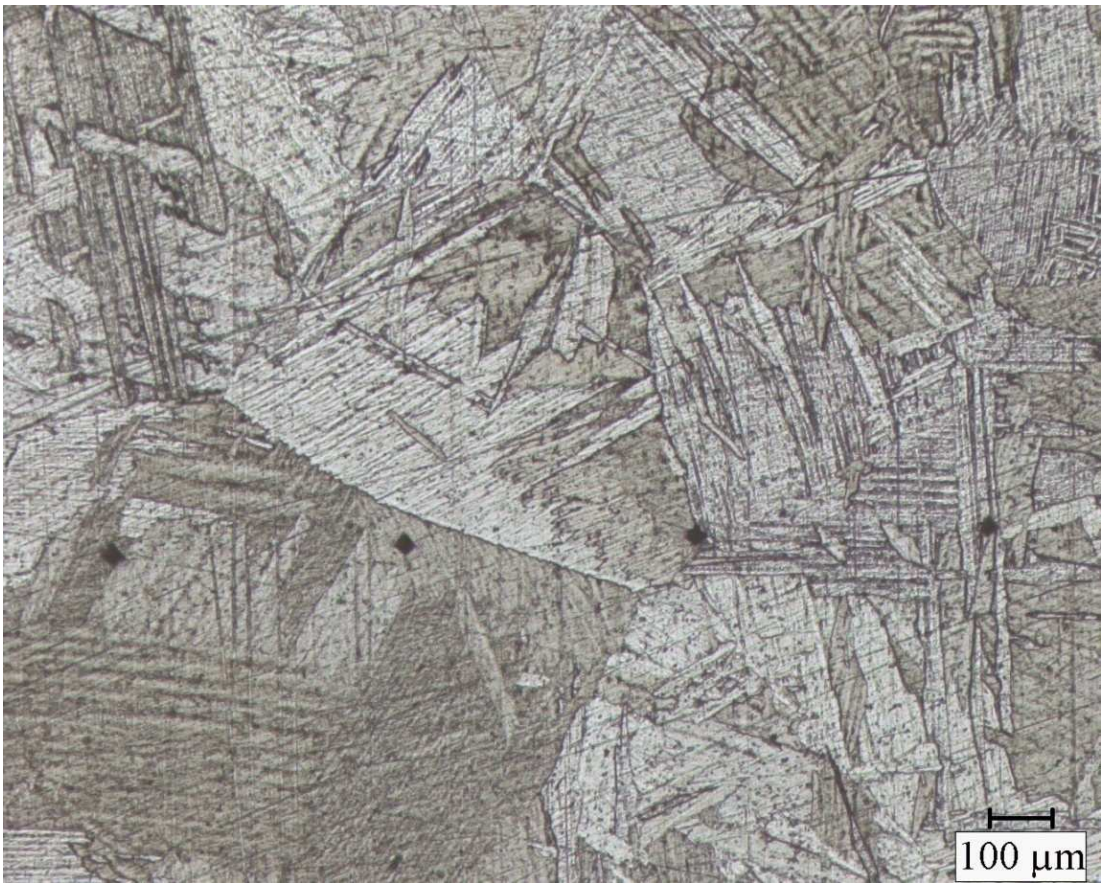

Figure 4.15. Microstructure of indentation in 500/1 AC specimen

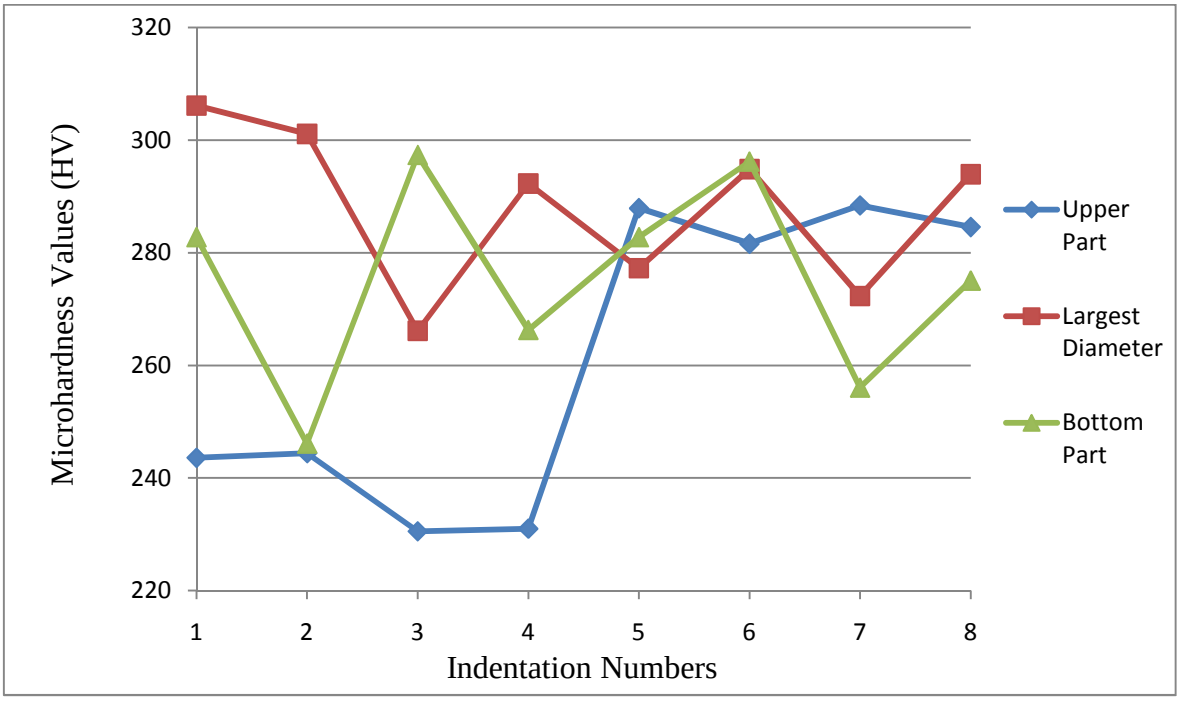

Figure 4.16. HV results for 500/1 AC specimen

4.2.4. 500/1 Annealed Specimen

Results for 500/1 AN specimen are illustrated in Table 4.4.

Table 4.4. Results for 500/1 AN specimen

500/1 AN	Maximum HV	Minimum HV	Average HV	SD
UP	307,75	262,27	279,00	17,26
LD	302,59	241,85	272,78	21,51
BP	318,58	269,60	290,56	14,66

Average HV values for UP and LD are very similar. Average HV for BP is higher than two other regions and this part has the best HV distribution (lowest SD). Figure 4.17 shows microstructure of indentation in 500/1 AN specimen. Figure 4.18 illustrates HV results for 500/1 AN specimen.

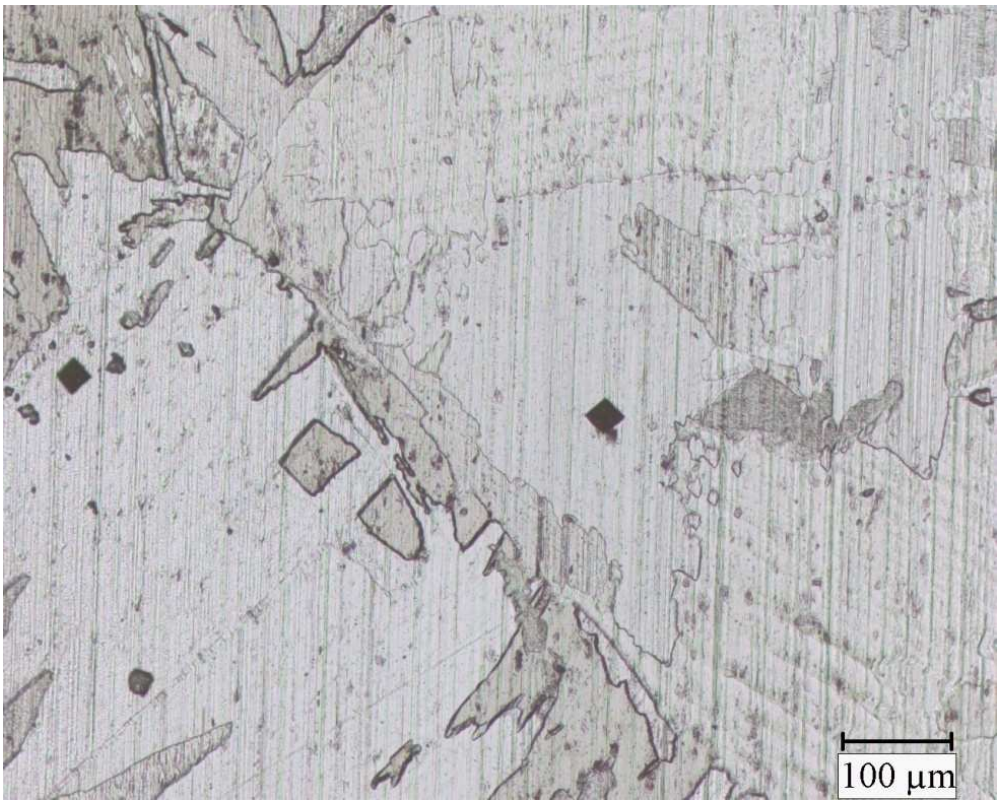

Figure 4.17. Microstructure of indentation in 500/1 AN specimen

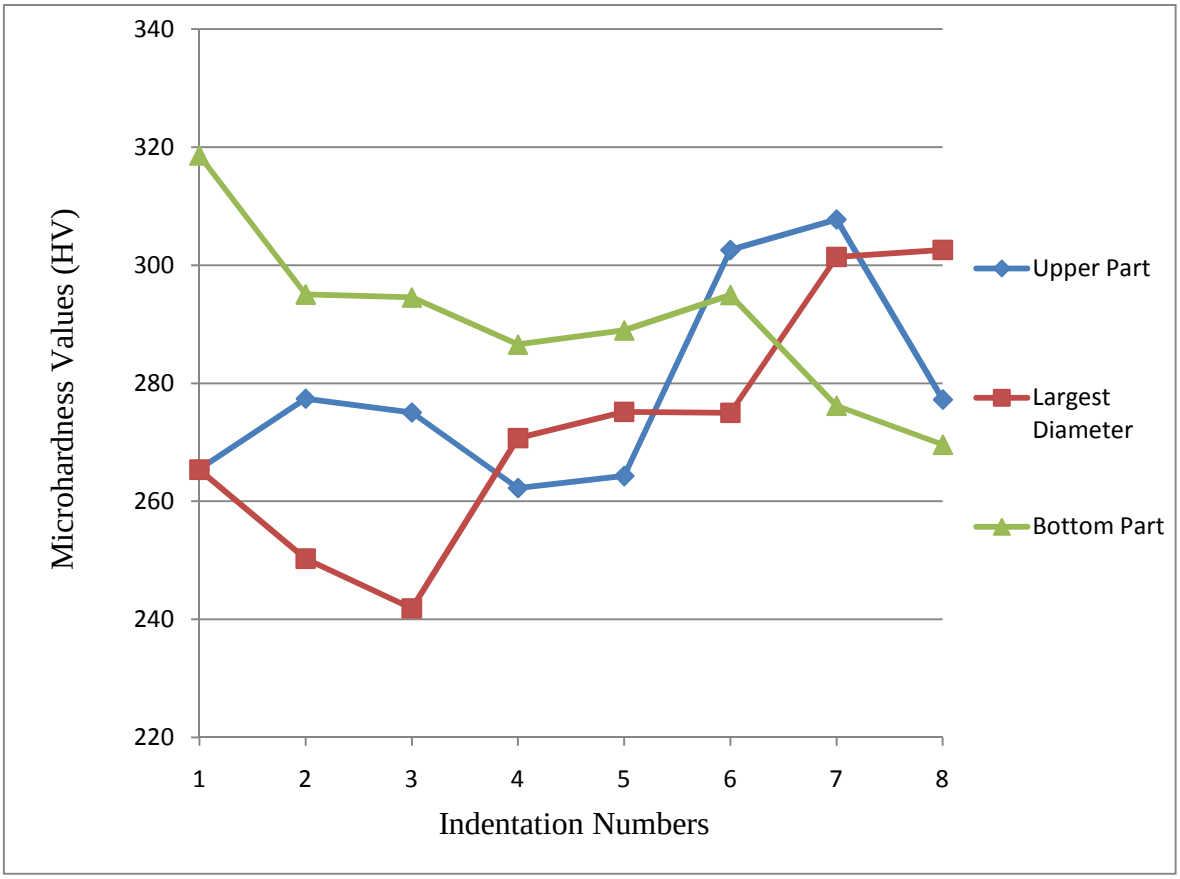

Figure 4.18. HV results for 500/1 AN specimen

4.2.5. Comparison Between Upper Parts

Results for UP of each specimen are shown in Table 4.5.

Table 4.5. Results for UP of each specimen

UP	Maximum HV	Minimum HV	Average HV	SD
300/1 AC	337,80	266,14	301,79	23,30
300/1 AN	382,35	288,41	326,42	34,03
500/1 AC	288,41	230,53	261,51	26,36
500/1 AN	307,75	262,27	279,00	17,26

It is found that 300/1 AN specimen has the highest average UP value (326,42). Also, this UP has the most unbalanced HV distribution (worst SD). 500/1 AN specimen has the best HV distribution. Figure 4.19 shows HV results for UP of each specimen.

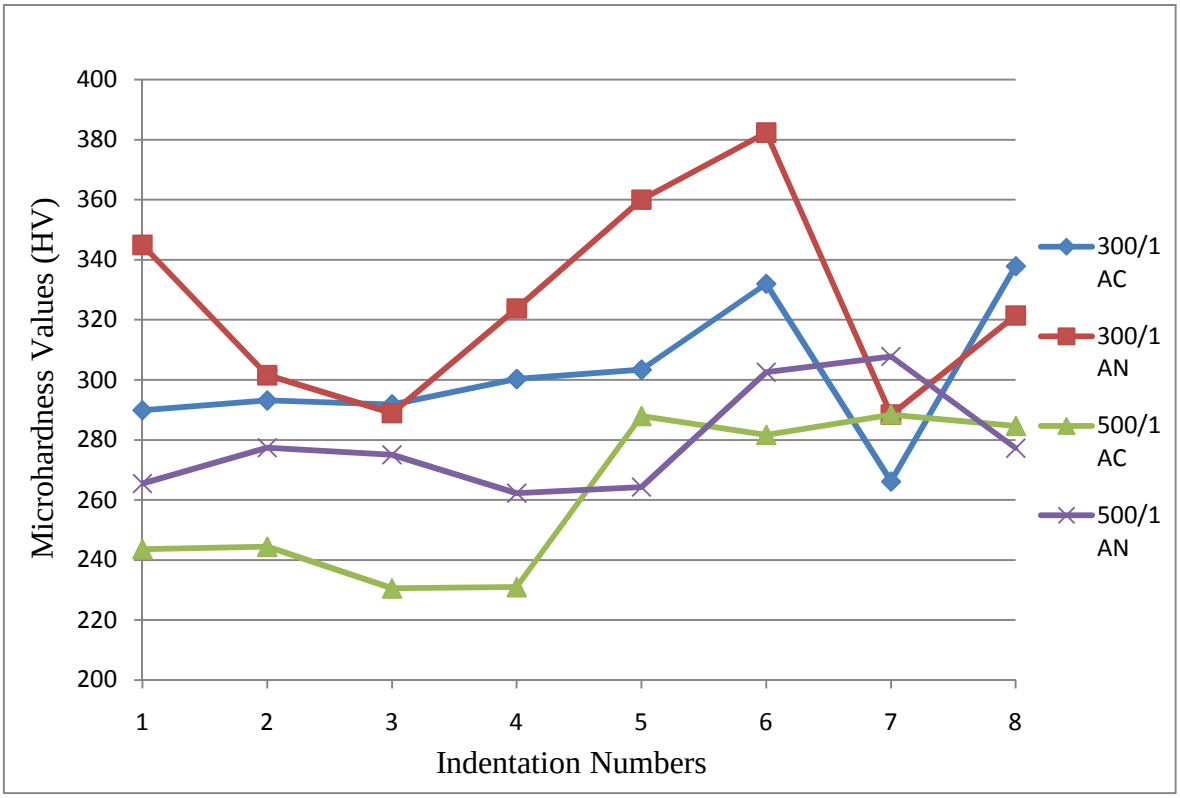

Figure 4.19. HV results for UP of each specimen

4.2.6. Comparison Between Largest Diameters

Results for LD of each specimen are illustrated in Table 4.6.

Table 4.6. Results for LD of each specimen

LD	Maximum HV	Minimum HV	Average HV	SD
300/1 AC	337,09	270,18	304,24	21,51
300/1 AN	320,36	256,44	293,27	22,76
500/1 AC	306,16	266,14	288,02	14,36
500/1 AN	302,59	241,85	272,78	21,51

300/1 AC specimen has the largest average LD value (304,24). All specimens have good HV distribution in this part. 500/1 AC specimen has better HV distribution than the others. Figure 4.20 illustrates HV results for LD of each specimen.

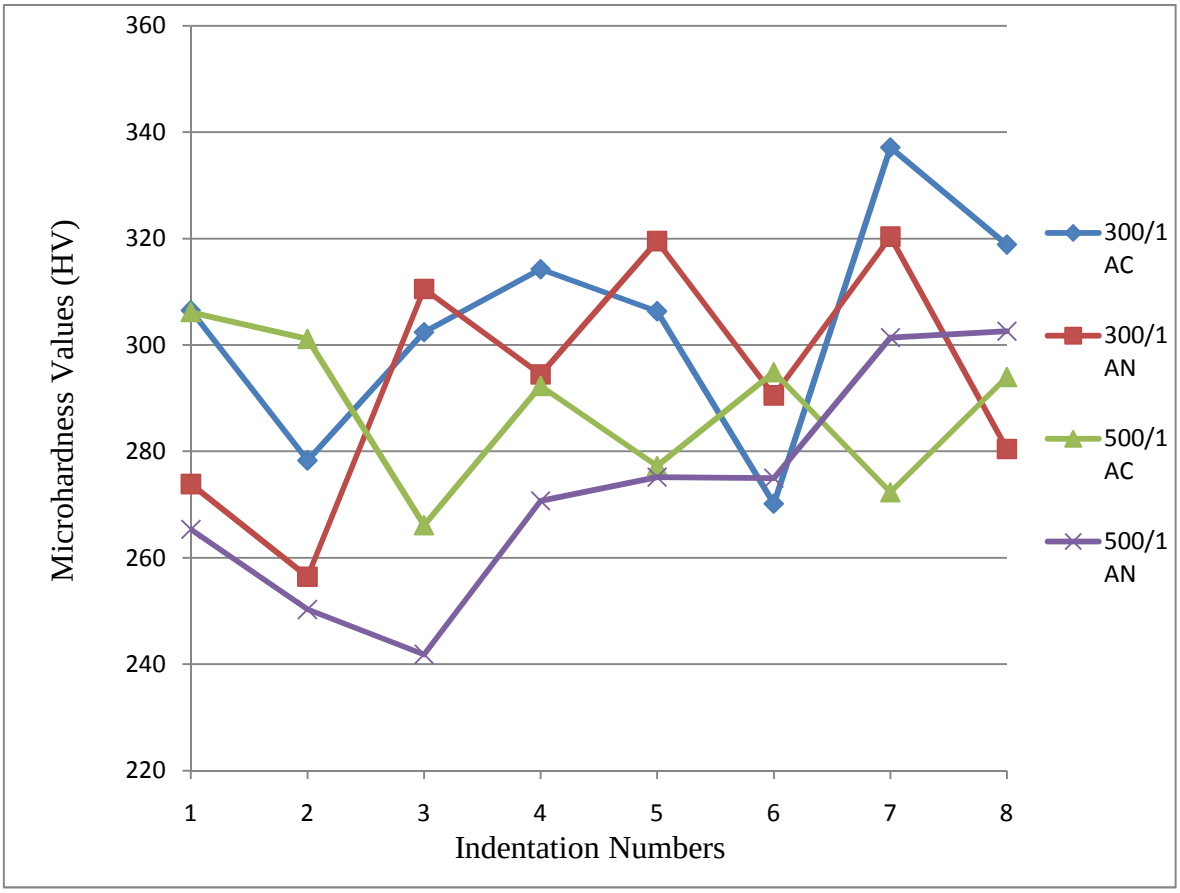

Figure 4.20. HV results for LD of each specimen

4.2.7. Comparison Between Bottom Parts

Results for BP of each specimen are illustrated in Table 4.7.

Table 4.7. Results for BP of each specimen

BP	Maximum HV	Minimum HV	Average HV	SD
300/1 AC	332,06	236,15	283,24	31,65
300/1 AN	300,35	283,41	292,60	5,63
500/1 AC	297,38	246,11	275,33	18,29
500/1 AN	318,58	269,60	290,56	14,66

300 AN has the highest BP value. But, there is not too much HV value difference between the BPs. AN implants have better HV distribution. Figure 4.21 shows HV results for BP of each specimen.

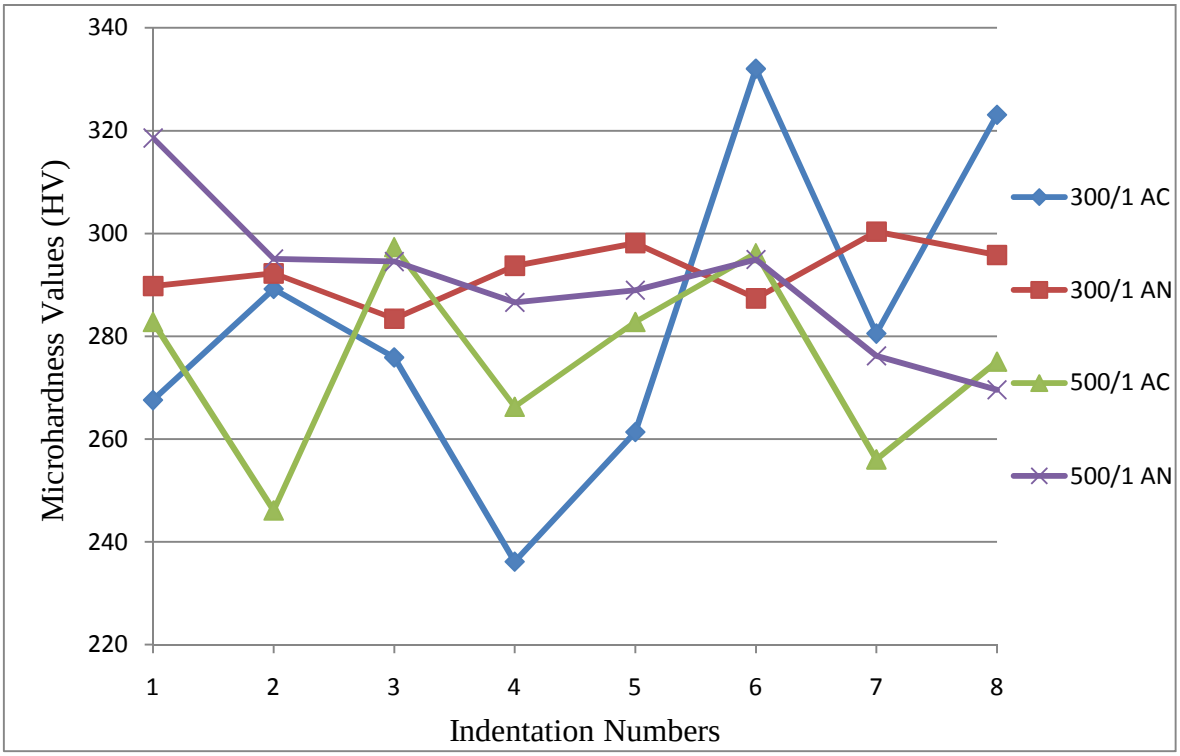

Figure 4.21. HV results for BP of each specimen

4.2.8. General Comparison

HV results for all implants are illustrated in Table 4.8.

Table 4.8. HV results for all implants

Specimens	Maximum HV	Minimum HV	Average HV	SD
300/1 AC	337,80	236,15	296,42	26,51
300/1 AN	382,35	256,44	304,09	27,93
500/1 AC	306,16	230,53	274,95	22,32
500/1 AN	318,58	241,85	280,78	18,80

From results, it can be seen that 300/1 AN specimen has the largest HV value. 500/1 AN has the best HV distribution (Lower SD). 300/1 AN specimen has slightly higher HV than 300/1 AC specimen. Also 500/1 AN specimen has slightly larger HV than 500/1 AC part. Annealing made a slight increase in HV. HV values are higher in 300/1 specimens. Raising RPM made a slight decrease in HV. This result agrees with the findings from literature [38, 39, 40]. SD values for each specimen are showed in Figure 4.22.

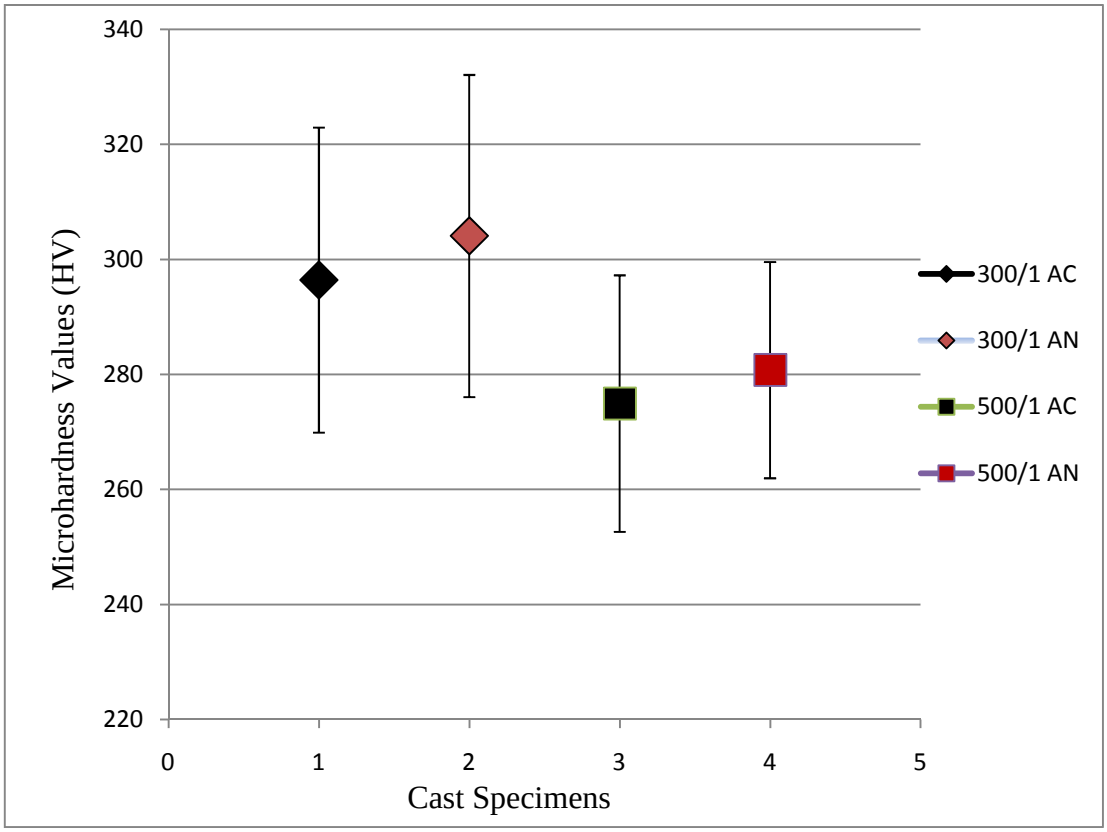

Figure 4.22. SD values for each specimen

All HV values of each specimen (8 from UP, 8 from LD and 8 from BP) can be seen in Figure 4.23. Values are taken from left to right in the specimens.

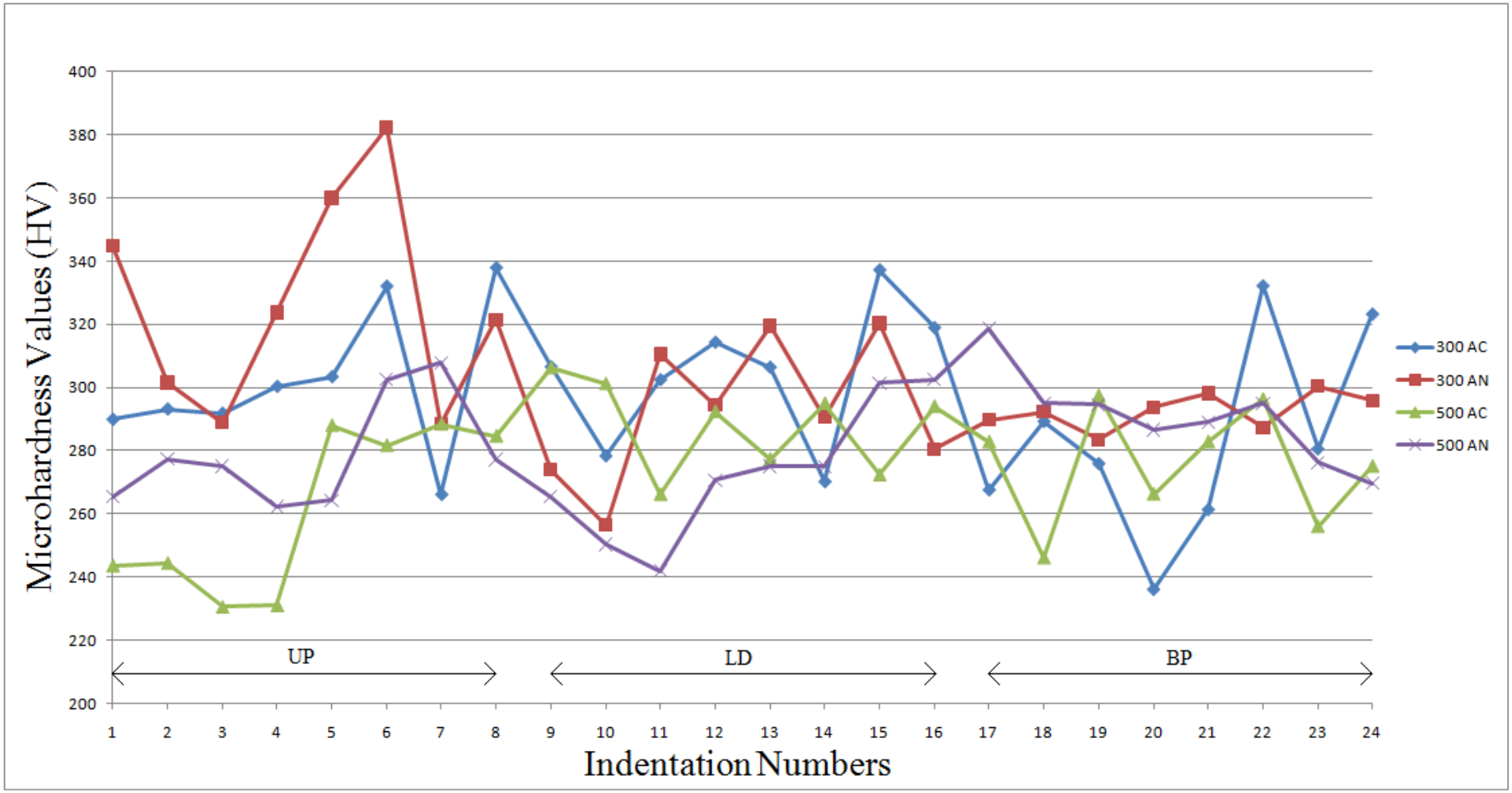

Figure 4.23. All HV values for each specimen

5. CONCLUSIONS AND FUTURE WORK

Dental implants are used to replace the missing teeth instead of dental bridges. Biocompatibility is important for living tissues in body and it is defined as the ability of a material to perform with an appropriate host response in a specific application or the quality of not having toxic or injurious effects on biological systems. Osseointegration is the contact between the metallic implant and the living tissues.

Biomaterials must simultaneously satisfy many requirements and possess properties such as non–toxicity, corrosion resistance, thermal conductivity, strength, fatigue durability, biocompatibility, and sometimes aesthetics.

To produce a dental implant that is concordant with the body, it is better to use Ti and its suitable alloys due to their excellent mechanical properties, good corrosion resistance in biological fluids and biocompatibility. The high corrosion resistance of titanium in various test solutions such as saliva and other physiological media is due to the formation of a very protective oxide layer on its surface. Ti is biocompatible, so osseointegration is seen between dental implant and the body.

Producing Ti dental implants with centrifugal casting is very common. Ti is biocompatible and has good mechanical properties, but it is a difficult metal to cast. Casting Ti with centrifugal casting technique is a good choice, because the centrifugal casting machine can exert approximately 40 – 60 times more force on the metal than the pressure difference casting unit. This force is good enough to produce sound castings

In the study, dental castings are produced via centrifugal casting method (High Frequency Casting Unit VACUTHERM 3,3 TITAN). For making centrifugal casting mould, rapid prototyping process was used for making the model and silicone moulding is used to make wax models. Wax models are evaporated inside the centrifugal casting mould.

The effects of different centrifugal speeds (RPM) in centrifugal casting machine and heat treatment to mechanical properties to Ti are investigated. For this purpose, dental implants are casted in 300 and 500 RPM by using raise time as 1. 2 implants are casted on each operation in one mould. Two implants (one from 300/1 and one from 500/1) are annealed at 700°C. Microstructure examination is performed and HV values are found by making microhardness test.

The obtained results are summarized:

- In 300/1 AC and 500/1 AC specimens, α grains are seen with acicular α grains.
- After annealing, most of the acicular α grains are converted to α grains (300/1 AN and 500/1 AN specimens).
- 300/1 AN specimen has the highest HV value.
- 500/1 AN has the best HV distribution (Lower SD).
- Annealing made a slight increase in HV (300/1 AN and 500/1 AN specimens).
- HV values are larger in 300/1 specimens.
- Raising centrifugal speed made a slight decrease in HV.

As a future work,

- Better rapid prototyping powders will be useful for making smooth rapid prototyping model surfaces.
- New wax types and techniques can be tried for better wax surface. Better wax surface means better casting surface.
- An avoiding system for the rapid cooling of cast Ti will provide better Ti microstructure.
- An extensive search should be made for investment material to protect chemical attack by highly reactive liquid Ti.

REFERENCES

1. Al-Mayouf, A. M., A. A. Al-Swayih, N. A. Al-Mobarak and A. S. Al-Jabab, "Corrosion Behavior of a New Titanium Alloy for Dental Implant Applications in Fluoride Media", *Materials Chemistry and Physics*, Vol. 86, pp. 320–329, Riyadh, Saudi Arabia, 2004.

2. Kurt, S. A., *Microstructure and Surface Topography of Cast Titanium as a Dental Material*, M.S. Thesis, Mechanical Engineering Department, Boğaziçi University, 1995.

3. Luo, X. P., T. W. Guo, Y. G. Ou and Q. Liu, "Titanium Casting into Phosphate Bonded Investment with Zirconite", *Dental Materials*, Vol. 18, pp. 512–515, China, 2002.

4. ADA Council Scientific Affairs, "Titanium Applications in Dentistry", Association Report, *the Journal of the American Dental Association*, Vol. 134, No. 3, pp. 347–349, 2003.

5. Alam, S. and R. I. Marshall, "Development and Metallurgical Evaluation of Centrifugally Cast Solid Bronze Bushes", *Journal of Physics D: Applied Physics*, Vol. 25, pp. 1335–1339, Leeds, U.K., 1992.

6. Schey, J. A., *Introduction to Manufacturing Processes*, Second Edition, the McGraw-Hill Companies, New York, U.S.A., 1987.

7. Eliopoulos, D., S. Zinelis and T. Papadopoulos, "Porosity of cpTi Casting With Four Different Casting Machines", *The Journal of Prosthetic Dentistry*, Vol. 92, No. 4, pp. 377–381, Athens, Greece, 2004.

8. Watanabe, I., M. Woldu, K. Watanabe and T. Okabe, “Effect of Casting Method on Castability of Titanium and Dental Alloys”, *Journal of Materials Science: Materials in Medicine*, Vol. 11, pp. 547–553, 2000.

9. Lütjering, G. and J. C. Williams, *Engineering Materials and Processes, Titanium*, Second Edition, Springer, Germany, 2007.

10. McCracken, M., “Dental Implant Materials: Commercially Pure Titanium and Titanium Alloys”, *Journal of Prosthodontics*, Vol. 8, No. 1, pp. 40–43, Alabama, U.S.A., 1999.

11. Lenntech Water Treatment and Purification, *Titanium*, http://www.lenntech.com/Periodic-chart-elements/Ti-en.htm.

12. Ping, W. S., L. D. Rong, G. J. Jie, L.C. Yun, S. Y. Qing and F. H. Zhi, “Numerical Simulation of Microstructure Evolution of Ti-6Al-4V Alloy in Vertical Centrifugal Casting“, *Materials Science and Engineering A*, Vol. 426, No. 1–2, pp. 240–249, Harbin, China, 2006.

13. Donachie, M. J., *Titanium: A Technical Guide*, Second Edition, ASM International, Ohio, U.S.A., 2000.

14. Iijima, D., T. Yoneyama, H. Doi, H. Hamanaka and N. Kurosaki, “Wear Properties of Ti and Ti–6Al–7Nb Castings for Dental Prostheses”, *Biomaterials*, Vol. 24, No. 8, pp. 1519–1524, Tokyo, Japan, 2003.

15. Ho, W. F., C. P. Ju and J. H. C. Lin, “Structure and properties of cast binary Ti-Mo alloy”, *Biomaterials*, Vol. 2, No. 22, pp. 2115–2122, Tainan, Taiwan, 1999.

16. Marples, M. and A. Partridge, *A Strategic Review of the Titanium Industry in the UK*, National Metals Technology Center, Rotherham, U.K., 2006.

17. Wessel, J. K., *The Handbook of Advanced Materials: Enabling New Designs*, Wiley-Interscience, New Jersey, U.S.A., 2004.

18. Roza, G., *Understanding the Elements of the Periodic Table: Titanium*, Rosen Central, New York, U.S.A., 2008.

19. Habashi, F., *Handbook of Extractive Metallurgy*, Wiley-VCH, Weinheim, Germany, 1998.

20. Chen, G. Z., D. J. Fray and T. W. Farthing "Direct Electrochemical Reduction of Titanium Dioxide to Titanium in Molten Calcium Chloride", *Nature*, Vol. 407, pp. 361–364, U.K., 2000.

21. Oak Ridge National Laboratory, *Opportunities for Low Cost Titanium in Reduced Fuel Consumption, Improved Emissions, and Enhanced Durability Heavy-Duty Vehicles,* http://www.ornl.gov/sci/propulsionmaterials/pdfs/Low-Cost_Titanium.pdf.

22. Rivard, J. D. K., C. A. Blue, D. C. Harper, J. O. Kiggans, P. A. Menchhofer, J. R. Mayotte, L. Jacobsen and D. Kogut, “The Thermomechanical Processing of Titanium and Ti-6Al-4V Thin Gage Sheet and Plate”, *JOM Journal of the Minerals, Metals and Materials Society*, Vol. 57, pp. 58–61, U.S.A., 2007.

23. International Titanium Powder, *The Armstrong Process, Low-cost High-Volume Production of Commercially Pure Titanium and Titanium Alloys, Potential and Limits of the Armstrong Process,* http://www.itponline.com/Presentations/Borys.pdf.

24. OSAKA Titanium technologies co., Ltd., *Titanium Manufacturing Process and Products,* http://www.osaka-ti.co.jp/e/e_product/titan/index.html.

25. Sunny Titanium Industry Co., Ltd., http://www.sino-ti.com/UploadFiles/200869203424510.jpg.

26. Taki, K. and A. Saito, *Method of Producing Titanium Material Resistant to Hydrogen Absorption in Aqueous Hydrogen Sulfide Solution*, United States Patent No. 5395461, 1995.

27. Niinomi, M., "Mechanical Properties of Biomedical Titanium Alloys", *Materials Science and Engineering: A*, Vol. 243, No. 1, pp. 231–236, Toyohashi, Japan, 1998.

28. Stock M. and P. Gehrke, *Underlying Mechanisms of Endosseous Integration at the Material-Biosystem Interface*, FRIADENT® CELLplus Scientific Bulletin, 2003.

29. International Titanium Association, www.titanium.org/files/ItemFileA3321.pdf.

30. University of Utah, Metallurgical Engineering, http://www.metallurgy.utah.edu/galleries/artifhp3.jpg/view.

31. Williams, D. F., *The Williams Dictionary of Biomaterials*, Liverpool University Press, Liverpool, U.K., 1999.

32. Dorland's Medical Dictionary, www.dorlands.com/.

33. Toumelin-Chemla F., F. Rouelle and G. Burdairon, "Corrosive Properties of Fluoride-Containing Odontologic Gels against Titanium", *Journal of Dentistry*, Vol. 24, No. 1–2, pp. 109–115, Paris, France, 1996.

34. Higuchi, Y., Y. Ohashi and H. Nakajima, "Biocompatibility of Lotus-type Stainless Steel and Titanium in Alveolar Bone", *Advanced Engineering Materials*, Vol. 8, No. 9, pp. 907–912, Osaka, Japan, 2006.

35. Braemer, W., "Biocompatibility of Dental Alloys", *Advanced Engineering Materials*, Vol. 3, No. 10, pp. 753–761, Hanau, Germany, 2001.

36. ASTM Standard E 384 – 99, Standard Test Method for Microindentation Hardness of Materials, 1999.

37. Gordon England, Independent Metallurgist and Consultant to the Thermal Spray Coating Industry, http://www.gordonengland.co.uk/hardness/vickers.gif.

38. da Rocha, S. S., G. L. Adabo, G. E. P. Henriques and M. A. de A. Nóbilo, "Vickers Hardness of Cast Commercially Pure Titanium and Ti-6Al-4V Alloy Submitted to Heat Treatments", *Brazilian Dental Journal,* Vol. 17, No. 2, Brazil, 2006.

39. Trillo, E. A., C. Ortiz, P. Dickerson, R. Villa, S. W. Stafford and L. E. Murr, "Evaluation of Mechanical and Corrosion Biocompatibility of TiTa Alloys", *Journal of Materials Science: Materials in Medicine*, Vol. 12, No. 4, Texas, U.S.A., 2001.

40. King, A. W., E. Lautenschlager, J. Chai and J. Gilbert, "A Comparison of the Hardness of Different Types of Titanium and Conventional Metal Ceramics", *The Journal of Prosthetic Dentistry,* Vol. 72, No. 3, pp. 314–319, Taiwan, 1994.

41. Rao, P. N., *Manufacturing Technology, Volume 1: Foundry, Forming and Welding*, Tata McGraw-Hill Publishing Company Limited, New Delhi, India, 1987.

42. Engineering Fundamentals, *Centrifugal Casting*, http://www.efunda.com/processes/metal_processing/centri_casting.cfm.

43. Southern Polytechnic State University, Mechanical Engineering Technology Department, http://met.spsu.edu/snasseri/ch11-Metal-Casting-2.pps.

44. Ray, R. and D. W. Scott, *Centrifugal Casting of Nickel Base Superalloys in Isotropic Graphite Molds Under Vacuum*, United States Patent No. 6634413, 2003.

45. Eastern Mediterranean University (EMU), Mechanical Engineering Department, http://me.emu.edu.tr/me364/ME364_casting_processes.pdf.

46. Grand Valley State University, School of Engineering http://www.eod.gvsu.edu/eod/manufact/manufact-199.html.

47. Welcome to B2B Marketplace for Metal Castings
http://www.themetalcasting.com/semi-centrifugal-casting.html.

48. The Mechanical Engineering, Indian Institute of Technology, Bombay, India
http://www.me.iitb.ac.in/~bravi/ME333/L04.pdf.

49. Wang, Q., Y. Wei, W. Chen, Y. Zhu, C. Ma and W. Ding, "In Situ Surface Composites of (Mg_2Si+Si)/ZA27 Fabricated by Centrifugal Casting", *Materials Letters*, Vol. 75, No. 24–25, pp. 3851–3858, Shanghai, China, 2003.

50. Chirita, G., D. Soares and F. S. Silva, "Advantages of the Centrifugal Casting Technique for the Production of Structural Components with Al–Si Alloys", *Materials and Design*, Vol. 29, No. 1, pp. 20–27, Guimarães, Portugal, 2008.

51. Pathak, J. P., S. Mohan, J. K. Singh and S. N. Ojha, ”Centrifugal Casting of Leaded Aluminium Alloys”, *International Journal of Cast Metals Research*, Vol. 19, No. 5, pp. 283–288, 2006.

52. Jovanović, M. T., B. Dimčić, I. Bobić, S. Zec and V. Maksimović, “Microstructure and Mechanical Properties of Precision Cast TiAl Turbocharger Wheel”, *Journal of Materials Processing Technology*, Vol. 177, No. 1, pp. 14–21, Belgrade, Serbia, 2005.

53. Jing, T., X. Shu-long, C. Yu-yong and C. Zi-yong, “Technology of Centrifugal Casting for Titanium Alloy”, *The Transactions of Nonferrous Metals Society of China*, Vol. 13, pp. 111−114, Harbin, China.

54. Liu, K., Y. C. Ma, M. Gao, G. B. Rao, Y. Y. Li, K. Wei, X. Wu and M. H. Loretto, “Single Step Centrifugal Casting TiAl Automotive Valves”, *Intermetallics*, Vol. 13, No. 9, pp. 925–928, 2005.

55. Halvaee, A. and A. Talebi, “Effect of Process Variables on Microstructure and Segregation in Centrifugal Casting of C92200 Alloy”, *Journal of Materials Processing Technology*, Vol. 118, No. 1–3, pp. 122–126, Tehran, Iran, 2001.

56. Vaidyanathan, T. K., A. Schulman, J. P. Nielsen and S. Shalita, "Correlation between Macroscopic Porosity Location and Liquid Metal Pressure in Centrifugal Casting Technique", *Journal of Dental Research*, Vol. 60, No. 1, pp. 59–66, New York, U.S.A., 1981.

57. Sherman, L. M., *Close-Up on Technology - Rapid Prototyping, 3D Printers Lead Growth of Rapid Prototyping*, Plastics Technology, http://www.ptonline.com/articles/200408cu3.html.

58. Z Corporation, http://www.zcorp.com/Products/3D-Printers/ZPrinter-310-Plus/ZPrinter-310-Plus---Technical-Sp/spage.aspx, 2007.

59. Z Corporation, http://www.zcorp.com/documents/15_CaseStudy-Jerde-FINAL.pdf, 2006.

60. ZPRINTER® 310 PLUS Hardware Manual, Z Corporation, 2007.

61. Bredt, J. F., T. C. Anderson and D. B. Russell, Assignee: Z Corporation, *Three Dimensional Printing Material System and Method*, United States Patent No. 6610429, 2003.

62. Alc Metal, *Investment Casting*, http://www.alcmetal.com/AlcMetal/eng/invesment_casting/invesment_casting.aspx.

63. Istanbul Technical University Mechanical Engineering Web Page, http://www.mkn.itu.edu.tr/bolumler/imalat/baglanti/dokum/hd/hd.htm.

64. Abréu, D., G. Castro, A. González, C. Martínez and M. Pérez, *Human Teeth: Biomaterials and Implants*, Applications of Engineering Biomechanics in Medicine, University of Puerto Rico, Mayagüez, 2003.

65. Watari, F., A. Yokoyama, F. Saso, M. Uo and T. Kawasaki, ”Fabrication and Properties of Functionally Graded Dental Implant”, *Composites Part B*, Vol. 28B, No. 1–2, pp. 5–11, Sapporo, Japan, 1997.

66. Rupp, F., J. Geis-Gerstorfer and K. E. Geckeler, “Dental Implant Materials: Surface Modification and Interface Phenomena”, *Advanced Materials*, Vol. 8, No. 3, pp. 254–257, Tubingen, Germany, 1996.

67. Massaro, C., P. Rotolo, F. De Riccardis, E. Milella, A. Napoli, M. Wieland, M. Textor, N. D. Spencer and D. M. Brunette, “Comparative Investigation of the Surface Properties of Commercial Titanium Dental Implants. Part I: Chemical Composition”, *Journal of Materials Science: Materials in Medicine*, Vol. 13, pp. 535–548, 2002.

68. University of California, San Diego, School of Medicine, *Osseointegration*, http://sdnp3.ucsd.edu/osseointegration.htm.

69. Welcome to The Web site for Dr. Martin Ruelas, D.M.D., PC, *Dental Implants,* http://www.martinruelas.com/services/.

70. Simunek, A., D. Kopecka, M. Cierny and I. Krulichova, “A Six-Year Study of Hydroxyapatite-Coated Root-Form Dental Implants”, *The West Indian Medical Journal*, Vol. 54, No. 6, pp. 393–397, 2005.

71. Mukherjee, D. P., N. R. Dorairaj, D. K. Mills, D. Graham and J. T. Krauser, “Fatigue Properties of Hydroxyapatite-Coated Dental Implants after Exposure to a Periodontal Pathogen”, *Journal of Biomedical Materials Research Part B: Applied Biomaterials*, Vol. 53, No. 5, pp. 467–474, U.S.A., 2000.

72. Bozkaya D. and S. Muftu, “Mechanics of the Tapered Interference Fit in Dental Implants”, *Journal of Biomechanics*, Vol. 36, No. 11, pp. 1649–1658, Boston, U.S.A., 2003.

73. Zimmer Dental, *Spline® Implant System Product Catalog* http://www.zimmerdental.com/pdf/lib_catSpline4857.pdf.

74. Oal, F., *Materials Selection Criteria for a Dental Implant*, M.S. Thesis, Boğaziçi University, 2005.

75. Dentaurum, *rematitan® Plus, Special investment for titanium castings*, http://www.dentaurum.de/eng/zahntechnik_2898.aspx.

76. Dentaurum, *rematitan® Plus, Instructions for use*, http://www.dentaurum.de/files/989-847-00.pdf.

77. Operating Instructions - High Frequency Casting Unit VACUTHERM-3,3-TITAN.

78. Linn High Therm Website, *Linn High Therm Dental*, neu.linn.de/docs/dental.pdf.

79. Struers A/S, *Struers Application Notes, Metallographic Preparation of Titanium*, http://www.struers.com.tr/default.asp?top_id=5&main_id=24&sub_id=185&doc_id=855.